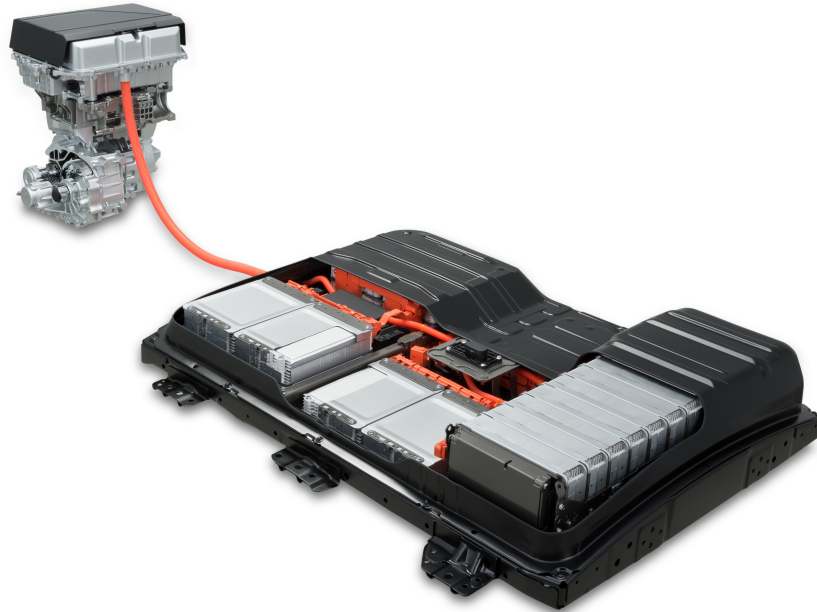© Nissan Motor Corporation

Life cycle assessment of nickel-rich lithium-ion battery for electric vehicles

A comparatative LCA between the cathode chemistries
NMC 333 and NMC 622

Master's thesis in Industrial Ecology

ADAM LEWRÉN

Life cycle assessment of nickel-rich lithium-ion battery for electric vehicles

A comparatative LCA between the cathode chemistries NMC 333 and NMC 622

ADAM LEWRÉN

Tutor, Chalmers: Felipe Bitencourt de Oliveira
Tutor, IVL: Lisbeth Dahllöf

Life cycle assessment of nickel-rich lithium-ion battery for electric vehicles
A comparatative LCA between the cathode chemistries NMC 333 and NMC 622
ADAM LEWRÉN

Cover: The battery pack and electric motor in the electric vehicle Nissan Leaf 2017.

Life cycle assessment of nickel-rich lithium-ion battery for electric vehicles
A comparatative LCA between the cathode chemistries NMC 333 and NMC 622
ADAM LEWRÉN
Department of Technology Management and Economics
Chalmers University of Technology

Abstract

Nickel-rich lithium-ion cells are entering the market for electric vehicles, due to their higher density (kWh/kg) and less content of cobalt which has been appointed as a critical raw material. With higher density, longer driving distance per charge can be achieved since greater energy capacity is obtained per kg battery. However, the increase in energy density may be at the expense of the lifetime of batteries. There is ongoing research on the aging of new Ni-rich Li-ion cells for vehicle applications on how the different factors affect aging such as material composition, cell design, temperature, and internal pressure.

This Master's thesis has investigated the environmental impacts of Ni-rich Li-ion battery by conducting a Life Cycle Assessment to get an overall picture of the total environmental impact throughout its life cycle - from raw material extraction, through manufacturing processes and use, to waste management. The cathode chemistry of the Ni-rich Li-ion battery has chosen to be NMC622 which consists of the following active electrode material: 60% nickel, 20% Manganese and 20% Cobalt. The NMC622 battery is compared NMC333 which more common cathode chemistry for electric vehicles and the comparison has been done with respect to how much energy (kWh) that has been provided over the service life.

According to the normalized and weighted LCIA results, NMC622 has around 2% higher environmental impact compared to NMC333. This is mainly due to that NMC622 has a higher contribution to the impact categories acidification and particulate matter from the production of nickel sulfate used in the cathode. The use phase was also considered as a hotspot in the life cycle where NMC622 has 2% lower plug-to-wheel consumption than NMC333 due to having around 8% higher energy density (kWh/kg). Other impact categories that accounted for the highest share of the total environmental impact was climate change and ionizing radiation which were also mainly due to the production of the cathode.

Although the difference in environmental impact between batteries is too small to draw any conclusions given the uncertainties, the study provides insight into potential hotspots in the life cycle. Furthermore, the study points out which components and materials which might have the greatest influence on the difference in environmental impact between NMC622 and NMC333.

Acknowledgements

Contents

Contents

Acronyms

LCA   Life Cycle Assessment

f.u   Functional Unit

ISO   International Organization for Standardization

ALINE   Aging of Lithium-ion Batteries with Nickel-Rich Cathodes for Electromobility

GHG   Greenhouse gases

BMS   Battery Management System

BatPac Battery Performance and Cost model

LCI   Life Cycle Inventory

LCIA   Life Cycle Impact assessment

LIBs   Lithium-ion batteries

BEV   Battery Electric Vehicle

PHEV   Plug-in Hybrid Electric Vehicle

BOMs   Bill-of-Materials

PEFCR   Product Environmental Footprint Category

ILCD   International Reference Life Cycle Data System

eLCAr   E-Mobility Life Cycle Assessment Recommendations

LMO   Lithium Manganese Oxide

LFP   Lithium Iron Phosphate

NCA   Nickel Cobalt Aluminum Oxide

NMC   Nickel Cobalt Manganese Oxid

LCO   Lithium Cobalt Oxide

WLTC   Worldwide Harmonized Light Duty Test Cycle

WLTP   Worldwide Harmonized Light Duty Test Procedure

NEDC   The New European Driv-ing Cycle

GWP   Global Warming Potential

FEP   Freshwater Eutrophication Potentia

MEP   Marine Eutrophication Potentia

TEP   Terrestrial Eutrophication Potential

AP   Acidification Potential

HTPC Human Toxicity Potential Cancer effects

HTPNC Human Toxicitiy Potential Non-Cancer effects

FETP   Freshwater Toxicity Potential

POFP Photo Oxidation Formation Potential

ODP   Ozone Depletion Potential

IR   Ionizing Radiation

PM   Particulate Matter

ADP   Abiotic Depletion Potential

1

Introduction

1.1 Background

The attention towards global warming and the identification of carbon dioxide (CO2) as the main driver has led to an increase of efforts to mitigate emissions (Stocker, 2013). One of the areas that has been encouraged to reduce its emissions is the transport road sector (Sims R. et al., 2014). This has pushed the research on development of light-duty and high-duty vehicles into a direction where the fossil-based fuel is replaced by electricity and among other things. Today there are selections of vehicles at different levels of electrification, such as plug-in-hybrid (PHEV) and fully electric vehicles (EV).

Lithium-ion batteries (LIBs) are the most dominant electric energy storage (EES) solution for portable electronics, but also the most preferred battery for electric vehicles (Zubi et al., 2018). There several other types of batteries that are available such as lead-acid and nickel-cadmium but according to Zubi et al. (2018) LIBs currently show the largest energy storage potential for portable electronic devices and electric mobility. This is due to the fact of lithium's relatively lightness and ability to donate electrons (Zubi et al., 2018). There are, however, some aspects to consider regarding LIBs such as high initial cost, low recovery and recycling rate and concerns regarding safety and material scarcity.

There are various LIB types with different characteristics primarily based on what materials that are used in the cathode (Romare & Dahllöf, 2017). In vehicle applications, most common cathode chemistries are Lithium Manganese Oxide (LMO), Lithium Iron Phosphate (LFP), Lithium Nickel Cobalt Aluminium Oxide (NCA), and Lithium Nickel Cobalt Manganese Oxide (NMC) (Pistoia & Liaw, 2018). Lithium Cobalt Oxide (LCO) is common chemistry for portable electronics but are due to safety reasons less relevant. According to Zubi et al. (2018) the market trend prediction for 2030, the NMC will be the most dominating LIB for vehicles with respect of relevant characteristics for electric vehicles such as durability, safety, specific energy and power. The market share on LFP is also expected to increase significantly but rather in a wider range of other applications than in vehicles (Zubi et al., 2018). The NCA seems to slightly increase as well but assumed to not be dominating in any particular application. As mentioned, the anode has a fewer options, where graphite is currently superior when combined with the cathode chemistries stated above (Romare & Dahllöf, 2017).

In the short term perspective, increased capacity is sought by further development of current available cathodes and anodes (Romare & Dahllöf, 2017). An emerging trend is to increase the nickel content in the NMC chemistry to improve the energy density. The Ni-rich NMC has been considered to be the next generation of LIBs for electric vehicles, however, according recent studies (Jung et al. 2018; Li et al. 2017; Jing et al. 2015 & Ma et al. 2015) the increase of nickel content could come of the expense of shorter lifetime.

There are already LCA studies available for the NMC batteries, but there has not yet been much on the nickel-rich ones. One of them that has been cited relatively widely and has been the basis of many other LCA studies on batteries is an LCA of a lithium-ion battery vehicle pack by Ellingsen et al. (2014). There are also LCA studies in which NMC battery has been compared with other batteries. There are, for example, two studies by Deng et al. (2017b) respective (Deng et al., 2017a) which compare the NMC battery with lithium-sulfur battery and molybdenum disulfide lithium-ion battery for electric vehicles.

The study's initiative comes from a project entitled Aging of Lithium-ion Batteries with Nickel-Rich Cathodes for Electromobility (ALINE). The aim of the project is to gain more knowledge regarding the performance, aging and environmental and societal impacts of nickel-rich LIBs with respect to vehicle applications. The project is conducted interdisciplinary with the involvement of various organizations focusing on different areas. The aim of this master thesis is to assist IVL in this project by providing a comparative life cycle assessment (LCA) on a nickel-rich lithium battery with the NMC cathode chemistry.

1.2   Methods

This study is primarily based on the LCA methodology according to ISO 14040 and 14044 but there are also other methods that have been used. The study has, for example, also been carried out by guidance from E-Mobility Life Cycle Assessment Recommendations (eLCAr), which is a project that supports the performance of life cycle assessment on electric vehicles (Del Duce et al., 2013). Furthermore, guidelines from the international reference life cycle data system (ILCD) handbook are followed, which includes the LCA standards ISO 14040 and 14044 (European Joint Research Centre, 2010). Finally, guidelines from the Product Environmental Footprint Category Rules for High Specific Energy Rechargeable Batteries for Mobile Applications will be considered if applicable (Siret et al., 2018).

1.3   LCA Methodology

LCA stands for Life Cycle Assessment and is a comprehensive method to analyze environmental impacts related to a product or a service (Baumann & Tillman, 2004). In figure 1.1 the main steps in LCA is presented; goal and scope, inventory analysis and impact assessment.
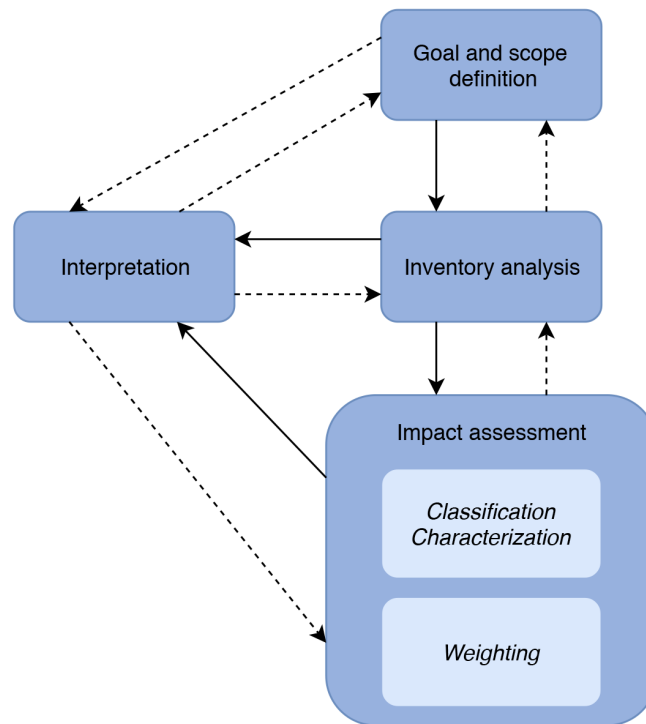
Figure 1.1: Illustration on the Life Cycle Assessment framework, adopted from Baumann & Tillman (2004).The boxes represent the main steps whereas the arrows show which order the steps are performed. The dashed arrows indicate possible iterations.

1.3.1 Goal and Scope definition

The goal specification of an LCA study is a central part which shapes the scope and sets the frame for the LCI and LCIA work (European Joint Research Centre, 2010). In addition, the goal definition can be viewed as the requirements of the study and can be used to ensure the overall quality of the analysis. Hence, a clear goal definition is essential for a correct interpretation of the results.

In the scope definition, the object of the LCA is defined and described. To ensure the breadth, depth and detail of the study are sufficient to address the stated goal(s), scope shall always be defined in line with the goal definition. For instance, deriving the methodology requirements based on the reasons for the study, the intended applications, and the audience.

1.3.2 Life Cycle Inventory

In the inventory analysis, the data collection and modelling of the product system is conducted in line with the goal and scope definition (European Joint Research Centre, 2010). The LCI is typically the most time-consuming step requiring the highest efforts and resources. Furthermore, results of the inventory analysis may provide new insights which need to be considered, leading to inevitable adjustments

in the initial scope definition. The data collection includes, for example, gathering information on energy and material flows between the processes along the product life cycle. Prior to the modelling, adjustments on the data sets are usually required to become compatible with the chosen functional unit. In addition to connecting and scaling data sets, modelling includes solving multifunctionality of processes in the system since the supply chain usually consists of processes producing more than just one product. The final step is to calculate the LCI results by summing up all inputs and output of all processes within the system boundaries.

1.3.3 Life Cycle Impact Assessment

In a life cycle impact assessment (LCIA) the results on the environmental loads from the LCI are translated into potential environmental impacts (Baumann & Tillman, 2004). There are several reasons to translate the elementary flows, i.e. inventory results, to environmental impact categories. One of reasons is to improve the *relevance*. By translation of the elementary flows, the results become more environmentally relevant, comprehensive and easier to communicate. For a lot of people environmental impacts, such as global warming, are easier to relate to than the amount of carbon dioxide emissions. Another reason is to improve the *readability*. The environmental impacts are an aggregation of the elementary flows and thus, easier to grasp since the number of result parameters decrease. Lastly, *comparability* is also a reason to aggregate the inventory results.

In figure 1.2, potential environmental impacts are explained by an environmental cause-effect chain (Masoni, 2016). The potential environmental impacts are effects of polluting activities and there are different types of effects depending on where in the cause-effect chain they are located. The effects are usually chronologically divided into three groups, where primary effects are the direct cause of the pollutants and secondary followed by tertiary effects are subsequent effects.

As seen in figure 1.2, an example of the environmental cause-effect chain could be activities that emit greenhouse gases (GHG) which causes a primary effect of changes in radiative forcing. This, in turn, causes an atmospheric temperature to rise as a secondary effect, followed by a tertiary effect such as raised sea levels, ice melting and changed weather patterns.

The potential environmental impacts correspond to these effects and are in the same way divided based on where they are located in the impact pathway. There are midpoint indicators which are in an intermediate point in the impact pathway, representing impact categories such as global warming, acidification, and eutrophication. There also endpoint indicators, relating to areas of protection, at the end of the impact pathway, including for example the ecosystem and human health. All these impact categories, located in different places along the impact pathway have different pros and cons when it comes to using them to assess environmental performance in LCA. The midpoint indicators are considered to be more scientifically valid as they are more closely linked to measurable effect, whereas endpoints are considered to be easier to interpret as they relate to things easier to grasp.
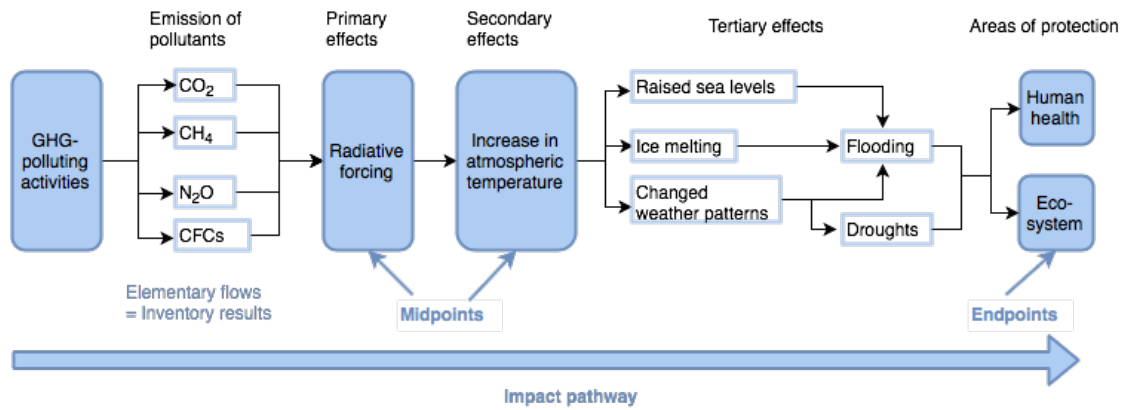
Figure 1.2: Cause-effect chain adopted from Masoni (2016)

According to Masoni (2016), the impact assessment consists of five steps. The first step is to select the impact categories with respect to the goal of the study (Masoni, 2016). The second step is called *classification* and this is where the inventory results are assigned to the selected impact categories. The third step, also the last mandatory step, is known as *characterization* where the elementary flows are multiplied with a specific characterization factor depending on which impact category they are assigned to. The purpose of characterization factor is to value the importance for each elementary flow for a specific impact category.

Two optional approaches after the characterization step are *normalization* and *weighting*. In these two steps, the resulting characterization indicator scores are weighted combined into one index. This enables a comparison of their relative magnitude since the sum of the indicator scores from each impact category can be put into the same scale. In the normalization step, the indicator scores from the characterization step are converted to a system used as a reference. The results of the normalization can also be used as a preparation for the weighting step. In the weighting step the resulting indicator scores are converted based on value-based choices and thus, comes in handy when the study consist of trade-offs as different categories can be related to each other. In addition to the possibility of comparing different impact categories on the same scale, normalization and weighting can ease the understanding and communication of the results for the intended audience of the study, if they are not used to analyzing a large number of impact categories side by side.

1.4 Electric vehicle battery

The following chapter explains the battery system used in electric vehicles and begins with cells followed by modules and finally the battery pack. The breakdown of the battery pack is shown in figure 1.3.

Figure 1.3: From left, a battery pack for an electric vehicle is shown followed by a battery module and battery cell.

1.4.1   Battery cell

Figure 1.4, illustrates the functionality of the lithium-ion cell, where the four main components are: cathode, anode, electrolyte and separator (Zubi et al., 2018). When the battery is charging, the cathode emits the positive Li-ion through the electrolyte to the receiving anode and opposite during discharge. The cathode and the anode both work as a receiver and transmitter, where cathode is made of lithium metal oxide powder and anode is commonly made of graphite powder.

The electrolyte works as a electric conductor and is a liquid mixture of lithium salt and organic solvent. The mobility of the passing Li-ions is increased by the organic solvent.

The separator's role is to prevent short circuit and this is done by preventing the cathode and anode to directly connect to each other, while still allowing the positive Li-ions to pass. The material content of the separator is commonly plastics such as polyethylene and polypropylene. The cathode and anode are supported by thin aluminum and copper foils respectively, and these foils also act as conductors.

A complete cell is created when the layered set-up described above is stacked several times. The electrical current from each layer is conducted to the positive and negative battery terminal by current collectors that are attached to the metal foils. To protect the layered structure an outer case is used, usually in stainless steel or aluminum (Pistoia & Liaw, 2018) For vehicle application, many lithium-ion cells need to be combined into a battery pack in order to provide enough power and energy (Romare & Dahllöf, 2017).

Cathode and anode chemistry

The characteristics of the lithium-ion battery that is considered most relevant when choosing what battery to use in a given application: specific energy and power and durability and safety (Zubi et al., 2018). The properties of the battery can be configured by different combinations of cathode and anode materials (Romare & Dahllöf, 2017). In vehicle applications, some material choices are more common due to certain demands on the battery chemistry with regard to power and energy per kg. For fully electric vehicles (BEVs), the specific energy (kWh storage/kg battery) is crucial, whereas for plugin hybrid vehicles (PHEVs) a certain balance of specific
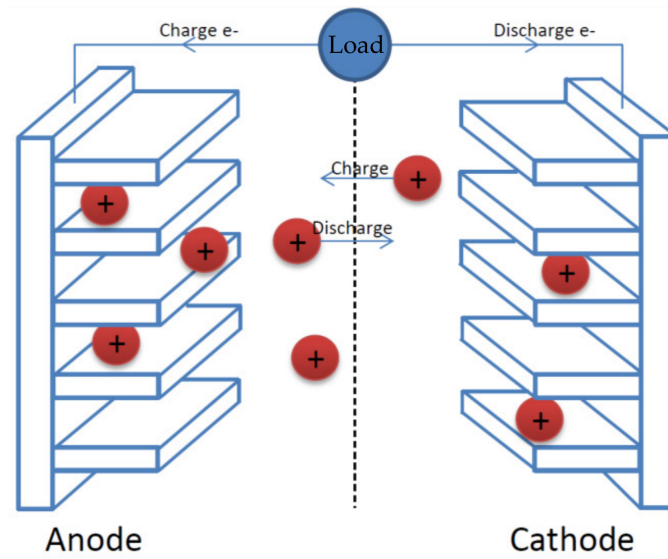
Figure 1.4: Illustration on a lithium-ion battery cell (Olofsson & Romare, 2013). The electricity is charged or discharged through the movement of the lithium ions between the active materials. In-between the active materials there is an electrolyte which serves as a catalyst promoting the movement of the ions. There is also a separator preventing the cathode and anode to react with each other causing a short circuit. Lastly, there are current collectors attached to the active materials with the role to support and transport the electrons to the load.

power and energy is required. A common cathode choice for PHEV, but specifically for BEV consists of a a mix of cobalt, nickel and manganese oxides together with lithium. For anode the material options are more limited. Graphite is currently the dominating choice but there are some cases where the graphite anode is combined with silicon or made of non-graphite material.

Cell design

The battery cell is mainly manufactured in two ways. They are stacked cells either in a flat or cylindrical design (Romare & Dahllöf, 2017). In the flat-design configuration, the large sheets of cathode-anode combination are cut into square shapes, stacked, and enclosed in a flat protective case. There are two kinds of cases: a *flexible pouch case* that is made of a plastic and aluminum laminate and a hard aluminum case, known as *prismatic case*.

The cylindrical design is manufactured by using the same large sheets as in the flat design configuration but instead rolled up and sealed in a cylindrical case usually made of aluminum. Historically, the cylindrical design has been used a lot in small scale batteries and therefor, the production cost is relatively low. However, the pouch and prismatic cell designs have, compared to cylindrical, more efficient packaging and are for this reason more commonly used in vehicles.

1.4.2   Battery module

Battery modules allow for management of a smaller number of cells within a larger pack and protect them by a cassette, consisting of an outer and inner frame (Ellingsen et al., 2014). Commonly, there are about 20 modules in a battery pack for electric vehicles and the number of cells in each is around 12 (Nelson et al., 2018). The weight is about 20 kg with a volume of 10 liters.

1.4.3   Battery pack

The purpose of having a battery pack is to be able to control certain units that are usually too large and complex to be handled only by cells and battery modules. Battery packs that are used for an electric vehicle consist of the following four main components: battery cells contained in modules, battery management system (BMS), cooling system and packaging (Ellingsen et al., 2014). The BMS controls and monitors the battery whereas the cooling system maintains the temperature.

1.5   Battery model

For the purpose of this study, the lithium-ion battery packs are theoretically designed in a tool developed by Nelson et al. (2018), called the *Battery Performance and Cost model* (BatPac). The design of the batteries is based on values that meet the *U.S. Advanced Battery Consortium LLC* (USABC) guidelines.

In figure 1.5, the BatPac framework is shown describing how the batteries are modelled. The battery modelling is conducted in an iterative spreadsheet where the following main categories are defined; cell chemistry, pack requirements and key constraints (Nelson et al., 2018).

In the spreadsheet, there were already ready-made cell chemistries available to choose from, including the ones that were chosen in this study namely NMC333 and NMC622. The values of the parameters in the pack requirements and key constraints were estimated based on predetermined conditions and performance of a battery in a vehicle application. For information see appendix A.2 and B. The output of the model are; the volume and mass, the specific energy and power, and bill-of-materials (BOM) for each battery. However, BOM was not entirely complete and thus literature studies were required to supplement the information that was missing. In addition, there was sometimes a need for derivation, which is explained in appendix A.1.

1.6   Vehicle model

To the BatPac model, an additional model has been added in the spreadsheet inspired by an LCA study by Deng et al. (2017b). The iterative integration between the battery and vehicle model is shown in figure 1.6a. The motivation to add an additional model is to create batteries that meet predetermined requirements with respect to vehicle applications. The original BatPac model offers a possibility to
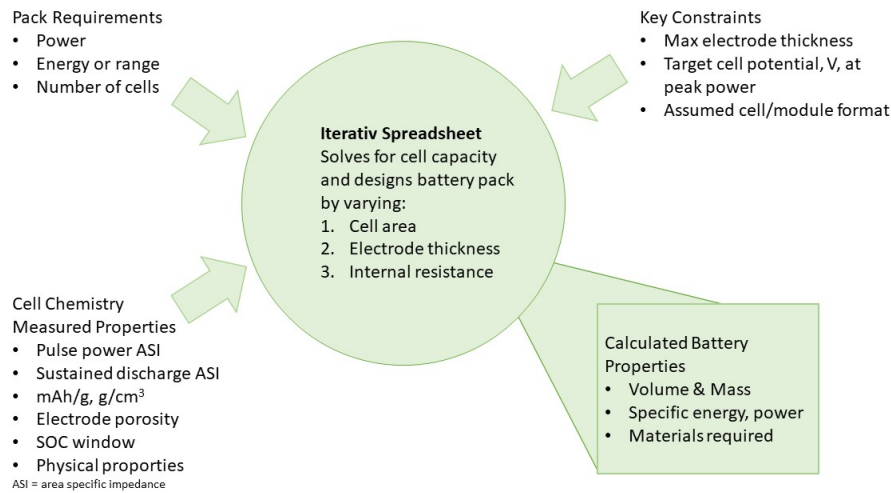
Figure 1.5: Illustration on the BatPac framework (Nelson et al., 2018)

choose a driving distance and energy consumption which subsequently calculates the required energy capacity and mass of the battery, see figure 1.6b. However, the original model fails to consider the feedback loop, confirmed by Del Duce et al. (2013), between the battery mass and energy consumption. The total vehicle mass, including the battery, influences the energy consumption, which again feeds back to the driving distance.
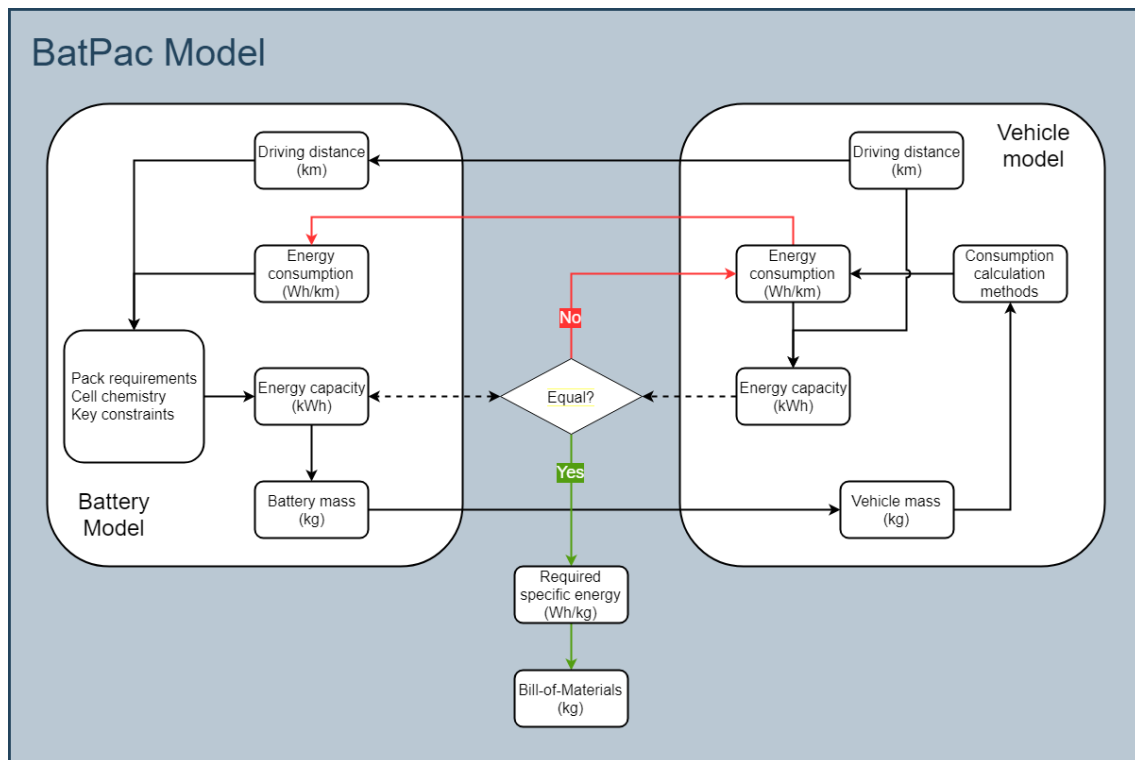
(a) An illustration on the iterative integration between the battery and vehicle model.
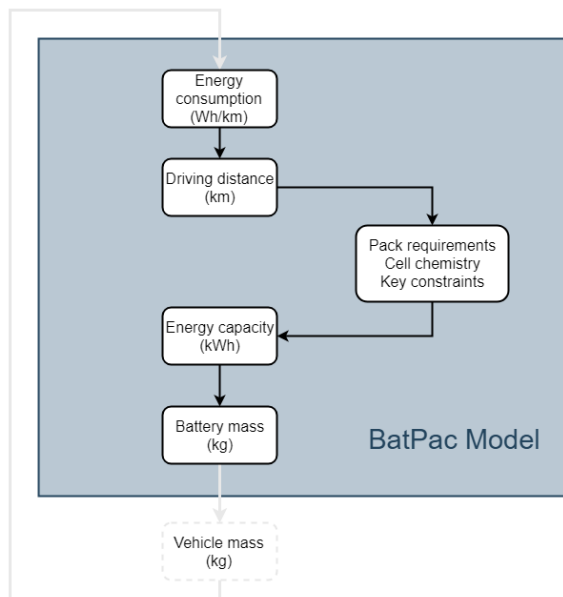
(b) An illustration on the original BatPac model. The gray box and arrows indicates the feedback loop that is missing.

Figure 1.6: Illustrations on a spreadsheet used to theoretically design batteries for the LCA study

In the new model, the iteration continues until the calculated energy capacity in the battery model is equal to the one calculated in the vehicle model. Once they are equal, the battery model has calculated the required specific energy that meets the predetermined requirements with respect to vehicle applications. It shall be noted that the calculations of the energy capacity inbetween the models are different. The battery model calculates the energy capacity with respect to a bundle of parameters within the the three main categories: pack requirements, cell chemistry and key constraints. Where the vehicle model calculates the specific energy by multiplying the energy consumption and the driving distance. More details on how the vehicle model calculates the energy consumption is found in chapter 3.3.

1.7 GaBi Software

The LCA modeling is conducted in an LCA software called GaBi developed by Thinkstep. The software offers a large range of datasets and facilitate the collection and management of data. In addition, the modeling is visualized with a drag-and-drop function that makes it easy to connect flows and processes and gives a complete picture of the product system. Lastly, the results can be delivered with different levels of aggregation which can ease the interpretation of them.

2

GOAL AND SCOPE DEFINITION

2.1 Goal definition

In the following chapter, the intended applications and reasons for carrying out the study will be explained, including research questions and limitations.

2.1.1 Research questions

The LCA study is a comparative analyze of life cycle environmental impacts associated with driving 180,000 km in a mid-size electric vehicle with 350 km driving range per charge having; (a) a NMC333 lithium ion battery with a specific energy of 0.164 kWh/kg and (b) a NMC622 lithium-ion battery with a specific energy of 0.177 kWh/kg.

The main objective is to analyze the environmental performance on the two chosen lithium-ion batteries and the research questions to be answered are the following:

- How is NMC622 performing environmentally compared with NMC333 throughout their life cycles?

- Which are the hotspots in the life cycle and what influence does the configuration of the cathode chemistry have in relation to them?

2.1.2 Limitations

In the following chapter, limitations will be presented which could affect the applicability of the study (European Joint Research Centre, 2010).

Impact coverage limitations

The impact assessment will not cover the endpoint categories as it is not recommended in the PEFCR (Siret et al., 2018)

Methodological limitation

In the production phase, manufacturing of the electric vehicles is not considered. Furthermore, manufacturing of other products related to electric vehicle such as

charging stations are also not covered in this study.

The transportation distances and modes which are not already included in the datasets corresponds to the guidelines provided from the PEFCR for lithium-ion batteries.

The calculations of the energy consumption in the use phase is limited to the guidelines provided by eLCAr.

The recycling processes of lithium-ion batteries is limited to one approach developed by the company Umicore.

Assumption limitations

The electricity mix for the use phase and majority of the production processes is assumed to be the EU-28 average consumption mix. Exceptions are made on processes with site-specific data such as the production of cobalt and lithium carbonate. The impact of using different electricity mixes are investigated in the sensitivity analysis section.

2.1.3 Reasons for carrying out the study

The reason for the study is to evaluate the environmental impact on NM622 compared to NMC333. In particular, it is of interest to investigate the relationship between environmental impacts and energy density as well as material use

2.1.4 Target audience

The study is available for everyone but the main targeted audience is IVL Swedish Environmental Research Institute and stakeholders involved in the ongoing project Ageing of Lithium-Ion Batteries with Nickel-Rich Cathodes for Electromobility (ALINE).

2.2 Scope definition

The scope definition is derived from the goal of the study starting with the identification and definition of the product system followed by clarification of requirements for method and quality (European Joint Research Centre, 2010).

2.2.1 Function, Functional Unit and reference flow

The product targeted in the LCA study are lithium-ion battery for electric vehicles and the functionality is the propulsion of a vehicle by supplying electrical energy at a desired voltage range that can be converted to mechanical motion. For mobile application, where the rechargeable battery is the main storage of energy, the functional unit shall according to PEFCR be defined as **"1 kWh of the total energy provided over the service life by the battery system"** (Siret et al., 2018, p. 28).

The functional unit has been defined by answering the following questions:

- What?

- How much?

- How well?

- How long?

The first question refers to what unit the functional unit shall be measured in and for batteries, watt-hour was believed to be most suitable. The second question refers to how much watt-hour the batteries shall produce which is obtained by multiplying the amount of charging cycles with the amount of energy that is delivered over each cycle. The third question refers to the technical properties of the batteries and in this case, it is the specific energy which is measured in watt-hour per kg batteries. The last questions refer to the total distance the batteries are supposed to deliver in a vehicle application.

The design of the batteries was strongly influenced by the predetermined requirements on the driving distance per charge in a mid-sized electric vehicle. The batteries are expected to deliver a driving distance of 350 km per charge and by the knowledge on the vehicle weight as well as other vehicle parameters explained in chapter 3.3, the energy consumption per km was calculated. By knowing how much energy the batteries were suppose to deliver the properties could be derived from the models explained in chapter 1.5 and 1.6. In table 2.1, a selection of parameters from the models have been compiled and for more details see appendix A.2.

Table 2.1: The design and characteristics of the NMC333 and NMC622 lithium-ion batteries

Characteristics	Battery pack with NMC333-Gr cells	Battery pack with NMC622-Gr cells
Energy storage capacity [kWh]	85.1	83.4
Weight [kg]	520	472
Specific energy [kWh/kg]	0.164	0.177
Battery lifetime [km]	180,000	180,000
Number of cells	240	240
Number of modules	20	20

Calculation of the reference flow and functional unit

The size of the battery has a significant role to achieve the amount of energy delivery per charge and therefore, the reference flow is defined as kg battery per kWh. There are three main steps to calculate the number of batteries needed per kWh. The first step is to calculate how much energy the battery can deliver over its service life, which is calculated with equation 2.1.

$$Qua = Edc \times Nc \times Acc \tag{2.1}$$

Where:

   Qua : is the total amount of energy delivered by the battery over its service life [kWh]
   Edc : is the energy delivered per cycle [kWh]
   Nc : is the number of cycles []
   Acc : is the amount of energy available [%]

The second step is to calculate the number of batteries that are needed to deliver the total driving distance which is calculated in equation 2.2. The total driving distance during the lifetime of the vehicle is assumed to be 180,000 km. By dividing the total driving distance with the driving distance per charge and multiply it with the energy delivered per cycle, the total energy required is obtained.

$$Nbatt = \frac{AS}{Qua} \tag{2.2}$$

Where:

   $Nbatt$: is the number of batteries []
   AS : is the total energy required per application [kWh]
   Qua : is the total amount of energy delivered by the battery over its service life [kWh]

The last step is to calculate how much kg batteries that are needed to deliver 1 kWh which by dividing the the mass of the battery with the total energy required for a total driving distance of 180,000 km, see equation 2.3.

$$Rf = \frac{Nbatt \times Mbatt}{AS} \tag{2.3}$$

Where:

   Rf : is the mass of the battery per kilowatt-hour [kg/kWh]
   $Mbatt$: is the mass of the battery []
   AS : is the total energy required per application [kWh]

The reason why the reference flow is needed is due to the fact that the batteries are modelled with respect to their mass. Hence, the environmental impacts calculated in the GaBi software will be per kg batteries. By multiplying the results from the life cycle impact assessment with the reference flow, they will be related to the functionality of the batteries, that is the ability to deliver energy. For mathematical terms, see equation 2.4.

$$\frac{Environmental\ impact_x}{Fu} = \frac{Environmental\ impact_x}{kg\ battery} \times Rf \tag{2.4}$$

2.2.2 Life cycle modelling framework

In the following chapter, the decisions on the life cycle inventory modelling principles and method approaches are explained. It is a crucial step which has implications on what data is collected or obtained (European Joint Research Centre, 2010).

Type of modelling principle

There are mainly two modelling principles, attributional and consequential modelling (European Joint Research Centre, 2010). In this study, the former is used which depicts potential environmental impacts that can be attributed to a system throughout its life cycle. The approach includes all involving processes to the system and use measurable data that is historical and factual. Hence, the system could be modeled in its current state, prior state or in a predicted state. Compared to consequential modelling, average data is more acceptable but ideally, producer-specific is the most appropriate.

Solving multifunctionality

Multifunctionality problems arise when a process has more than one function (European Joint Research Centre, 2010). It could, for example, be a process producing several products, where only one is of interest. There are different approaches to solve multifunctionality and the appropriateness could depend on, for example, the goal definition, available data, and the characteristics of the multifunctional process or product. There is also a hierarchy for solving multifunctionality available provided by ISO 14044:2006 which ranks the appropriateness as follow:

1. Subdivision of multifunctional processes

2. System expansion (including substitution)

3. Allocation

In the production phase, a mix of the different solutions for multifunctionality have been used and are mentioned in chapter 3.1. Typically, the multifunctionality issues have been already been dealt with in the data sets that have been used in this study. In the use phase, there were no multifunctionality issues since it was solely based on the energy consumption which was modelled together with an electricity grid mix. In the end-of-life phase, it was decided to not include environmental credits from recycling and thus, no system expansion was conducted.

2.2.3 System boundary and cut-off criteria

Figure 2.1 depicts the system boundary of the product system between the techno- and ecosphere. The LCA has a cradle-to-grave approach which implies that a complete life cycle is studied, from raw material extraction to disposal or recycling (European Joint Research Centre, 2010). Transportation has been excluded in the flowchart and is instead described in chapter 3.2.

If there are parts within the system boundary that are considered not relevant, they can be omitted which is referred to as cut-offs (European Joint Research Centre,

2010). These can be, for example, processes or elementary flows that are less qualitatively relevant and thus, not worth the effort in relation to their contribution to the results. In the following bulleted lists, the included cut-offs are presented:

- Production and maintenance of capital goods and infrastructure (buildings, machines, vehicles, power distribution grid etc.) used within the life cycle stages.

- Personnel-related environmental impacts.

- Packaging material used to transport battery components or complete battery packs.

- Road and charging infrastructure required for the use phase.

2.2.4 Choice of impact categories

According to eLCAr and the PEFCR for batteries, which are both in line with the ILCD handbook, the following impact categories should be assessed:

- Climate change

- (Stratospheric) Ozone depletion

- Human toxicity

- Respiratory inorganics

- Ionizing radiation

- (Ground-level) Photochemical ozone formation

- Acidification (land and water)

- Eutrophication (land and water)

- Ecotoxicity

- Land use

- Resource depletion (water, metal, mineral, fossils and renewables)

From the bulleted list, the PEFCR points out the following impact categories to be the most relevant: climate change (fossil), resource depletion (energy, minerals, and metals) and respiratory inorganics (Siret et al., 2018).

Initially, results will be taken out for all impact categories, but depending on recommendations and the results, a selection will be made of those considered more relevant to answering the research questions.

2.2.5 Method of impact assessment

The life cycle impact assessment is conducted in the LCA software GaBi and the LCIA methods are chosen according to the Recommendations for Life Cycle Impact Assessment in the European context (European Commission-Joint Research Centre, 2011).

2.2.6 Data requirements

Time-related coverage

The study will analyze the electric vehicle and the battery as if they were produced and operated in a present or near future. Hence, the endeavour is that the data represent the current situation and are up-to-date.

Geographical coverage

For the production phase, the geographical scope is global. In case site-specific data is not available, average datasets are used as default. The use and end-of-life phase is assumed to take place in Europe and thus, data related to the use and recycling of batteries represent only the European average.

Technological coverage

The NMC333 and NMC622 are assumed to be produced with the same processes and technologies. One of the recurring problems in previously published LCA studies has been the restriction to production LCI data based on engineering calculations or pilot-scaled operations (Dai et al., 2017). It has been commonly assumed from the literature review that there is a lack of credible information on battery manufacturing. This study uses recent LCI data on battery manufacturing from Argonne National Laboratory which based on two visits to battery manufacturing facilities in China (Dai et al., 2017). In addition, the LCA study includes site-specific data on the production of battery-grade cobalt sulfate from Dai et al. (2018a) which is one of the materials that require a lot of processing and plays an essential role for lithium-ion batteries.
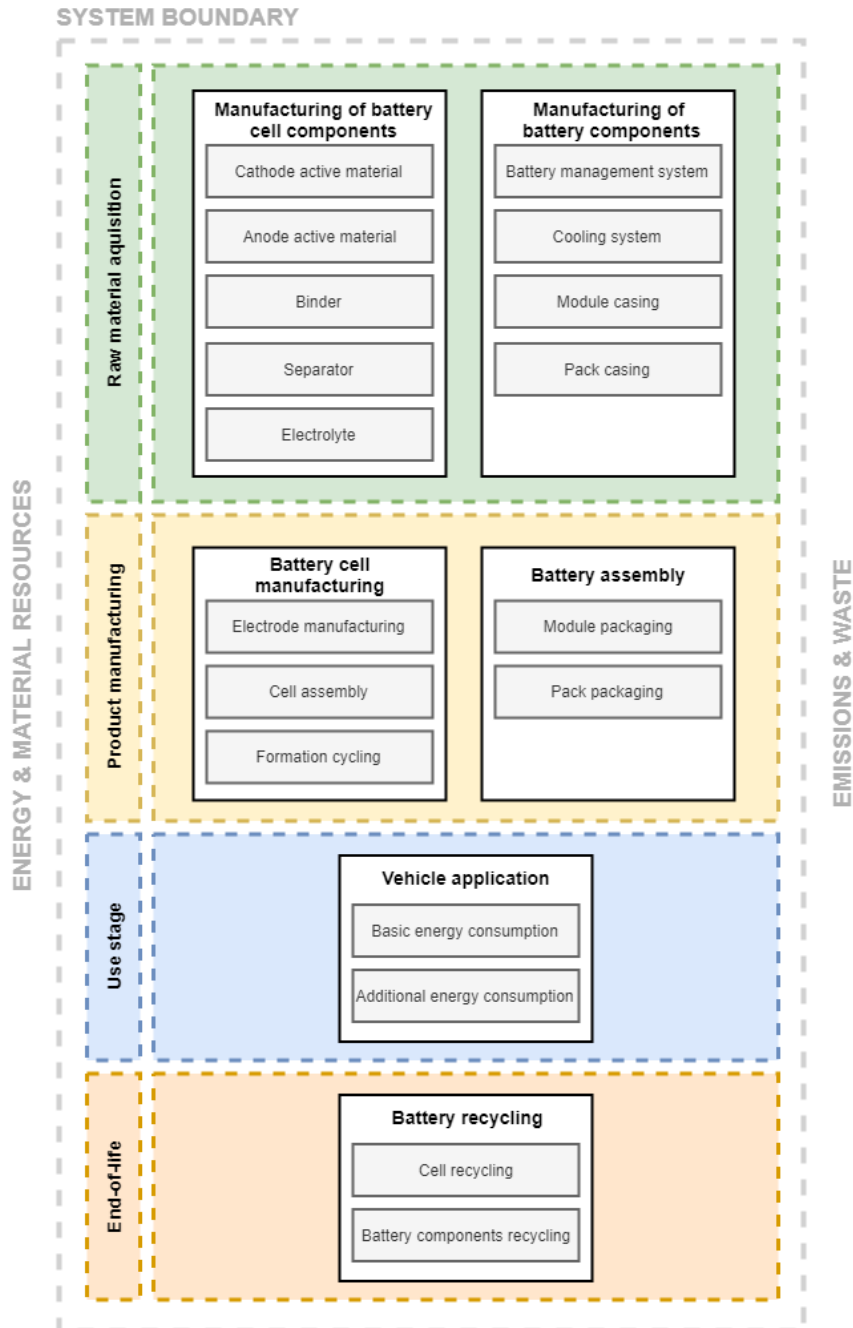
Figure 2.1: The flowchart depicts the system boundary of the product system including the main stages: extraction, production, usage and disposal or recycling. The boxes within each stage represents the main processes in the LCA.

3

LIFE CYCLE INVENTORY ANALYSIS

3.1 Production phase

In the following chapter, the production of a battery pack is explained and which data inventory that has been collected. An overview of the supply chain and processing steps is shown in figure 3.1.
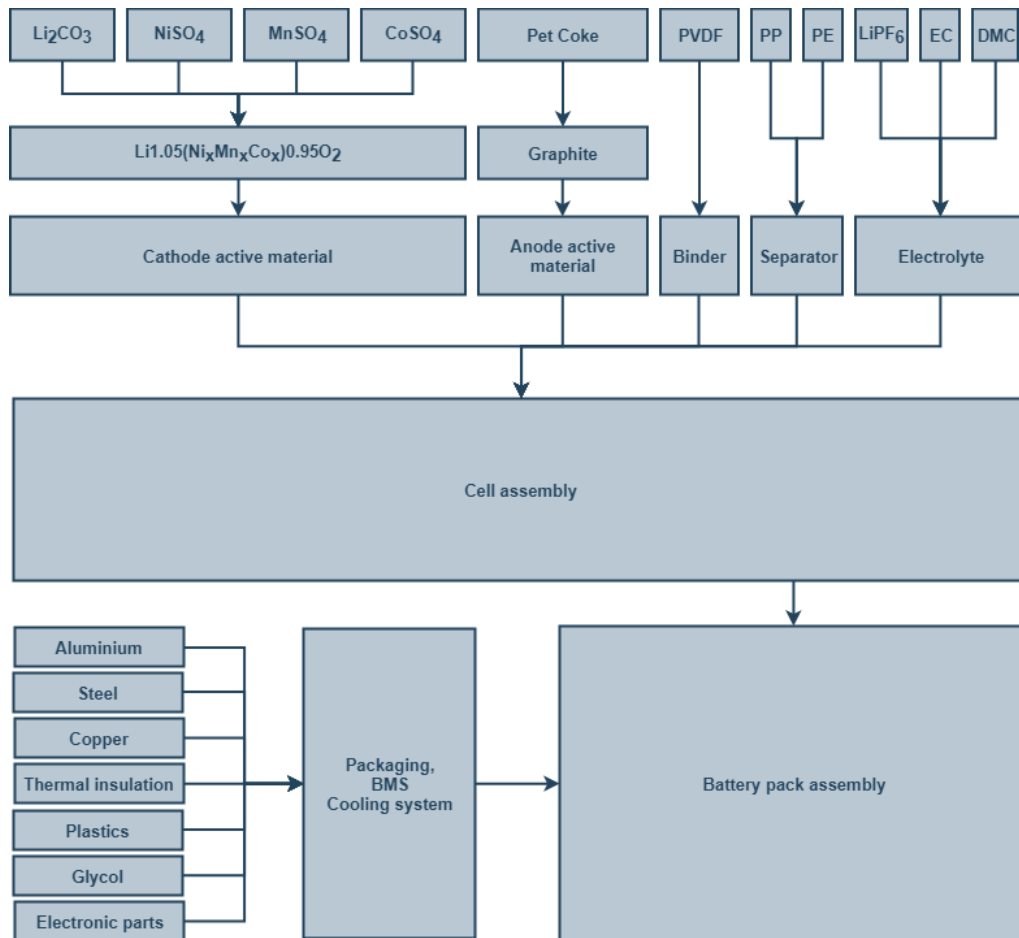
Figure 3.1: Flowchart showing a simplified supply chain in the production of a battery pack.

3.1.1   Battery cell, module and pack

The battery packs are designed in BatPac by selection of cell chemistry and additional configuration on performance and battery components (Nelson et al., 2018). The BatPac model includes several of different cell chemistries, where NMC333 and NMC622 where two among them. Additional configuration is limited by a number of parameters available in the model and for the two batteries that are compared, the default values are used. When the design is determined, bill-of-materials (BOMs) are provided of the cells, modules and pack. The BOMs are typically referred to as ingredient lists and contains information on materials required to produce a product. In the BatPac model, the weights on the different components are listed. The recent update of the BatPac model was made 2018 and the results of BOMs from modelling NMC333 and NMC622 is presented in table 3.1.

Table 3.1: Material inventory of NMC333 and NMC622 battery packs.

Input	NMC333	NMC622
Positive electrode		
Active cathode matetrial (Li-NMC)	27%	24%
Conductive additive (Carbon black)	1.8%	1.6%
Binder (PVDF)	1.5%	1.3%
Current collector (Aluminium)	3.6%	3.8%
Negative electrode		
Active anode material (Synthetic graphite)	15%	15%
Binder (PVDF)	0.77%	0.80%
Current collector (Copper)	8.3%	8.7%
Separator		
Outer layer (PP)	0.96%	1.0%
Inner layer (PE)	0.24%	0.25%
Electrolyte		
LiPF6	1.7%	1.6%
Ethylene carbonate	4.7%	4.6%
Dimethyl carbonate	4.7%	4.6%
Cell container		
Multilayer film (Aluminium)	1.2%	1.2%
Multilayer film (PET)	0.18%	0.18%
Multilayer film (PP)	0.08%	0.08%
Positive terminal (Aluminium)	0.55%	0.56%
Negative terminals (Copper)	1.8%	1.9%
Module packaging		
Module state-of-charge regulator assembly (Electronic part)	0.34%	0.37%
Module thermal conductor (Aluminium)	2.2%	2.2%
Module terminals (Copper)	0.21%	0.21%
Thermal Inslutation (Fiberglass)	0.05%	0.05%
Module closure (Aluminium)	1.5%	1.6%
Module spacer (PE)	0.05%	0.06%
BMS		
Battery Management System	0.71%	0.77%
Cooling system		
Cooling System Exterior	1.2%	1.3%
Coolant (Glycol)	2.2%	2.3%
Pack packaging		
Battery jacket (Aluminium)	8.8%	9.0%
Thermal Insulation (Fiberglass)	0.27%	0.27%
Mass of battery pack heaters (Electronic part)	0.07%	0.08%
Mass of both battery pack terminals (Copper)	0.02%	0.02%
Mass of each module inter-connect (Electronic part)	0.32%	0.34%
Mass of module compression plates and steel straps (Steel)	0.67%	0.67%

3.1.2 Preparation of the cathode active material

The production of the active electrode material NMC (nickel-manganese-cobalt), that is used in the cathode, can be divided into three stages: production of metal sulfates, production of lithium carbonate and synthesis of NMC, see figure 3.1 (Dunn et al., 2015).

Production of metal sulfates

The metal sulfates that are used in the NMC synthesize are nickel sulfate $NiSO_4$, manganese sulfate $MnSO_4$ and cobalt sulfate $CoSO_4$ (Dunn et al., 2015). In the following text, the production of the metal sulfates will be detailed, starting with nickel sulfate followed by manganese and cobalt sulfate.

The production of battery-grade nickel sulfate is depicted in figure 3.2 and is primarily based on an LCA study sponsored by the Nickel Institute (Gediga et al., 2015). The LCI data are based on a economic allocation and system expansion of the extraction and processing of nickel. Economic allocation was used to treat the metal co-products based on the average market value from the year 1996 to 2011. The system expansion is used to treat the non-metal co-product, sulfuric acid. The geographical scope of the LCA study is global and represents following regions: North America, South America, Europe and Russia. The final processing from refined nickel to nickel sulphate is based on the study by (Dunn et al., 2015).
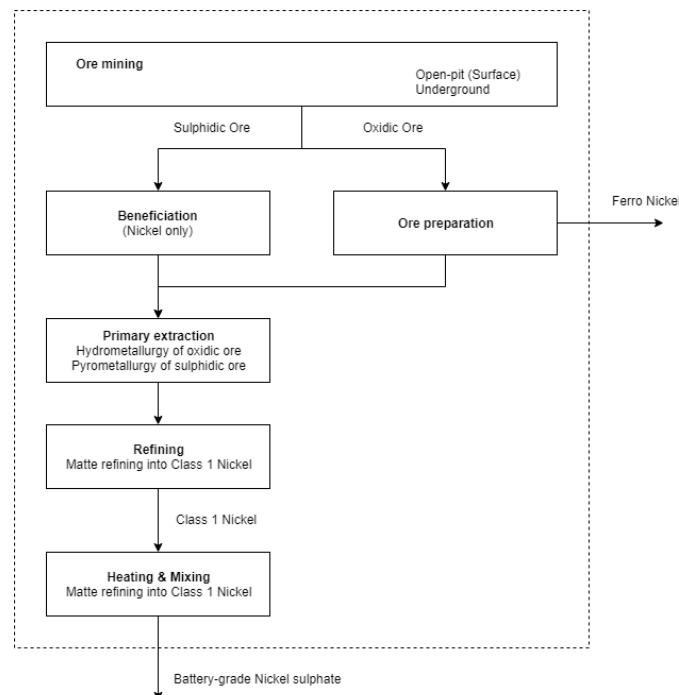
Figure 3.2: Process flow diagram for production of battery-grade nickel sulfate, adopted from Gediga et al. (2015).

Nickel can be extracted from two different ores, sulfidic and oxidic ores (also referred to as laterite ore) which are mined in open-pit and underground mines Gediga et

al. (2015). The oxidic ores have slightly higher nickel content than sulfidic ores. However, the latter is extracted more which could be due to the fact that it is extracted in both open-pit and underground mines whereas oxidic are only extracted from underground mines. After the ore mining, the sulfidic ores undergo a beneficiation process where the ores are crushed, ground and separated through magnetic or flotation separation. For oxidic ores, the processing is different since it consists of higher moisture content and thus need to be dried after it has been crushed and screened. In the primary extraction step, the nickel concentrates and prepared ores are converted into the following products: nickel oxide, nickel matte, ferronickel, nickel cobalt intermediates, and other nickel and non-nickel co-products. The ores can either undergo a hydrometallurgical or a pyrometallurgical extraction, however, in the LCA-study, hydrometallurgical extraction from sulfidic ore is not included. In the refining process, nickel matte and nickel cobalt intermediates are converted to class 1 nickel products. Refined nickel is divided into two classes, where class I has a higher purity level (>99%) than class II and thus, more preferable in batteries. The refining of nickel can include the following processes: crushing, grinding, leaching, purification, electrolysis, electrowinning, cutting and reduction processes. In the final step, the class 1 nickel products undergoes a process where it is mixed with sulphuric acid in high temperature (Dunn et al., 2015).

As for the production of battery-grade manganese sulfate, the processing has been simplified due to lack for data. It is assumed that manganese oxide is extracted from manganese ores with 55% manganese content (Dunn et al., 2015). Without further processing, the manganese oxide undergoes a simple mixing process with sulfuric acid, which do not require any heat.

The production of cobalt sulfate consists mainly of three processes: ore mining, hydrometallurgical ore processing and refining (Dai et al., 2018a). In figure 3.3, the LCI data is presented in a flowchart. The material and energy flows associated with producing battery-grade cobalt sulfate is based on economic allocation, where the average ore grade is 2.44% copper and 0.47% cobalt. In addition, the LCI data have been calculated by multiplying the cobalt content of cobalt sulfate since $CoCL_2$ is also produced in the same production pathway. There is also a cobalt yield of 80% from cobalt ore processing that has been accounted in the LCA study. Cobalt sulfate is produced by two raw materials; concentrated cobalt ore and crude $Co(OH)_2$, where only the latter is considered. Data on ore mining and hydrometallurgical ore processing is collected from three major mines in DRC (Democratic Republic of the Congo): the Komato mine, the Mutanda mine and the Tenke Funfurume Mine (TFM) The cobalt-rich ore either extracted from open-pit or underground mining, where 17 % of the total ore mining in DRC is through handpicking (also referred to as artisanal mining). Other mining equipment is fueled by either diesel or electricity.

The processing of copper-cobalt ore takes place in a hydrometallurgical plant, where they first go through a milling process (Dai et al., 2018a). Once the particle size of the ore has been reduced to a suitable size for subsequent mineral extraction and leaching processes, the ores are converted to enriched concentrate through flotation processing. The resulting concentrates are either sulfidic or oxidic, where sulfide concentrates require additional processing before the leaching process. To convert
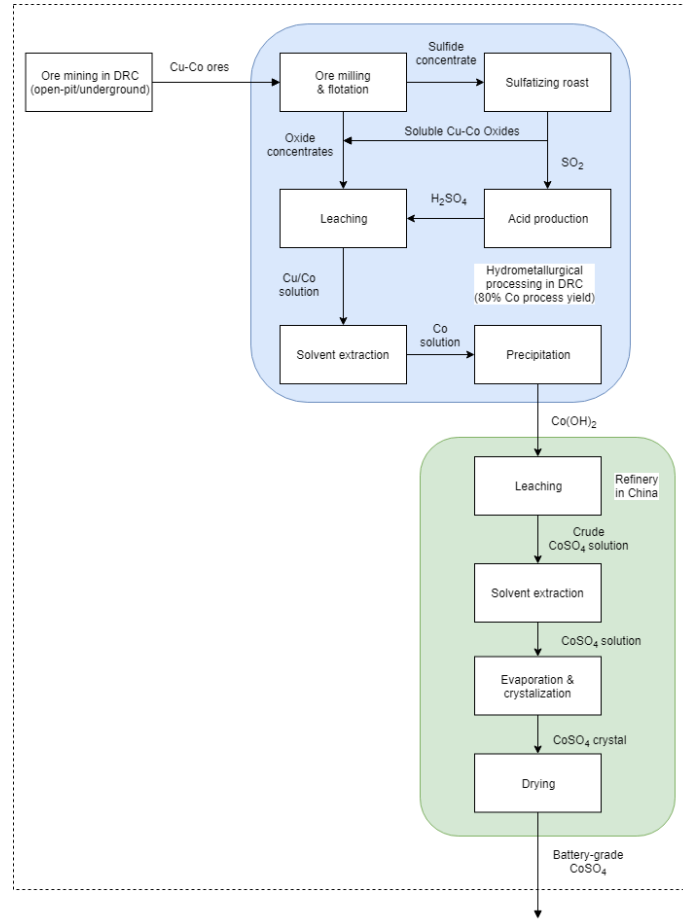
Figure 3.3: Process flow diagram for production of battery-grade cobalt sulfate, adopted from Dai et al. (2018a)

the sulfide concentrates to soluble Cu-Co oxides they undergoes a sulfatizing roast process. Through leaching and solvent extraction, the oxide concentrates are turned into copper and cobalt solution. Lastly in the hydrometallurgical processing, the cobalt-rich solution undergoes several precipitation steps to recover copper that are still left in the solution and to remove aluminum, iron and manganese impurities. In the last precipitation step, the cobalt solution is mixed with magnesium oxide which results in a precipitation of $Co(OH)_2$. The process yield for Co is assumed to be 80% and is also considered in the LCI calculation. It is assumed that there are no other material losses throughout the production of battery-grade cobalt sulfate.

From the hydrometallurgical processing, the crude $Co(OH)_2$ is assumed to have a cobalt content of 35 % and for further refining, it is sent to China (Dai et al., 2018a). For the refining process, the LCI data has been collected from Huayou Cobalt which is one of the top three cobalt refineries in China. To produce battery-grade cobalt sulfate $CoSO_4$, four processes are conducted, leaching, solvent extraction, evaporation and crystallization, and drying. In the leaching process, the purchased crude $Co(OH)_2$ is converted to cobalt sulfate by mixing it with sulfuric acid. Thereafter, the cobalt sulfate is refined by several precipitation steps, followed by a solvent extraction. Finally, battery-grade $CoSO_4$ crystals are produced by evaporation,

crystallization and drying.

Production of lithium carbonate

The lithium carbonate (Li_2CO_3) is assumed to be produced in Chile and in figure 3.4, the LCI data together with the process flow diagram is presented (Dunn et al., 2014). The energy and mass flow associated with lithium carbonate is based on mass allocation. The production of lithium carbonate begins with extraction of lithium brine from wells. From wells, the brine undergoes a series of evaporations in ponds, where the lithium concentration increases from 1,500 ppm to 60,000 ppm. Thereafter, the concentrated lithium brine is transported to a processing plant in Chile that produces lithium carbonate. The extraction of lithium carbonate from the concentrated Li-brine begins with removal of boron by mixing it with HCl, sulfuric acid, alcohol, and an organic solvent. Then the resulting solution undergoes two additional extraction steps, wherein the first step, soda ash is added in the solution to precipitate magnesium carbonate $MgCO_3$. In the second, magnesium hydroxide $Mg[OH]_2$ and calcium carbonate $CaCO_3$ are removed by adding lime to the solution. When the Li-brine has undergone the three previously mentioned extraction processes, it is sent to a precipitation reactor where the solution is mixed with soda ash. During the process, the lithium carbonate is precipitated from the solution, which is subsequently washed, filtered, dried and packaged.
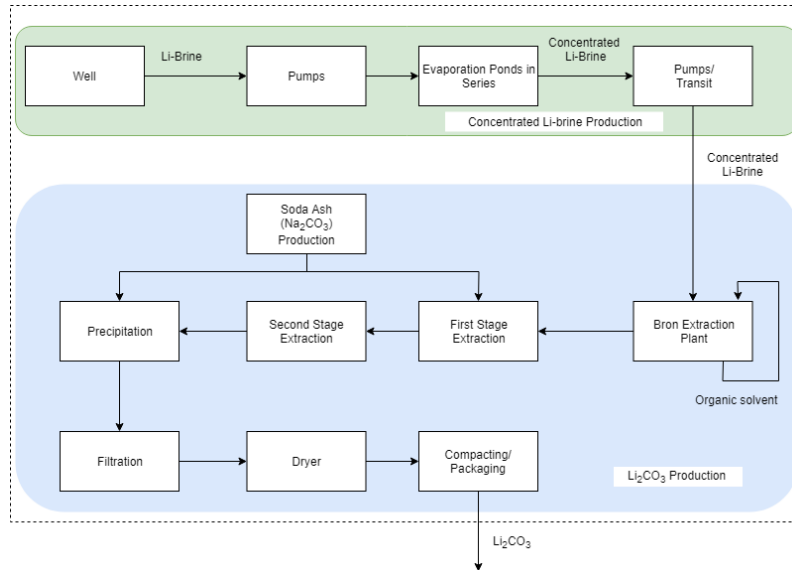
Figure 3.4: Process flow diagram for production of lithium carbonate, adopted from Dunn et al. (2014).

Synthesis of NMC

The synthesize of NMC consist primarily of two processes: 1) the production of the NMC-precursor by mixing the metal sulfates; 2) the production of NMC by mixing the dried precursor with lithium carbonate, followed by calcination (Dai et al., 2017). In figure 3.5, the LCI data is presented in a process flow diagram, where material

and energy flows are based on mass allocation. The data have been collected from a leading cathode materials producer in China (Dai et al., 2018b). It should be noted that the two processes mentioned above are conducted at two different plants in China.

The production of the NMC-precursor begins with dissolving and mixing the metal sulfates in a continuously stirred tank reactor (CSTR). Once the metal sulfates have been completely dissolved and mixed into a solution, sodium and ammonium hydroxide is added. Thereafter, the metals sulfates co-precipitate to $Ni_xCo_xMn_x(OH)_2$ by heating the tank at a temperature of 50 °C. The tank is heated by steam produced by natural gas with a boiler efficiency of 80% Out of the tank, the solid NMC-precursor undergoes filtration, washing and drying.

In the next production plant, the NMC cathode powder is produced through calcination (also known as the solid state synthesization). The number of calcination steps depends on the cathode material, where NMC requires two. The processes in the production plant is completely automated and powered solely by electricity, where the calcination steps are responsible for almost the entire consumption. This is due to the fact that the products are calcinated up to 12 hours at a temperature of 1000°C. In addition, the calcining furnaces are not shut down when idling because it takes too long to reach the required operating temperature. The production plant has been designed to maximize the material efficiency, which is close to 100%. The material loss is recovered by; transporting intermediate materials through tubes; and by collecting and reusing dust generated from the crushing and sieving process.
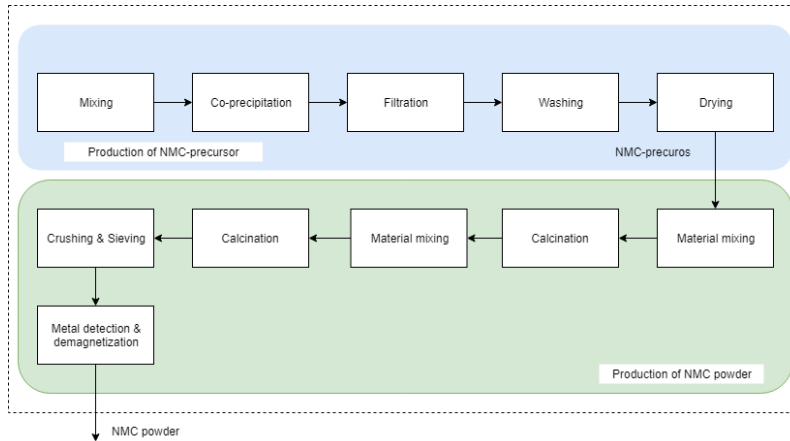
Figure 3.5: Process flow diagram for synthesis of NMC, adopted from Dai et al. (2018b)

3.1.3   Preparation of the anode active material

The graphite used as the active material in the anode and can be divided into natural graphite (NG) and synthetic graphite (SG) (Ellingsen et al., 2014). In this study, only synthetic graphite is considered which is made of petroleum coke and coal tar pitch. The petroleum coke is residues from thermal processing of crude oil, that has been produced by delayed cooking (Dunn et al., 2015). The coal tar pitch is

derived from coal and commonly produced as a by-product from the coke oven for steel production. The petroleum coke is the main raw material, while the coal tar pitch is used as a binder.

The production of synthetic graphite, depicted in figure 3.6, begins with grinding and sizing the petroleum coke to a desirable particle size (Dunn et al., 2015). It is then mixed with coal tar pitch in a mixer that is heated to a temperature of 160-170 °C to keep the coal tar pitch in a liquid state. Once the coal tar pitch has partially penetrated the pores of the coke, the mixture is cooled down and undergoes an extrusion process. After the extrusion, the product starts to resemble the final product and the density has been maximized. To successfully convert the coal tar pitch into coke, the product is fed into a furnace heated by natural gas. The baking process (also known as carbonization) typically takes 18-24 hours at a temperature range of 800-1000 °C and the product loses around 30-40% of its weight. Before the product is sent to the graphitization furnace, it is impregnated with pitch and baked a second time to improve its properties. In the last process, graphite crystals are formed by slowly heating the product to a temperature of approximately 3000 °C. The graphitization process is powered by electricity and last up to three weeks when cooling time is included.
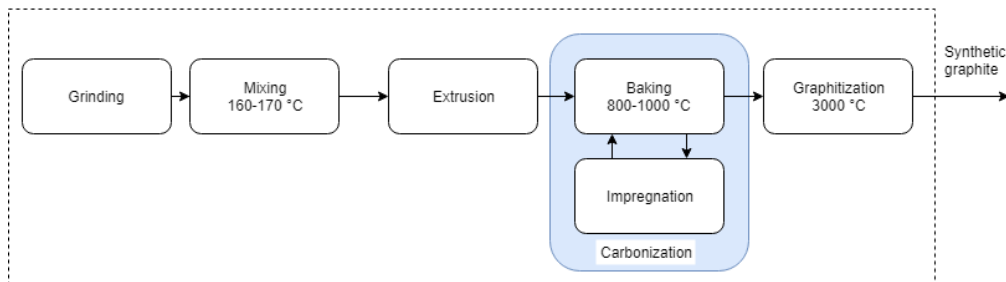
Figure 3.6: Process flow diagram for synthetic graphite, adopted from Dunn et al. (2015)

3.1.4 Production of binder

To hold the active electrode materials together in batteries, a polymeric binder material is used and the most common material is polyvinylidene fluoride (PVDF) (Dunn et al., 2014). To produce the binder, the PVDF undergoes an injection moulding process (Ellingsen et al., 2014).

3.1.5 Production of separator

The separator is a porous membrane that keeps the active electrode materials apart to prevent short circuit (Dunn et al., 2014). The outer layers consist of polypropylene (PP) and the inner layer consist of polyethylene (PE). The relative share is 80% PP and 20% PE. The battery cell component is assumed to be processed by injection moulding (Ellingsen et al., 2014).

3.1.6 Production of electrolyte

The most common electrolyte consist of lithium hexafluorophosphate ($LiPF_6$) which is a salt produced by a chemical synthesis of lithium fluoride (LiF) and phosphorus pentachloride (PCI_5) (Dunn et al., 2014). To increase the permittivity of the electrolyte, the $LiPF_6$ is mixed with dimethyl carbonate (DMC) and ethylene carbonate (EC) solvent. The DMC can be produced from EC which in turn is produced from ethylene oxide followed by ethylene. According to Ellingsen et al. (2014), relative shares of the electrolyte are 12% $LiPF_6$ and 88% EC and DMC, where the volume ratio of the solvents is 6:4 (Deng et al., 2017b). In figure 3.7, the LCI data is presented in a process flow diagram. Due to lack of data, the production of lithium fluoride LiF and PCI_5 is not considered.
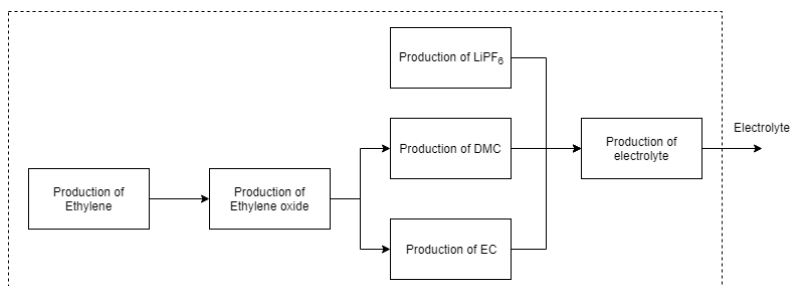
Figure 3.7: Process flow diagram for synthesis of electrolyte, adopted from Dunn et al. (2014)

3.1.7 Production of multilayer pouch, terminals and current collectors

The BatPac model uses prismatic cells which are sealed in a multilayer pouch (Nelson et al., 2018). The cell container consists of three layers, where the outer layer is polyethylene terephthalate (PET), the middle layer aluminum and the inner layer polypropylene (PP) (Deng et al., 2017b). The cell container surrounds all other components in the cell and leads the current via attached terminals which are linked to current collectors on the cathode and anode. Aluminum is used to conduct current through the cathode while copper is used for the anode. The LCI data is collected from an LCA study by Ellingsen et al. (2014).

3.1.8 Cell manufacturing

The cell manufacturing has been considered as a complex and energy demanding procedure, not least due to the number of processing steps but also because some of them need to take place in a dry room where the temperature and level on the moisture content in the air is controlled (Dai et al., 2017). The dry room is required to prevent a harmful reaction between the electrolyte salt and water, which occurs when the moisture level of the air exceeds 100 parts per million by volume (ppmv). The main manufacturing processes for NMC-graphite cells, based on previous LCA studies on lithium-ion batteries by Dai et al. (2017) & Deng et al. (2017b), is shown

in figure 3.8. The LCI data have been collected from the LCA study by Dai et al. (2017), which is based on visits to two lithium-ion battery manufacturing facilities in China.
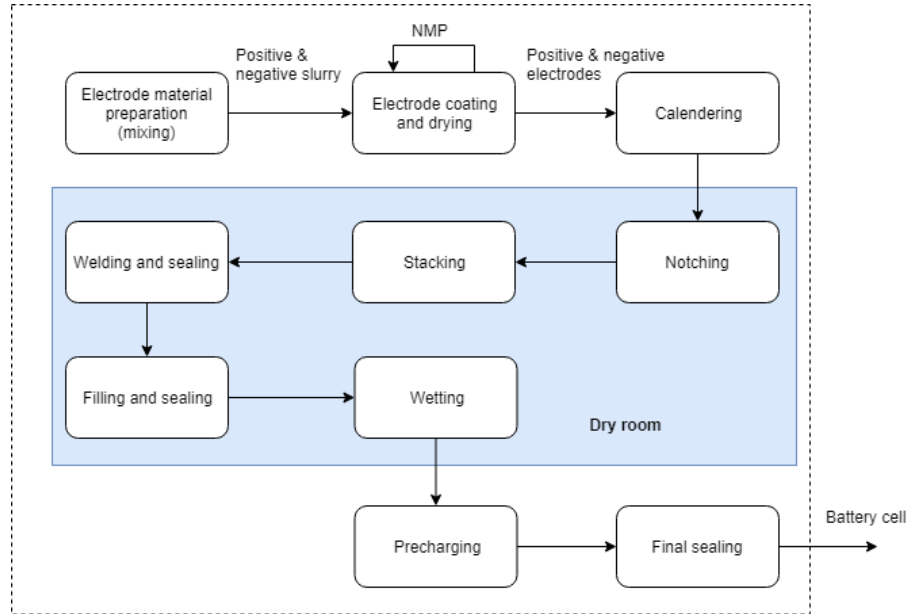
Figure 3.8: Process flow diagram for cell assembly, adopted from Dai et al. 2017 and Deng et al. 2017b.

The first step is to produce positive and negative electrode slurry which done by mixing the electrode active materials with solvents, binders and conductive additives. (Deng et al., 2017b). For positive electrode materials N-Methyl-2-Pyrrolidone (NMP) is used as a solvent, while for negative electrode material water is typically used (Dai et al., 2017). For binders and conductive additives, PVDF respective carbon black is used (Deng et al., 2017b). The slurry subsequently undergoes a coating process where it is coated onto electrodes. The negative electrode paste (formerly referred to a slurry) is coated on the anode, while positive electrode paste is coated on the cathode. Before the electrodes are fed into an oven for drying, it goes through an intermediate step where almost all NMP solvent (99.5%) is recovered by evaporation. When the coated electrodes have dried, it is pressed through heated rollers in a so-called calendaring process to achieve a uniform thickness and density.

After the electrodes have been coated and pressed they enter the dry room where they are cut into a final shape (Deng et al., 2017b). The electrodes are then stacked on each other together with separators, forming the "guts" of a battery cell. Thereafter, the positive and negative current collectors, made of aluminum and copper, respectively, are welded on the cell and sealed within a pouch. Before the cell leaves the dry room, it is filled and saturated with electrolyte.

When the cell has left the dry room, it is charged for the first time by slowly applying electricity, also known as *formation cycling*. This is done to form the solid electrolyte interface layer to prevent drastic and irreversible capacity losses before the batteries are put on the market (An et al., 2017).

During the formation cycling, the first charging cycles on unstable voltage ranges are performed on the battery cells which cause the electrolyte to decompose and precipitate. In low voltages a solid electrolyte interphase (SEI) layer is built up on the anode through reduction reactions, while in high voltages a cathode electrolyte interphase (CEI) layer is built up on the cathode through oxidation reactions. The formation of electrolyte interphase layer is highest on the first cycle and drastically reduces in the next charging cycles. In cases where the anode is made of graphite, the irreversible capacity losses from the first charging cycle are approximately 10% while during the third charging cycle the capacity losses are less then 0.05%. The resulting capacity fade from the formation of electrolyte interphase layer is due to the insulation of the active electrode materials which are followed by irreversible consumption of electrolyte and lithium ions.

The formation cycling processes can take up to several days or weeks in order to create a stable electrolyte interphase layer, which is when the whole surface of anode and cathode are evenly covered. Finally, after the formation cycling is complete, the cell is degassed and sealed for the last time (Deng et al., 2017b).

The overall energy consumption for cell manufacturing has been estimated by Dai et al. (2017) to be 170 MJ per kWh battery pack produced, where the relative share of the energy input is 82.4% natural gas and 17.6% electricity. Electrode drying (including NMP recovery) and dry room operation have been confirmed as the biggest contributors to energy consumption (Dai et al., 2017). The dry room operation stands for the entire electricity consumption and half of the total heat energy consumption, whereas electrode drying stands for the rest. The reason for the high energy intensity from electrode drying is due to the use of NMP as solvent. In a gas form, NMP is highly flammable and thus, it must be carefully controlled during the evaporation process. It should be noted that economies of scale have been shown to affect the process energy intensity from previous studies, but this has not been taken into account.

3.1.9 Module and pack level packaging

The packaging consist mainly of three components; module packaging, battery retention and battery tray (Ellingsen et al., 2014). The material inventories for these components are derived based on the BatPac results and the documentation of each components by Ellingsen et al. (2014). The battery packs that are designed in the BatPac have 12 battery cells in each module and the battery pack consist of 20 modules in total (Nelson et al., 2018). The modules are kept in place by a battery retention and are within the battery tray which is the outer shell of the battery pack (Ellingsen et al., 2014). More details on the material choice and processing can be found in appendix C

3.1.10 Battery management and cooling system

To ensure batteries longevity and safety, a collection of electronic components are installed within the battery pack, referred as the battery management system (BMS) (Dunn et al., 2014). The BMS consists of measurements devices and can control, for

example, the voltage, current, and temperature. The battery pack is also equipped with a cooling system for thermal management and insulation. The BMS and cooling system consist of several sub-components which are documented transparently by Ellingsen et al. (2014) and used in this study together with the results from BatPac.

3.2 Transportation

The transportation for the majority of the raw materials are included in the background datasets available in the GaBi software and the transport for the foreground system is based on transportation data from the PEFCR (Siret et al., 2018). Exceptions are made on the production of cobalt sulfate since site-specific data were available. The battery cells are assumed to be manufactured in Asia as they according to Siret et al. (2018) currently dominate the market. The rest of the components for the battery pack are assumed to be produced in Europe. In table 3.2, a summary of the transportation data for the foreground system are presented.

Table 3.2: Transportation modes and distances

Materials/Components	Truck (km)	Rail (km)	Ship (km)
Crude cobalt hydroxid (Congo to China)	2700		13000
Active material (China to Korea)	300	200	10000
Passive material (Japan)	300	200	18000
Battery Cell (Asia to Europe)	300	200	18000
From component supplier to OEM factory (Europe)	130	240	270
From OEM factory to user (Europe)	200	-	-
Transport to the EoL recycling (Europe)	200	-	-

3.3 Use phase

The use phase contains all activities that are involved in the operation of the electric vehicle (Del Duce et al., 2013). In this study, only the vehicle energy consumption is considered, implying that the following main elements in the use phase are left out; road and vehicle infrastructure, maintenance, and non-exhaust emissions. The energy consumption from a typical mid-size electric vehicle, using either NMC333 or NMC622 battery pack, is calculated using consumption calculation methods described in eLCAr (Del Duce et al., 2013). The overall energy consumption can be divided into five parts:

- Basic consumption through driving from point A to B without considering the use of additional devices which is not directly needed for the action of driving.

- Additional consumption by the use of heating and air conditioning of the passenger compartment

- Additional consumption by the use of auxiliaries such as, light, radio and navigation

- Additional consumption from internal battery losses in standstill

- Additional consumption from battery charging losses.

3.3.1 Basic consumption

The energy needed for driving an electric vehicle from point A to B is mainly determined by; the mechanical power required to put the vehicle in motion; the energy losses from drivetrain efficiencies and the recovery of energy from decelerating (Del Duce et al., 2013).

To calculate the mechanical energy needed to sustain the motion of a specific vehicle it is first necessary to know which trajectory and what driving profile the car is driven (Del Duce et al., 2013). This would, however, imply an infinite amount of information of different driving situations. Instead, driving cycles are used, which represents everyday vehicle operations and consist of measured data on vehicle speed versus time under standardized conditions. There are two different type of driving cycles, steady-state and transient driving cycles (Hofer, 2014). The significant different between them is that transient driving cycles are based on more dynamic driving patterns and thus, considered to be more realistic. The New European Driving Cycle (NEDC) is a test procedure which uses steady-state driving cycles and was commonly used in relation to consumption measurements. However, the test procedure has recently been criticized on the grounds that it fails to represent the real-world driving conditions and underestimates the fuel consumption. To tackle the challenge, countries around the world have collaborated with United Nations Working Party on Pollution and Energy (UNECE) to develop a new test procedure with transient cycles, called the Worldwide Harmonized Light Duty Test Procedure (WLTP). This test procedure is the one used in this study and consists of four different speed phases; low, middle, high and extra high (Tutuianu et al., 2013). In addition, the test procedure is divided into three classes with different driving cycles based on vehicle classifications. The vehicle used in this study is classified as a class 3b since it has a power-to-mass ratio over 34 W/kg and a maximum speed over 120 km/h. In figure 3.9, the driving cycle used to calculate the energy consumption is presented.

When the driving cycle is determined, the wheel power demand can be calculated on every vehicle operating point shown in figure 3.9. The wheel power is calculated in equation 3.1, where the laws of mechanics are applied on the vehicle (Del Duce et al., 2013). The formula is derived by the assumption of driving on a float road and uses following vehicle parameters: mass (m), cross-sectional area (A), drag coefficient (cw) and rolling resistance coefficient (cr).

$$P(t)_{wheel} = m \times a \times v + \frac{cw \times \rho_{air} \times A \times v^3}{2} + cr \times m \times g \times v \qquad (3.1)$$

The mass of the vehicle is assumed to be solely dependent on the drivetrain which is typically composed of; a battery that provides the electrical power; a collection of power electronics which processes the electrical power; a electric motor that converts
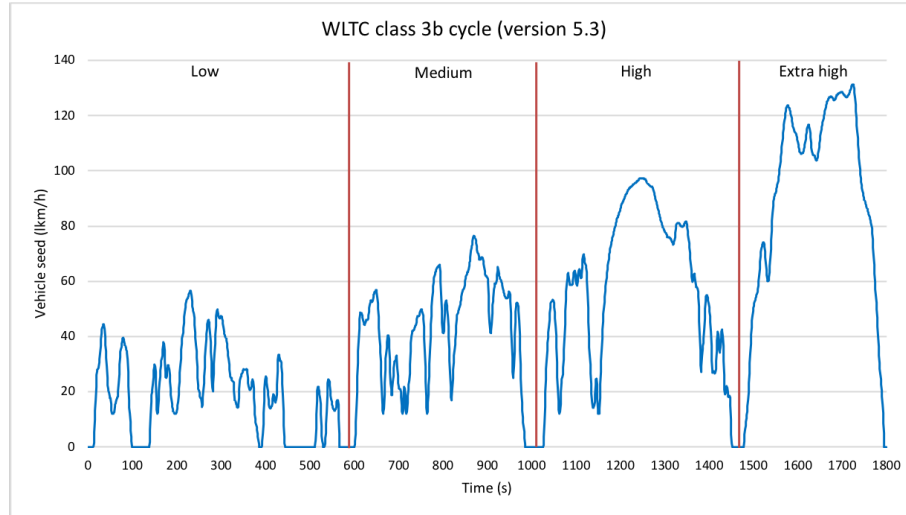
Figure 3.9: Illustration on the Worldwide Harmonized Light Duty Test Cycle (WLTC), constructed with data collected from Tutuianu et al. (2013).

the electrical power into mechanical power; and a transmission which is act as a link between the electric motor and the wheels (Del Duce et al., 2013). The total vehicle mass is calculated according to equation 3.2.

$$m_{BEV} = m_{battery} + m_{electric\ motor} + m_{transmission} + m_{glider} \qquad (3.2)$$

The mass of the electric motor is calculated to 132 kg by multiplying a mass-power coefficient of 0.9 $kg\ electric\ motor\ kW^{-1}$ with a battery power of 147 kW. Similarly, the mass of a transmission is derived to be 59 kg considering a 0.4 $kg\ kW^{-1}$ mass coefficient for transmission. The NMC333 and NMC622 lithium-ion batteries have equal battery power and thus the mass for the transmission and electric motor are also equal. In case of the battery mass, no further calculations are needed since the mass is already determined in the BatPac model.

The glider can be seen as the backbone of the vehicle keeping the other components together (Bauer et al., 2015). Since the NMC333 and NMC622 lithium-ion batteries weights differently, the mass of the glider is also different. It is assumed that the mass of the glider changes by 0.57 kg per kg change of the other components. To measure the difference in weight between the vehicle with NMC333 and NMC622 batteries, a baseline is used. The baseline is simulated by Bauer et al. (2015) and represents an average mid-sized BEV from the year 2012. The calculation results on the weight of the vehicles are shown in table 3.3.

The values of the cross-sectional area, the drag coefficient, and the rolling resistance coefficient shown in table 3.4 are derived from an LCA on passenger vehicles by Bauer et al. (2015).

By knowing the mechanical power required to put the vehicle in motion, the amount of electrical power that needs to be taken from the battery can be calculated (Del Duce et al., 2013). This is done by backtracking the energy losses that occurs along the electric drivetrain shown in figure 3.10

Table 3.3: The calculated mass on the electric vehicles with NMC333 and NMC622 battery packs. The electric vehicle used as a baseline is simulated by (Bauer et al., 2015)

	Glider	Transmision	Battery	Electric motor	Total weight
BEV-baseline [kg]	1295	86	448	147	1976
BEV-NMC333 [kg]	1319	59	520	132	2031
BEV-NMC622 [kg]	1281	59	472	132	1944

Table 3.4: Vehicle characteristics used in equation 3.1 to calculate the wheel power demand

Cross-sectional area	2.2
Drag coefficient	0.28
Rolling resistance coefficient	0.01

Each component in the drivetrain has its own dynamic behavior which implies that its efficiency can vary under different circumstances (Del Duce et al., 2013). In this study, the dynamic behaviors are not considered and is according Del Duce et al. (2013), only necessary to include if optimization of the drivetrain is desired. Instead, a simplified method is used which has its focus on energy consumption.

The method is called the *Willans approximation* and uses a mean drivetrain efficiency that is developed based on a linear relationship between mean positive wheel power and battery power demand (Del Duce et al., 2013). In equation 3.3, the battery power demand is calculated by parameter A and B. The first corresponds to the power needed to run all components, such as power electronics, that is necessary for the vehicle to operate while it is standstill. The latter parameter is used in conjunction with parameter A to describe the relationship between the overall drivetrain efficiency and the battery power demand. From measurements by Bütler & Winkler (2013) at Empa, parameter A and B has a value of 1.118 and 0.436, respectively. The mean positive wheel power is computed from the equation 3.1 described above by setting all negative values to zero. It should be noted, this implies that the recuperation power is not considered in following equation.

$$P_{el.bat.out} = A \times P_{wheel.m.pos} + B \tag{3.3}$$

The electricity consumption in Wh/km is calculated in equation 3.4, where battery power demand is divided by the mean cycle speed (Del Duce et al., 2013).

$$C_{el.bat.out} = \frac{P_{el.bat.out} \times 1000}{v_{cycle.m}} \tag{3.4}$$

A significant feature of electric vehicles to consider when calculating the electricity consumption is the ability of recuperation of kinetic energy (Del Duce et al., 2013). By the motion of the vehicle, the electric motor can act as a generator during the
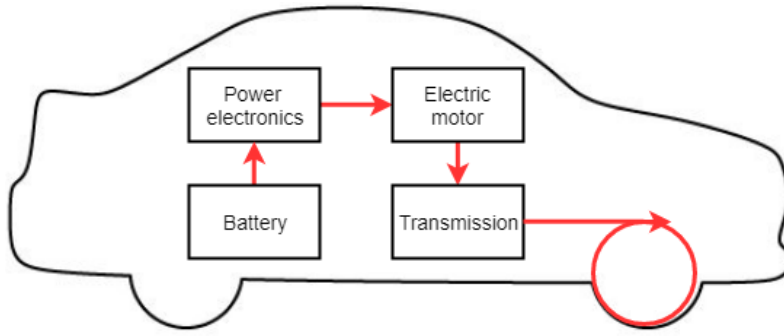
Figure 3.10: Illustration on an electric drivetrain, adopted from Del Duce et al. (2013)

time when no energy is withdrawn from the battery. When the electric motor spins by the motion of the vehicle, energy is fed back to the battery and a braking effect occur. The recuperative behavior is considered to be complex since it is affected by different systems and highly dependent on the operating point.

To calculate the maximum recuperated energy that is possible for the vehicle on given driving cycle, the theoretical maximum recuperation is compared to a speed-dependent limit set by the vehicle's control software. The theoretical maximum recoverable energy is calculated in equation 3.5 for every operating point of the driving cycle. Since the energy flow is reversed to the battery the calculated value is negative.

$$P(t)_{el.recu.max} = \frac{1}{1.118} \times P(t)_{wheel} + 0.436 \qquad (3.5)$$

The value to be compared, is the maximum recuperation power that is limited by the vehicle. It is calculated in equation 3.6 where data on the cycle speed for every operating point is used (Del Duce et al., 2013).

$$P(t)_{el.recu.limit} = -0.36 \times v(t)_{cycle} + 1.8 \qquad (3.6)$$

In figure 3.11, values from $P(t)_{el.recu.max}$ and $P(t)_{el.recu.limit}$ are compared to each other to examine which of the values that are practically possible for the specific vehicle and the given driving cycle. For each operating point where the maximum values exceed the limit, they are reduced to the limit value.

To determine the kinetic energy that is recovered per km driving, a mean value is calculated on the values of recuperated power that is within the limit. It should be noted that before the mean value was calculated, values on $P(t)_{el.recu.max}$ based positive wheel power was set to zero since kinetic energy can only be recovered by deceleration (Del Duce et al., 2013). By equation 3.7, the reversed electricity consumption (wheel-to-battery) in Wh/km was calculated by dividing it with the mean cycle speed.
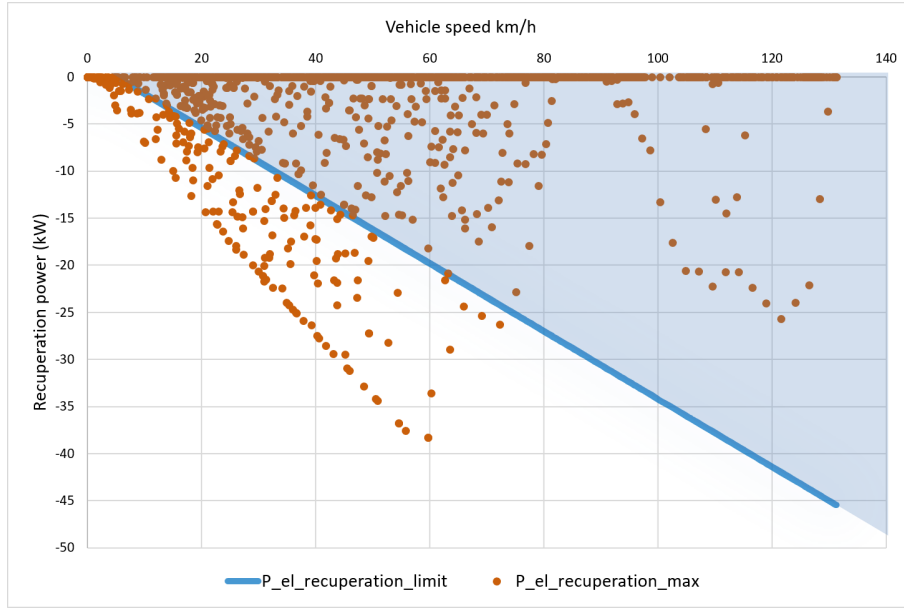
Figure 3.11: Illustration on the maximum theoretically possible recuperation (red dots) and limited recuperation versus vehicle speed (blue line) for the WLTC driving cycle.

$$C_{el.\ in} = \frac{P_{el.recu.m} \times 1000}{v_{cycle.m}} \tag{3.7}$$

Finally, the basic consumption was calculated by equation 3.8 which describes how much power the battery needs to provide to the drivetrain when recuperated energy is considered.

$$C_{el.\ tot} = C_{el.\ out} + C_{el.\ in} \tag{3.8}$$

3.3.2 Heating and air conditioning

To calculate the electricity consumption from heating and air conditioning in BEVs, the usage of the devices concerned need to be defined (Del Duce et al., 2013). Following information is required;

- Geographical temperature profile of minimum and maximum temperatures per day

- Comfortable ambient temperature range

- Usage pattern of the heating and air conditioning

In this study, the following three locations have been chosen to represent the European temperature profile: Frankfurt, Madrid, and Oslo. The data on the temperature is collected from Tank et al. (2002) and figure 3.12 represents the average temperatures from the three locations in the year 2017.
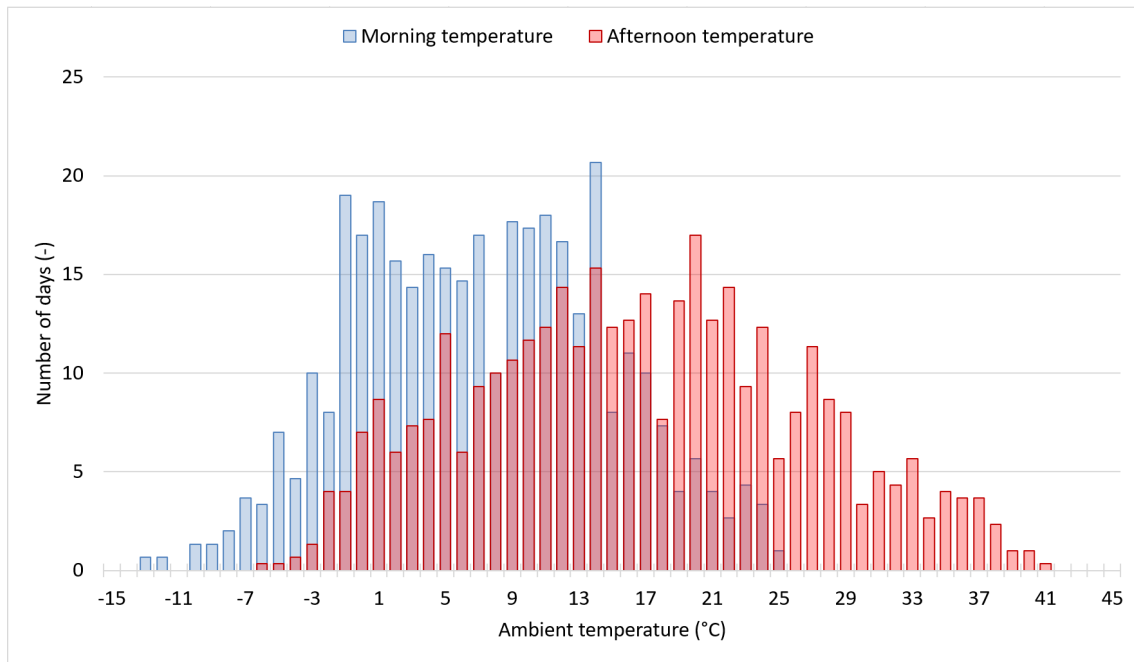
Figure 3.12: Illustration on a temperature profile showing the number of days with a specific temperature during the year 2017.

The comfortable ambient temperature has been assumed to be between 20 and 23 °C in the vehicle and the usage pattern of the heating and air conditioning to maintain the temperature interval is described by Del Duce et al. (2013) in table 3.5. The temperature range 15-20 °C is not included in the table and it is assumed that no heating or air conditioning is needed at that temperature interval.

Table 3.5: Usage pattern to maintain a comfortable temperature interval inside the vehicle

Heating set to maximum:	ambient temperature < 10 °C
Heating set to medium:	10 °C ≤ ambient temperature < 15 °C
Air conditioning set to medium:	20 °C < ambient temperature ≤ 25 °C
Air conditioning set to maximum:	ambient temperature > 25 °C

By relating the temperature profile and the usage pattern of heating and air conditioning per day, the number of operation days for different use of heating and air conditioning can be identified. In figure 3.13 have the results compiled in a diagram. The total operation days for the year 2017 is calculated by weighting the morning and afternoon trips. It is assumed that the use of heating and air conditioning is 1/3 during morning trips and 2/3 during afternoon trips.

Apart from the comfort related usage of heating and air conditioning, the devices is also used to remove the fog from the windscreen for safety reasons (Del Duce et al., 2013). The fog appears on the windscreen when the temperature on the glass is either equal to or lower than the dew point temperature which is dependent on the humidity and temperature inside the car. Usually, heating and air conditioning
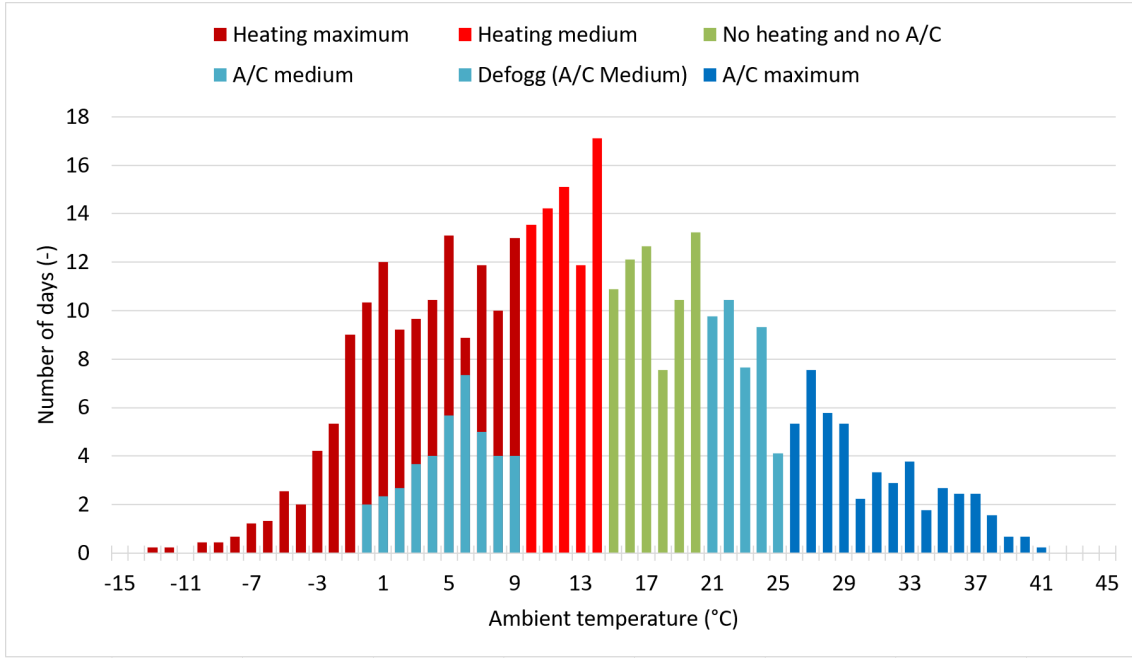
Figure 3.13: Illustration on a temperature profile showing the use of heating and air conditioning devices in different settings with respect to the temperature intervals.

is used simultaneously to remove the fog but in this study, only air conditioning at medium setting is considered. This is due to the complexity to model the actual defogging phenom where the interaction of humidity, inner and outer temperature is considered.

It is assumed that fog appears on the windscreen when the temperature inside the vehicle is 20 °C at days where the humidity is over 80% and the outside temperature is at a range of 0°C ≤ T < 10°C. The estimation on the use of A/C for defogging the windshields was an annual share of 11% with the assumption that air conditioning is used 1/3 during morning trips and 2/3 during afternoon trips.

In addition to total operation days, the power demand for the use of heating and air conditioning needs to be determined. The vehicle used is equipped with a PTC heater (Positive Temperature Coefficient heating element) and standard ICE air conditioning system, which have a power demand of 5 kW and 1 kW per hour, respectively. (Del Duce et al., 2013). When the heating and air conditioning are set to a medium setting, the power demand is assumed to be reduced to half. The annual vehicle operation time in hours is calculated in equation 3.9, where annual vehicle mileage in km is divided with mean cycle speed.

$$t_{ann.oper} = \frac{D_{ann}}{v_{cycle.m}} \quad (3.9)$$

The individual energy consumption in Wh/year for heating and air conditioning is calculated in equation 3.10, where the input parameters are: the total time in

days when the device is operating ($t_{dev.days}$) and power demand for heating or air conditioning (P_{device}) (Del Duce et al., 2013).

$$C_{el.ann.heating(cooling)} = \frac{t_{dev.days}}{365} \times (t_{ann.oper} \times P_{device}) \times 1000 \qquad (3.10)$$

In equation 3.11, the results on the individual energy consumption are divided by the annual vehicle operation time in hours to get it in per km (Del Duce et al., 2013).

$$C_{el.heating(cooling)} = \frac{C_{el.ann.heating(cooling)}}{D_{ann}} \qquad (3.11)$$

3.3.3 Auxiliaries

The auxiliaries in the vehicle that are considered in the energy consumption are lighting, radio/navigation and seat heating. In table 3.6, data has been gathered on the mean use and power demand for each auxiliary (Del Duce et al., 2013). The systems are assumed to be connected to a 12V grid in the vehicle which is powered by the battery through a DC-to-DC converter. The power electronic is assumed to have a efficiency of 90%.

Table 3.6: Auxiliaries that is assumed to be used in an electric vehicle.

Auxiliaries	Mean power demand (W)	Use ratio
Lighting	140	75%
Radio/Navigator	20	75%
Seat heating	30	75%

The energy consumption from auxiliaries is calculated in equation 3.12, where the mean power demand for each auxiliary is multiplied by its mean use ratio and the DC-to-DC efficiency, divided by the mean cycle speed (Del Duce et al., 2013).

$$C_{el.aux} = \frac{eff_{dc/dc} \times P_{device.m} \times r_{use.m}}{v_{cycle.m}} \qquad (3.12)$$

3.3.4 Battery losses in standstill

For lithium-ion batteries, internal battery losses from periods of standstill are mostly due to self-discharge (Del Duce et al., 2013). The energy consumption from this loss is highly dependent on battery designs, where the loss of state of charge varies. Data on how much battery capacity that was lost during standstill was only available for the time frame per day. Since the vehicle is assumed to only be parked unplugged for 8 hours per day, the loss of state of charge per hour was calculated by assuming a linear relationship. It should be noted that this is probably a underestimate of the actual loss. The energy consumption was calculated by equation 3.13.

$$C_{el.standstill} = \frac{B_{cap} \times Loss_{selfdischarge} \times t_{standstill.period} \times 1000}{D_{period}} \qquad (3.13)$$

Where:

$$
\begin{aligned}
B_{cap} &: \text{is the battery capacity in kWh} \\
Loss_{selfdischarge} &: \text{is the mean loss of state of charge per hour} \\
t_{standstill.period} &: \text{is the number of hours the vehicle is parked unplugged for a year} \\
D_{period} &: \text{is the annual driving distance}
\end{aligned}
$$

The mean loss of state of charge was assumed to be 0.014% and during one year the vehicle has been parked unplugged for 2920 hours. The annual driving distance is 21 700 km which is the mean annual driving distance according to Federal Highway Administration (2018).

3.3.5 Battery charging

Up to now, the energy consumption has been calculated with the respect of the energy withdrawn from the battery. However, to include the total consumption, the energy losses caused by charging the battery need to be considered (Del Duce et al., 2013). The additional energy consumption is dependent on the efficiency of the devices that are used to charge the battery.

The overall efficiency is dependent on various parameters (Del Duce et al., 2013). One of them is the type of charging devices used, ranging from low to high voltage charger. Furthermore, even with the given type of charging devices that are used, there is a large range of charging devices with different efficiencies to an extent below 80% and up to 90%. There are also different charging strategies that dependence on the design and performance of the battery, for instance, the size of the battery and cell, temperature and voltage level etc.

The data on the average influence of the charger to the energy consumption is currently unavailable and instead, a simplified approach is used. The method is based on data analysis from Bütler & Winkler (2013) and derived from the assumption of using a standard charging device like those used at home. It is also assumed that BEVs are charged in a garage and thus, influence on charging efficiency caused by temperature is neglected. By equation 3.14, the overall plug energy demand for one discharge cycle is calculated by characterization of the energy storage efficiency. From the data analysis, it was discovered that the overall charge efficiency is strongly influenced by the initial state of charge. After every charge, the voltage level for all cells need to be balanced which requires a relatively high amount of energy. This is associated with the charging strategy, where a high state of charge (for example, caused by short driving distances) yields low charging efficiency and vice versa. This aspect was also considered when equation below was derived.

$$E_{tot.plug} = 1.213 \times E_{tot.bat} + 0.1925 \qquad (3.14)$$

Finally, the additional energy consumption from battery charging is calculated with equation 3.15

$$C_{el.charge} = \frac{E_{tot.plug} - E_{tot.bat}}{D_{discharge}} \qquad (3.15)$$

3.3.6 Total energy consumption

The results on the five energy sub-consumption are summarized in figure 3.14. The total energy consumption for NMC333 and NMC622 was calculated to 239 and 234 Wh/km, respectively. The difference in energy consumption between the two battery packs is due to their mass. The basic consumption approach considers the mass of the vehicle when calculating the wheel power, see equation 3.1. Further, the battery charging is in turn dependent on the results on the basic consumption, see equation 3.14
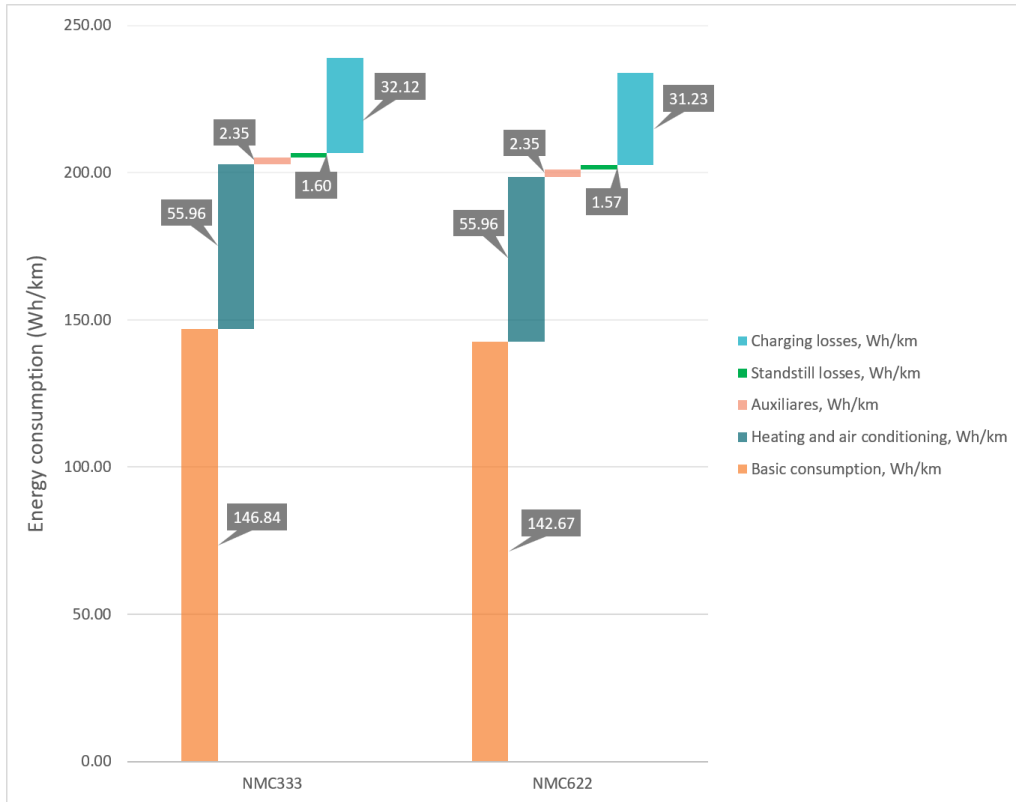
Figure 3.14: Plug-to-wheel energy consumption for NMC333 and NMC622.

3.3.7 Electricity mix

By the look on overall results from a number of LCA studies on electric vehicles, it is confirmed that the choice of electricity sources have a significant impact (Del Duce et al., 2013). Among countries around the world, different resources are used to produce electricity and these country specific mixes of production paths are usually referred to as electricity mixes. The use of batteries in BEVs are assumed to be in

Europe and therefore, EU-28 average consumption mix has been chosen to represent the resource use for, and emissions from, producing electricity. In figure 3.15, the relative shares of the resources used in the production of electricity are shown.
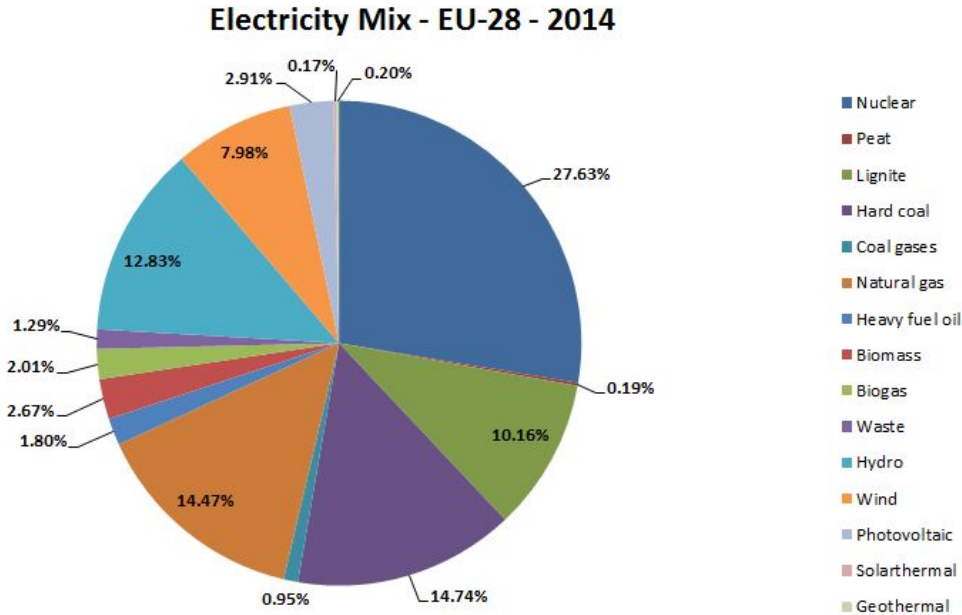
Figure 3.15: Relative share of different energy sources in the EU-28 average consumption mix.

3.4 End-of-life phase

Over the past decade, many different recycling methods for electric-vehicle batteries have been developed (Elwert et al., 2015). Recycling plants that are located in Europe are obliged to follow a battery directive (Directive 2006/66/EC), which requires that at least 50% of the materials in the batteries are recycled. In an economic point of view, cobalt (99,8%) and nickel (99,8%), followed by copper (grade A) and lithium (lithium carbonate) are the main drivers for recycling. Since the cobalt and nickel have the highest economic value, different recycling methods mainly aim to recover the layered oxides that are found in the cathode.

3.4.1 Umicore's recycling process

In the report by Dunn et al. (2014), the recycling processes are divided into four processes: pyrometallurgical, hydrometallurgical, intermediate and direct physical processes. In this study, Umicore battery recycling process will be used to model the end-of-life phase. The recycling process is based on a combination of pyrometallurgical and hydrometallurgical processing and is considered to be one of the most advanced recycling methods for lithium-ion batteries (Elwert et al., 2015). In essence, the recycling method recovers cobalt, nickel, and copper as an alloy by pyrometal-

lurgical processing which then undergoes further separation by hydrometallurgical processing.

Battery pack dismantling and recycling

The dismantling of battery packs by Umicore does either take place in Hanau in Germany or in Maxton, NC in USA (Tytgat, 2013). The battery packs are first disassembled to its main components; battery pack packaging, battery modules (containing the cells), cooling system and battery management system. Prior to the dismantle, the state-of-charge is measured to determine whether a discharge is needed (Elwert et al., 2015). Due to the low quantities of recycled batteries in relation to the high diversity of battery designs, only manual dismantling is currently used.

Most of the components are recycled locally except for the battery modules which are sent to Hoboken in Belgium for further processing (Tytgat, 2013). The material generated from the disassembly can be divided into the following fractions: metals, plastics, mixed materials and electrochemical parts. The mixed materials are metals and plastics that are difficult to separate, such as printed circuit boards. Electrochemical parts are found in the modules and cells which are separated by pyrometallurgical and hydrometallurgical processing. The pure metals are further treated in smelters to convert them into tradeable shape and quality. The recycling efficiency is assumed to be 98% for pure metals. It is possible to recycle the plastics, in particular, the larger parts, but in practice, all plastic parts are currently incinerated with energy recovery. The mixed materials are treated in a smelter, where the focus is on the recycling of copper. The recycling efficiency of the metal content in the mixed materials is estimated to be 30%.

Cell recycling

Without further mechanical pre-treatment of the battery modules, the separation processing, shown in figure 3.16, begins with a smelting process where the battery modules are fed into a high-temperature shaft furnace together with slag-forming agents: limestone, sand, and slag (Dunn et al., 2014). The shaft furnace consists of three heating zones which operate in different temperatures. The first heating zone is known as the pre-heating zone where the electrolyte evaporates. The temperature is below 300 °C which is the lowest temperature compared to other heating zones with the reason to reduce the risk of explosion. The second heating zone is known as the plastics pyrolizing zone and is where the plastics are burned at a temperature of approximately 700 °C. When the electrolyte and the plastic have been separated, a higher operating temperature is possible which reduces the overall energy consumption. The last step referred to as the smelting and reducing zone operates at a temperature range of 1200-1450 °C and is where metals are turned into either a slag or an alloy. The smelting process does also produce gas which need to be treated, typically in a post-combustion chamber at temperature approximately 1150 °C and followed by additional gas clean-up steps. However, the gas treatment is not included in this study.
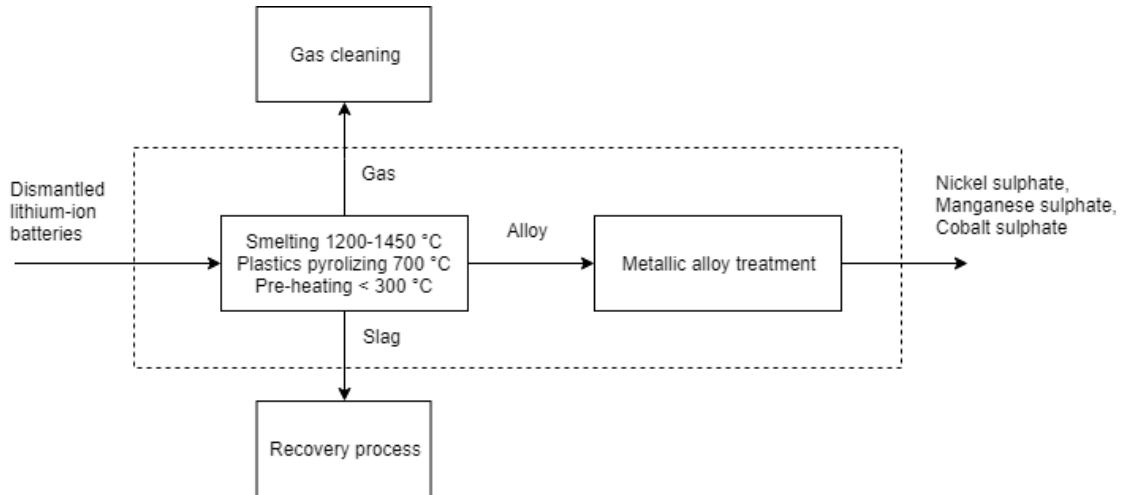
Figure 3.16: Process flow diagram for recycling of battery cells developed by Umicore and adapted from Dunn et al. (2014).

The materials that end up in the slag are lithium, aluminium, silicon, calcium, manganese, and some iron (Dunn et al., 2014). These are not recycled because there is no financial incentive and the processing requires relatively much energy. Typically, the slag is instead used as an aggregate in concrete, but the option is not considered in this study. The remaining metals are formed to an alloy consisting of copper, cobalt, nickel, and some iron (Dunn et al., 2014). The separation of each metal from the alloy is conducted with hydrometallurgical processing where sulphuric acid and sodium hydroxide are used.

The LCI data for the recycling processes are collected from the PEFCR which refer to the procedure developed by Umicore (Siret et al., 2018). The collection rate for recycling is assumed to be 95% and the remaining unsorted battery fraction is assumed to end in a landfill.

4

LIFE CYCLE IMPACT ASSESSMENT

In the following chapter, the results from the life cycle impact assessment are presented. The contribution to the environmental impact categories from each life cycle phase is found in appendix D.

4.1 Climate change

Figure 4.1 present the results on the midpoint category *climate change*. The NMC622 has around 2% lower contribution to the total impact compared to NMC333. The impact from the use phase is solely from the production of electricity, which also the case for the rest of the impact categories, and in the production phase, cathode accounts for the highest contribution. Further details on the cause of the impact of climate change and the other impact categories are discussed in section 5.3.

The characterization factors is derived from the IPCC 2013 report for a time horizon of 100 years (Fazio et al., 2018). The drivers of global warming are anthropogenic emissions of greenhouse gases which increases the radiative forcing leading to higher absorption of solar radiation (Pachauri et al., 2014). The involved gases are the following: carbon dioxide (CO_2), methane (CH_4), nitrous oxide (N_2O), chlorofluorocarbons ($CFCs$) and other trace gases.
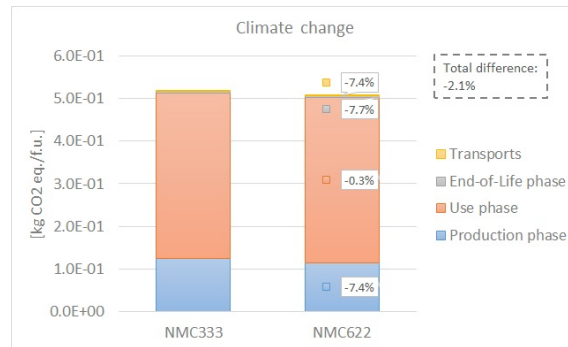
Figure 4.1: Results on climate change throughout the life cycle on NMC333 and NMC622 batteries.

4.2 Eutrophication

Figure 4.2 present the results in the midpoint category *eutrophication*, where sub-figure 4.2a, 4.2b and 4.2c illustrate the impact category in the following three areas: freshwater, marine and terrestrial. The NMC622 has a lower contribution to all three impact categories compared to NMC333 where the highest difference is in terrestrial eutrophication (-3.5%) followed by marine (-3.1%) and freshwater (-0.5%). As for freshwater eutrophication, the production phase account almost for the total impact and the difference between the batteries are relatively low compared to the end-of-life phase and transports. As for marine and terrestrial eutrophication, the use-phase account for the highest contribution followed by the production phase. The differences between the batteries are relatively low in the use-phase compared to the rest. In the production phase, cathode accounts for the highest contribution to terrestrial and marine eutrophication whereas for freshwater eutrophication, mostly is from the production of the module and pack packaging.

The characterization factors on terrestrial eutrophication is derived from the method of Accumulated Exceedance (AE) and the aquatic eutrophication from the ReCiPe method (European Commission-Joint Research Centre, 2011). The adverse effects are caused by the excessive flows of N- and P-compounds to soil and water (Fazio et al., 2018) An example of the effects on aquatic eutrophication is oxygen deficiency in lakes from the increase in algae blooming. For terrestrial eutrophication, it could be nutrient leaching in the soil.

4.3 Acidification

Figure 4.3 present the results on the midpoint category *acidification*. The NMC622 has around 17% higher contribution to the total impact compared to NMC333. The production phase accounts for the highest share of the total impact and the difference between the batteries is also greatest compared to the other life cycle stages. The production of the cathode accounts for the highest impact in the production phase.

The characterization factors are derived from the method of Accumulated Exceedance (AE) where the dispersion of air pollutants to land area and major lakes/rivers are modelled together with the European critical load database (European Commission-Joint Research Centre, 2011). The main air emission causing acidification to land and water are ammonia (NH_3), nitrogen dioxide (NO_2) and sulphur oxides (SO_x) (Fazio et al., 2018). An example of adverse effects from aquatic acidification is fish mortality and for terrestrial acidification, an example is deforestation.

4.4 Human toxicity

Figure 4.4 present the results on the midpoint category *human toxicity*, where sub-figure 4.4a illustrates the human toxicity with non-cancer effect while subfigure 4.4b show with cancer effects. The NMC622 has around 1% and 6% lower contribution to the total impact of human toxicity non-cancer effects respective with cancer effects

(a) Freshwater

(b) Marine

(c) Terrestrial
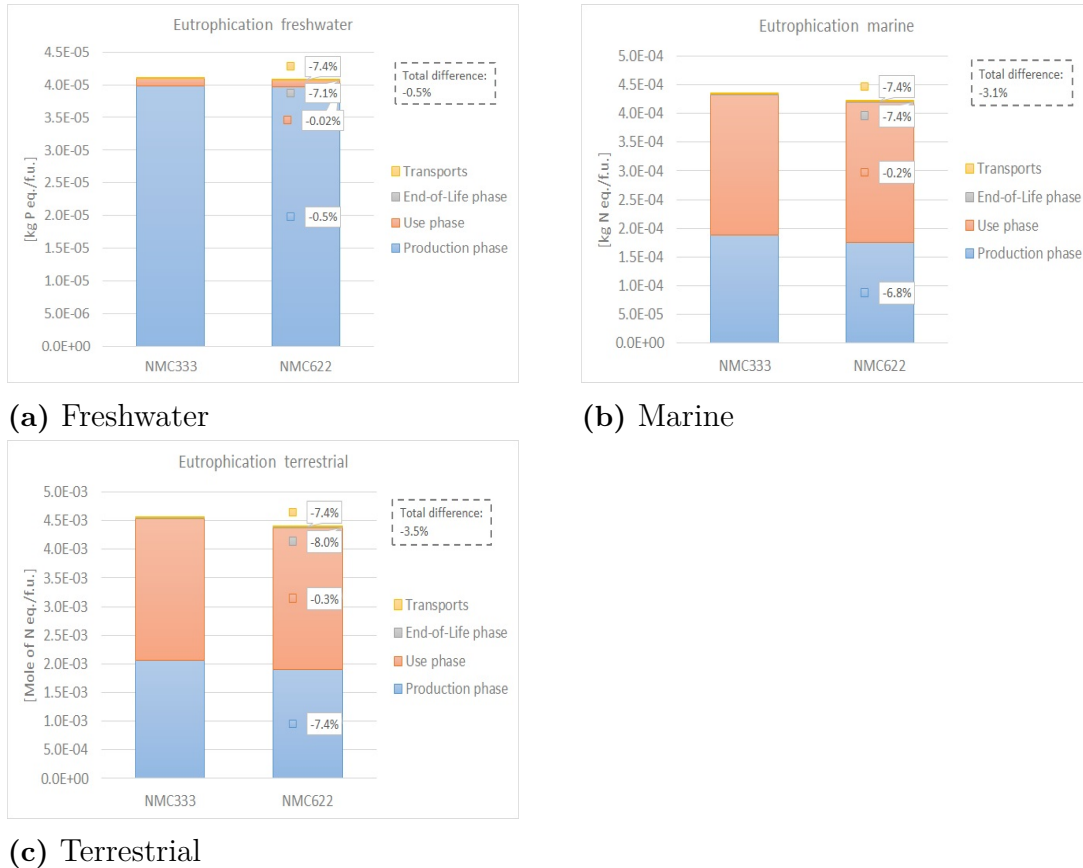
Figure 4.2: Results on eutrophication throughout the life cycle on NMC333 and NMC622 batteries.

compared to NMC333. The production phase account for the highest share of the total impact and the difference between the batteries is more prominent for human toxicity with cancer effects. The production of the module and pack packaging are responsible for the highest impact in the production phase.

The characterization factors are derived from the USEtox model combining chemical fate and exposure with toxicological data and includes emissions to all three compartments: air, water and soil (European Commission-Joint Research Centre, 2011).

4.5 Ecotoxicity freshwater

Figure 4.5 present the results on the midpoint category *ecotoxicity freshwater*. The NMC622 has around 0.5% lower contribution to the total impact compared to NMC333. The production phase account for the highest share of the total impact but the difference between the batteries are relatively low. The production of the module and pack packaging are responsible for the highest impact in the production phase.

Same as for human toxicity, the characterization factors are derived from the USEtox
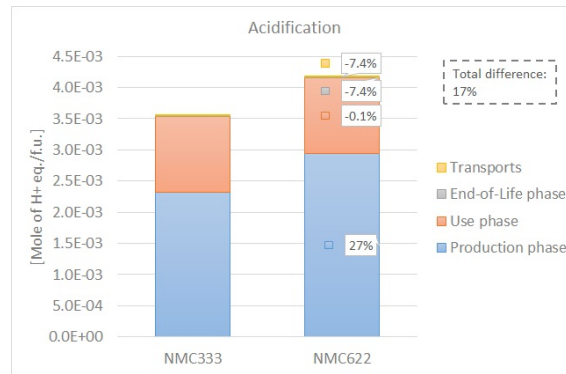
Figure 4.3: Results on acidification throughout the life cycle on NMC333 and NMC622 batteries.

(a) Non-cancer effects

(b) Cancer effects
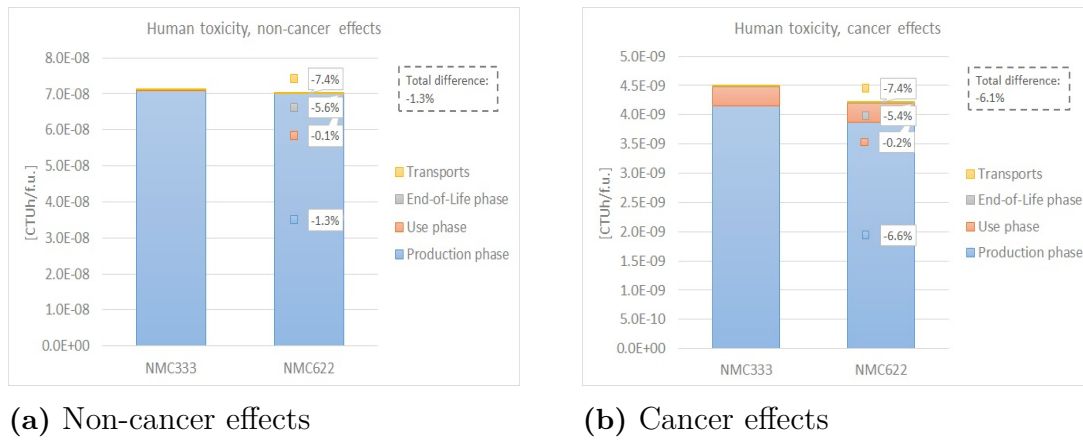
Figure 4.4: Results on human toxicity throughout the life cycle on NMC333 and NMC622 batteries.

model but European Commission-Joint Research Centre (2011) recommends only freshwater to be analyze since there are currently no suitable models for marine and terrestrial.

4.6 Photochemical ozone formation

Figure 4.6 present the results on the midpoint category *photochemical ozone formation*. The NMC622 has around 0.3% higher contribution to the total impact compared to NMC333 which is due to the production phase that accounts for a relatively high share and in which the batteries are slightly different from each other. The production of the cathode is responsible for the highest impact in the production phase.

The characterization factors are derived from the ReCiPe model which models marginal increase in ozone formation caused by emissions of non-methane volatile organic compounds ($NMVOC$) or carbon monoxide (CO) in the presence of nitrogen oxides (NO_x) and sunlight (European Commission-Joint Research Centre, 2011).
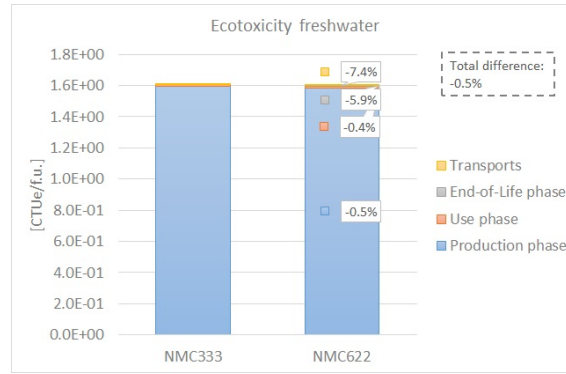
Figure 4.5: Results on ecotoxicity freshwater throughout the life cycle on NMC333 and NMC622 batteries.
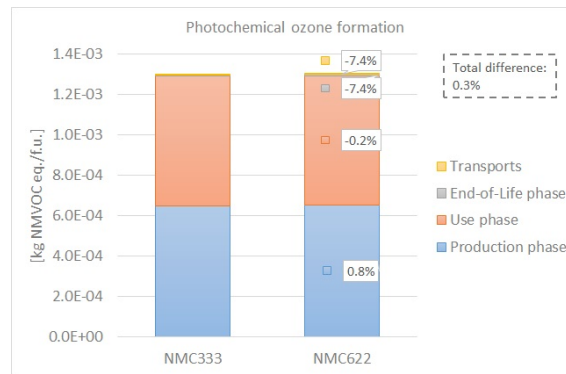
Figure 4.6: Results on photochemical ozone formation throughout the life cycle on NMC333 and NMC622 batteries.

4.7 Ozone depletion

Figure 4.7 present the results on the midpoint category *ozone depletion*. The NMC622 has around 3% lower contribution to the total impact compared to NMC333 which is almost entirely due to production phase in which the difference between the batteries is relatively high. The production of the cathode is responsible for the highest impact in the production phase.

The characterization factors are derived from the World Meteorological Organisation (WMO) steady state method which models the cause thinning of the stratospheric ozone layer due to ozone-depleting substances (ODS) such as CFCs, HCFCs and Halons (European Commission-Joint Research Centre, 2011). The adverse effect of the decrease in ozone concentration is increased UV-B level which subsequently harms the ecosystem and humans.

4.8 Ionizing radiation

Figure 4.8 present the results on the midpoint category *ionizing radiation* with respect to human health impact. The NMC622 has around 0.4% lower contribution
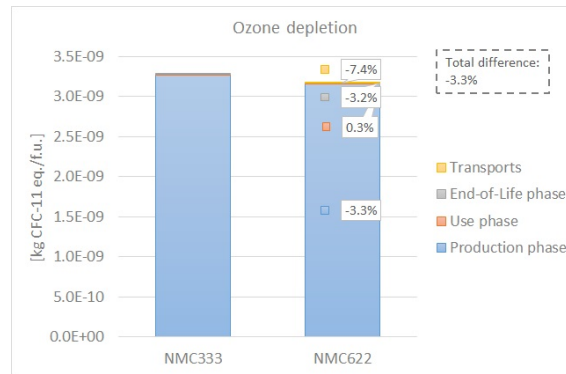
Figure 4.7: Results on ozone depletion throughout the life cycle on NMC333 and NMC622 batteries.

to the total impact compared to NMC333. The use-phase accounts for the highest share of the total impact but the difference between the batteries are relatively low compared to the other life cycle stages. The production of the cathode is responsible for the highest impact in the production phase.

The characterization factors are derived from method described by Frischknecht et al. (2000) providing separated and intermediary results on fate and exposure (European Commission-Joint Research Centre, 2011). The method is also used in the following LCIA methodologies: Ecoindicator 99, IMPACT 2002, ReCiPe and Swiss Ecofactor.
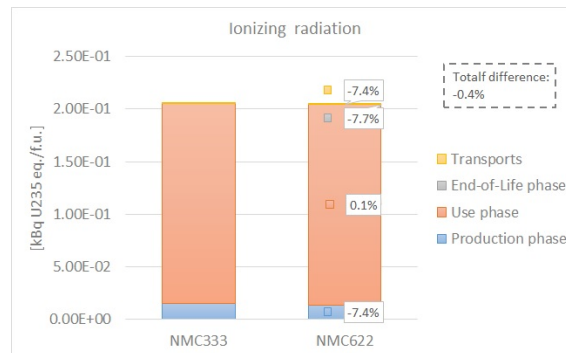
Figure 4.8: Results on ionizing radiation throughout the life cycle on NMC333 and NMC622 batteries.

4.9 Particulate matter/Respiratory inorganics

Figure 4.9 present the results on the midpoint category *particulate matter/respiratory inorganics*. The NMC622 has around 2.5% higher contribution to the total impact compared to NMC333 which is mainly due to the production phase that has the highest share and where the difference between the batteries are relatively high. The production of the cathode is responsible for the highest impact in the production phase.

The characterization factors are derived from a model developed by the UNEP-SETAC Task Force (TF) on PM in 2016 (Fazio et al., 2018). The model assesses the indoor and outdoor emissions of primary and secondary ($PM_{2.5}$) in urban and rural areas and what damage it causes on human health. The model does not assess (PM_{10}) since it is less significant, however, it is included in the impact category and the CF is calculated by multiplying the CF for ($PM_{2.5}$)) by 23%.
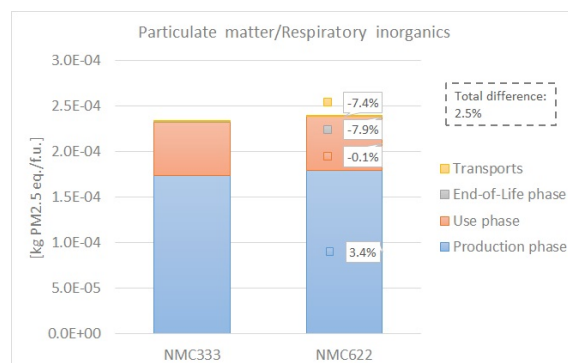
Figure 4.9: Results on particulate matter/respiratory inorganics throughout the life cycle on NMC333 and NMC622 batteries.

4.10 Resource depletion

Figure 4.10 present the results on the midpoint category *resource depletion*. The NMC622 has around 1.8% and 0.9% lower contribution to the total impact compared to NMC333 for depletion of mineral, fossils and renewable respective water. As for depletion of mineral, fossils and renewable, the production phase accounts for the highest share of the total impact and where the difference between the batteries are relatively high. However, when it comes to depletion of water, the use-phase accounts for the highest share of the total impact but the difference between the batteries is relatively low compared to the other life cycle stages. In the production phase, the cathode is responsible for the highest impact of water scarcity whereas the production of the module and packaging accounts for the highest impact of depletion on mineral, fossils, and renewables.

The characterization factors for minerals and metals are derived from a model developed by Van Oers et al. (2002) which is referred to as the Abiotic Resource Depletion (ADP) ultimate reserve version. There are no recommended methods to assess renewable resources and information was not found on the methodology (Fazio et al., 2018). The characterization factors for water scarcity is from the available water remaining per area (AWARE) model which is developed by WULCA, a working group of the UNEP SETAC Life Cycle Initiative.

4.11 Land use

Figure 4.11 present the results on the midpoint category *land use*. The NMC622 has around 1% lower contribution to the total impact compared to NMC333. The
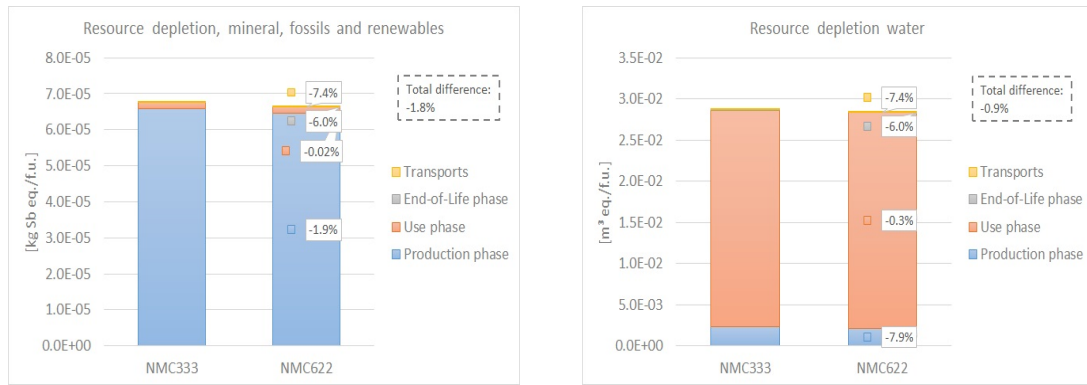
(a) Mineral, fossils and renewables **(b)** Water

Figure 4.10: Results on resource depletion throughout the life cycle on NMC333 and NMC622 batteries.

use-phase has the highest share of the total impact but the difference between the batteries is relatively low compared to the other life cycle stages.

The characterization factors for land use is derived from the Land Use Indicator Value Calculation Tool (LANCA) LCIA model which assess the following impacts caused by the use of soil: erosion resistance, mechanical filtration, physico-chemical filtration, groundwater regeneration, and biotic production (Fazio et al., 2018).
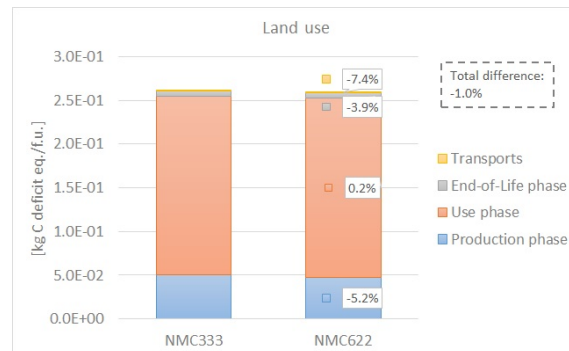
Figure 4.11: Results on land use throughout the life cycle on NMC333 and NMC622 batteries.

5

INTERPRETATION OF RESULTS

5.1 Benchmark

In the following chapter, the LCIA results are compared with the results from a PEF screening report on High Specific Energy Rechargeable Batteries for Mobile Applications (Bonell et al., 2015). The representative product used for the PEF study is lithium-ion battery for electric mobility with a chemistry composition based on market share. The included chemistries are LCO ($LiCoO_2$), NMC ($LiNi_xMn_yCo_zO_2$), LiMn ($LiMn0_2$), LFP ($LiFePO_4$). The battery is virtually designed and in table 5.1, its technical specification is compared with NMC333 and NMC622.

Table 5.1: Technical specifcations on the battery designed in the PEFCR report provided by European Commission (2017) compared to NMC333 and NMC622

Technical specifications	PEFCR	NMC333	NMC622
Mass (kg)	225	520	427
Amount of cells	250	240	240
Number of cycles	400	514	514
Specific energy capacity (kWh/kg)	0.09	0.16	0.18
Total energy delivered over the service life (kWh)	8000	43784	42895
Reference flow (kg/kWh)	0.028	0.012	0.011

The purpose of the benchmark is to identify similarities and potential diversion between the LCIA results from this study and the PEFCR report. The LCIA results per kWh energy delivered over the service life are shown in table 5.2 where the difference in percent was calculated by comparing the benchmark values with average values between NMC333 and NMC622.

The differences in the LCIA results that were considered to be significant are marked gray in table 5.2, which includes the following midpoint impact categories: freshwater eutrophication, marine eutrophication, freshwater ecotoxicity and water scarcity. The reason why there is a high difference in freshwater eutrophication is assumed to be due to the use of different datasets. Over 60% of the total impact is solely from a dataset of an electronic component used in module and pack packaging, see table H.3 in appendix H. However, in the PEFR study, they also find that the largest

Table 5.2: Benchmark results on the following midpoint impact categories: Global Warming Potential (GWP100), Freshwater Eutrophication Potential (FEP), Marine Eutrophication Potential (MEP), Terrestrial Eutrophication Potential (TEP), Acidification Potential (AP), Human Toxicitiy Potential (HTP), Freshwater Toxicity Potential (FETP), Photo Oxidation Formation Potential (POFP), Ozone Depletion Potential (ODP), Ionizing Radiation (IR), Particulate Matter (PM), Water scarcity, Abiotic Depletion Potential (ADP) and Land use. The gray marked values are considered to have a relatively high difference.

Midpoint Impact Categories	NMC333	NMC622	PEFCR	Difference
GWP100 [kg CO2 eq./fu]	5.2E-01	5.1E-01	6.1E-01	-16%
FEP [kg P eq./fu]	4.1E-05	4.1E-05	2.6E-06	1496%
MEP [kg N eq./fu]	4.4E-04	4.2E-04	5.1E-05	742%
TEP [Mole of N eq./fu]	4.5E-03	4.4E-03	7.1E-03	-37%
AP [Mole of H+ eq./fu]	3.5E-03	4.2E-03	3.8E-03	0%
HTC [CTUh/fu]	4.5E-09	4.2E-09	5.6E-09	-23%
HTNC [CTUh/fu]	7.1E-08	7.0E-08	1.1E-07	-34%
FETP [CTUe/fu]	1.6E+00	1.6E+00	1.5E-01	967%
POFP [kg NMVOC eq./fu]	1.3E-03	1.3E-03	2.0E-03	-34%
ODP [kg CFC-11 eq./fu]	3.3E-09	3.2E-09	1.8E-09	82%
IR [kBq U235 eq./fu]	2.1E-01	2.0E-01	1.8E-01	14%
PM [kg PM2.5 eq./fu]	2.3E-04	2.4E-04	3.6E-04	-34%
Water scarcity [m³ eq./fu]	2.9E-02	2.8E-02	3.6E-03	686%
ADP [kg Sb eq./fu]	6.8E-05	6.6E-05	9.8E-05	-32%
Land use [kg C deficit eq./fu]	2.6E-01	2.6E-01	2.6E+00	-90%

contribution to the eutrophication of freshwater is from electronic components but in this case printed wiring boards in OEM components which could be the battery management system and/or cooling system. As for marine eutrophication, the highest contribution is from oceanic transportation of the active cathode material, see table H.5 in appendix H. In similar case on the freshwater eutrophication, the highest contribution in the PEF study is from printed wiring boards in OEM components but also from production of active materials for the cathode. There was no information on the freshwater ecotoxicity hotspots but the highest contribution in this study is from production of electronic components used in the pack and module packaging. Likewise for water scarcity, there was no information on which components/processes that contributed the most but for this study it is from the electricity usage in the cathode production and the assembly of the battery cell, see table H.25 in appendix H.

5.2   Screening and hotspot analysis

In the following chapter, the interpretation of the results begins by identifying the most important impact categories by normalization and weighting. Thereafter, each environmental impact is analyzed to identify components and processes that account for a relatively high share of the emissions, also referred to as hotspots.

5.2.1 Normalization

The normalization factors that have been used is recommended by the PEFCR and can be found in table E.2 in appendix E. The results of the normalization shown in table 5.3 are expressed as impact per person within the EU and has the purpose to identify the most relevant impact categories for a product system (Bonell et al., 2015). The ILCD handbook has classified the impact categories into three different quality levels to facilitate the understanding of the importance of each of them. The ones with the lowest quality level are considered to be non-representative according to the PEFCR and are thus excluded in the screening analysis. For information about the quality levels and complete results of the normalization see table E.1 respective E.3 in appendix E. The impact categories that were considered the most important after the normalization are gray marked in table 5.3 which are the following: ionizing radiations, acidification, particulate matter, climate change and photochemical ozone formation.

Table 5.3: Results on the normalization of the cradle-to-grave impacts. The normalization factors that were used are recommended by the PEFCR and are expressed as impact per person within EU. The values that are gray marked are considered as the most important impact categories.

Impact categories	NMC333	NMC622	Relative	Cumulative
Ionising radiations	1.8E-04	1.8E-04	37%	37%
Acidification	7.5E-05	8.8E-05	15%	52%
Particulate matter/ Respiratory Inorganics	6.1E-05	6.3E-05	12%	64%
Climate change	5.6E-05	5.5E-05	11%	76%
Photochemical ozone formation	4.1E-05	4.1E-05	8.3%	84%
Eutrophication - freshwater	2.8E-05	2.8E-05	5.6%	90%
Eutrophication - terrestrial	2.6E-05	2.5E-05	5.2%	95%
Eutrophication - marine	2.6E-05	2.5E-05	5.2%	100%
Ozone depletion	1.5E-07	1.5E-07	0.03%	100%
SUM	4.9E-04	5.1E-04		

5.2.2 Weighting

The weighting factors that have been used is recommended by the PEFCR and can be found in table F.1 in appendix F. The LCIA results after normalization and weighting are shown in table 5.4 where the following gray marked impact categories have been considered to be the most important ones: climate change, ionizing radiations, particulate matter, and acidification. The results are calculated by multiplying the normalized results with a set of weighting factors that are determined based on value judgments of the perceived relative importance of the impact categories. In the same way as the normalization step, the impact categories with lowest quality levels are excluded but a complete list is provided in table F.2 in appendix F.

Table 5.4: LCIA results of the cradle-to-grave impact after normalization and weighting. The weighting factors that were used are recommended by the PEFCR and are derived from an aggregated weighting set and robustness factors. The impact categories that are gray marked are considered most important. The relative values are the share of the total environmental impact and the cumulative value is the accumulation of the relative values. The environmental impact categories that account for a relatively high share and are responsible for 80% of the total environmental impact are considered the most important ones.

Impact categories	NMC333	NMC622	Relative	Cumulative
Climate change	1.2E-03	1.2E-03	32%	32%
Ionising radiations	9.8E-04	9.7E-04	26%	58%
Particulate matter/ Respiratory Inorganics	5.8E-04	6.0E-04	16%	74%
Acidification	5.0E-04	5.8E-04	14%	88%
Photochemical ozone formation	2.1E-04	2.1E-04	5.5%	93%
Eutrophication - terrestrial	1.0E-04	9.8E-05	2.6%	96%
Eutrophication - freshwater	8.2E-05	8.1E-05	2.1%	98%
Eutrophication - marine	8.0E-05	7.8E-05	2.1%	100%
Ozone depletion	1.0E-06	9.9E-07	0.03%	100%
SUM	3.78E-03	3.85E-03		

The weighting step allows impact categories to be compared with each other and also summed into one-dimensional impact indicator. The summed results indicate that NMC622 has 2% higher environmental impact than NMC333. The impact categories that are mostly responsible for NMC622 having a lower environmental performance than NMC333 are particulate matter and acidification. The reason why NMC622 has a relatively high contribution to these impact categories is due to the production of nickel sulfate which discussed more in section 5.3.

5.3 Contribution & structural path analysis

The purpose of the contribution and structural path analysis is to identify the differences in the environmental impact categories between NMC622 and NMC333 in more detail. By looking into which components and processes that account for the highest contribution a deeper understanding of the hotspots are provided. In some cases, it is also interesting to identify which elementary flows that accounts for the highest contribution in the datasets. The structural path analysis that is found in appendix H is a compilation of all components and datasets that are used in the modeling and includes the share of what they contribute to each impact category.

The structure of the analysis is dependent on the results from the previous analysis where the impact categories were weighted to determine how important they are with respect to predetermined quality levels from the ILCD handbook and value judgments of the perceived relative importance of the impact categories from the

PEFCR. Table 5.5 shows an overview of how much each impact category contributes to the total environmental impact in each life cycle stage. For example, climate change is the most significant impact category according to the table where most of the emissions are from the use phase. The second most important impact category is ionizing radiation and so forth. Furthermore, the table indicates that the use phase has the highest total environmental impact compared to the other life cycle stages. The remaining share is almost entirely from the production phase as end-of-life and transports have both relatively low environmental impact.

Table 5.5: The contribution to the environmental impact categories on each life cycle step for NMC622.

NMC622	Production phase	Use phase	End-of-life phase	Transport	Relative	Cumulative
Climate change	7.6%	24%	0.25%	0.02%	33%	33%
Ionising radiations	1.8%	23%	0.04%	0.00%	26%	59%
Particulate matter/Respiratory Inorganics	12%	3.9%	0.05%	0.00%	15%	74%
Acidification	9.9%	5.2%	0.06%	0.00%	13%	87%
Photochemical ozone formation	2.7%	2.7%	0.03%	0.00%	5.5%	93%
Eutrophication - terrestrial	1.1%	1.4%	0.01%	0.00%	2.7%	96%
Eutrophication - freshwater	2.06%	0.06%	0.00%	0.00%	2.2%	98%
Eutrophication - marine	0.87%	1.14%	0.01%	0.00%	2.1%	100%
Ozone depletion	0.03%	0.00%	0.00%	0.00%	0.03%	100%
	38%	62%	0.4%	0.04%		

Apart from how much each impact category contributes to the total environmental impact, it is also of interest to see the differences between NMC622 and NMC333 on each of them. Table 5.6 shows the difference in percentage on how much NMC622 contributes to the weighted environmental impacts compared to NMC333. The impact categories that are not advantageous for NMC622 are acidification and particulate matter. The major reason for this is that nickel production has a higher contribution to the two impact categories than the production of cobalt which lead to a higher environmental impact from NMC622 as it consists of a higher share of nickel. These two impact categories also account for a large part of the total environmental impact, as shown in table 5.5, which makes the difference between the two batteries more evident. This is not the case for ozone depletion which has a high difference in percentage in table 5.6 but accounts for a low share of the total environmental impact as shown in table 5.5.

Table 5.6: The difference in percentage on how much NMC622 contributes to the weighted environmental impacts compared to NMC333.

GWP	IR	PM	AP	POFP	TEP	FEP	MEP	ODP
-2.3%	-0.61%	2.3%	17%	-0.15%	-3.3%	-0.11%	-3.1%	-8.9%

5.3.1 Production phase

The production phase is considered to be the most important life cycle stage. As seen in chapter 4, the production and use phase was almost entirely responsible for the

total impact on all impact categories, however, the differences between the batteries were much greater in the production compared to the use phase. Thus, the analysis will have a greater focus on the production of the batteries to identify in which components and processes the differences in the impact categories arise between the NMC622 and NMC333. Figure 5.1 provides an overview of the cradle-to-gate environmental impacts of NMC622 with respect to the main battery components and the manufacturing process of battery cells.
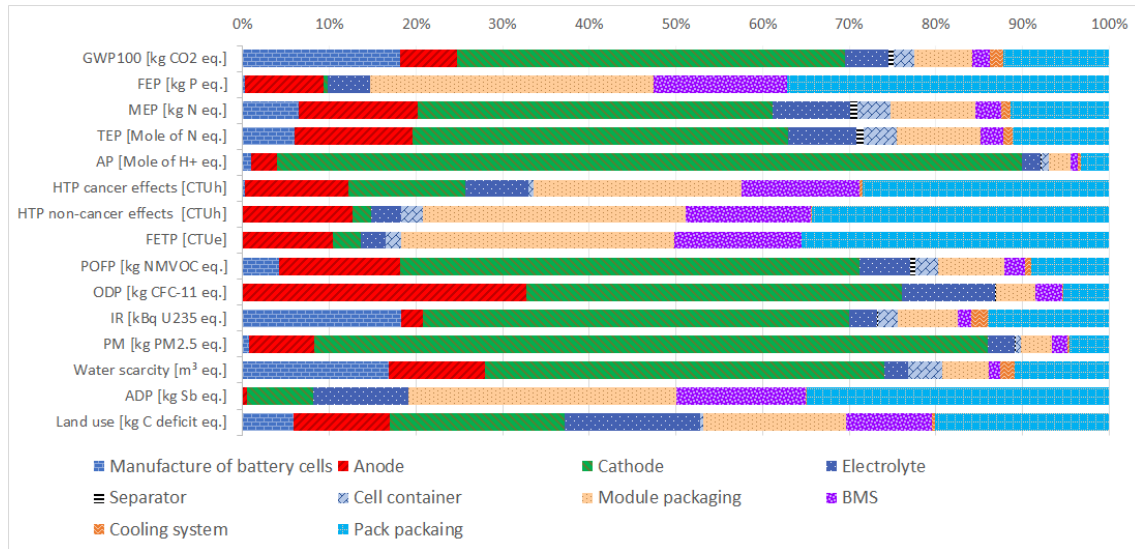
Figure 5.1: Contribution of cradle-to-gate environmental impacts of NMC662 from main battery components and first-tier processes

As seen in the figure 5.1, the cathode has a relative high share of contribution to majority of the impact categories: climate change (45%), marine eutrophication (41%), terrestrial eutrophication (43%), acidification (86%), photochemical formation (53%), ionizing radiation (43%), ozone depletion (49%), particulate matter (78%) and water scarcity (46%). An overall explanation why cathode has a high contribution to these categories is because it accounts for a relatively high share of the battery weight, it is energy-intensive to produce and it consists of cobalt and nickel sulfate which requires relative high amount of energy and material to produce. The anode has a relative high contribution to ozone depletion (33%) which is also the same reason for the cathode and that is from the production of PVDF, used as a binder in the battery cell. The module and pack packaging has a relative high share of contribution to freshwater eutrophication, abiotic resource depletion and the toxicity impact categories. The main reason for a high contribution to these categories is due to their weight and the production of electronic components.

5.3.1.1 Climate change

Figure 5.2 represents a comparison between NMC333 and NMC622 on the absolute and relative contribution to climate change from each component or process. The cathode stands for the highest contribution (37%) where the major reason is because the production is energy intensive. The results of the structural pathway analysis

point out that the synthesis of NMC requires a relatively high amount of energy which accounts for about 14-15% of the total impact on climate change. About half of the share comes from the production of the precursor with the use of thermal energy from natural gas and the other half to produce the active cathode material with the use of electricity. Further upstream, it was found that metals in the precursor accounted for a high share: cobalt (NMC333: 11%, NMC622: 6%), nickel (NMC333: 6%, NMC622: 11%) and lithium (4%).

The manufacturing of battery cells has the second-highest impact on climate change due to relatively high energy usage. Most of it comes from the use of electricity and thermal energy from natural gas to maintain the operation room dry during assembly accounting for 11% of the total impact. The other process is electrode drying and NMP recovery which uses electricity and accounts for 6% of the total impact. Pack packaging has a relatively high impact since the battery-pack casing is made of aluminum which is energy-intensive to produce. The most noticeable difference between the batteries is from the cathode and the major reason is that the material composition of NMC333 consists almost 3% more active cathode material than NMC622, see table 3.1. Another reasons is that the production of cobalt sulfate emits around 40% more CO_2 equivalents than the production of nickel sulfate.

Figure 5.2: Contribution of different components and processes to the cradle-to-gate environmental impacts on climate change for NMC333 and NMC622. The right axis represents the absolute value whereas the left represents shares of the total impact on climate change.

5.3.1.2 Ionizing radiation

Figure 5.3 represents a comparison between NMC333 and NMC622 on what proportion each component or process contributes to ionizing radiation. The cathode stands for the highest contribution to ozone depletion where the highest share (29%) is from the electricity for the synthesis of NMC. The manufacture of battery cells has the second highest contribution to ionizing radiation (17%) where the electricity to maintain the dry room is almost entirely responsible for the total impact.

The results from the structural path analysis show that the majority of the impact is from the amount of electricity required to manufacture the cathode and battery cells. However, there is also a relatively high contribution to ionizing radiation from the amount of aluminum that is used in the pack packaging, accounting for 10% of the total impact. The reason for this is that the component is relatively heavy and due to the fact that the production of aluminum is energy-intensive. Furthermore, sodium hydroxide accounts for a relatively high proportion of the total impact used for the production of the cathode (6%) and cobalt sulfate (4%). The most noticeable difference between the batteries is on the cathode, where NMC3333 has a higher impact since it has a higher proportion of the amount of active cathode material.

Figure 5.3: Contribution of different components and processes to the cradle-to-gate environmental impacts on ionizing radiation for NMC333 and NMC622. The right axis represents the absolute value whereas the left represents shares of the total impact on ionizing radiation.

5.3.1.3 Particulate matter/Respiratory inorganics

Figure 5.4 represents a comparison between NMC333 and NMC622 on what proportion each component or process contributes to particulate matter/respiratory inorganics. The cathode stands for the highest contribution to the impact category where the highest share is from the production of nickel sulfate. The results of the structural path analysis show that the nickel refining process accounts for about 38% and 55% on the total impact from the production of NMC333 and NMC622, respectively. Furthermore, the production of cobalt has the second highest contribution to the impact category where the mining of cobalt is the most responsible process accounts for about 26% and 12% of the total impact of the production of NMC333 and NMC622, respectively. The most noticeable difference between the batteries is on the cathode, where NMC622 has a higher impact since it consists of a higher share of nickel. The production of nickel sulfate has a higher contribution to the impact category compared to production of cobalt sulfate, which is mainly due to the emission of sulfur dioxide from processing nickel.
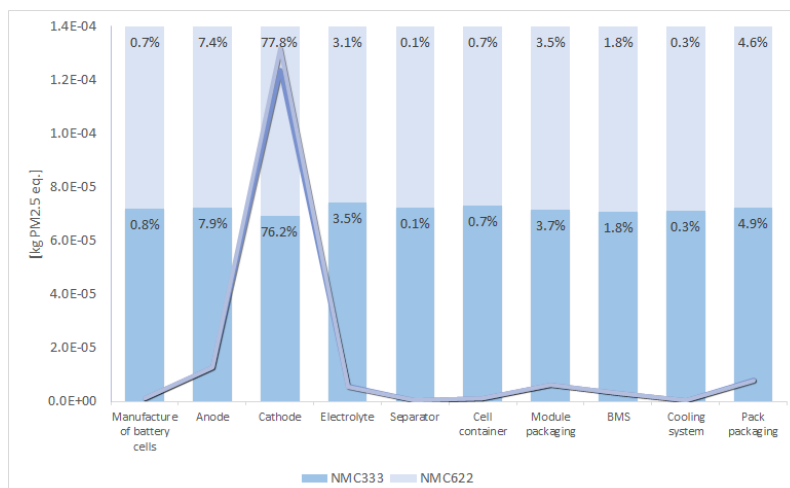
Figure 5.4: Contribution of different components and processes to the cradle-to-gate environmental impacts on particulate matter/respiratory inorganics for NMC333 and NMC622. The right axis represents the absolute value whereas the left represents shares of the total impact on particulate matter/respiratory inorganics.

5.3.1.4 Acidification

Figure 5.5 represents a comparison between NMC333 and NMC622 on what component or process contributes to acidification. The cathode stands for the highest contribution to acidification where the highest share is from the production of nickel sulfate. Since the proportion of nickel content in the active cathode material is higher for NMC622, the impact on acidification is significantly higher compared to NMC333, even though the total material use is less.

The impact on acidification from the production of nickel sulfate compared to cobalt sulfate is almost twice as large. The results from the structural path analysis show that the refining process for nickel accounts for around 64% for NMC333 and 74% for NMC633 of the total impact, which is mainly due to the emissions of sulfur dioxide. The impact is notably high for the single process as the second-highest impact from the primary extraction of nickel stands for around 3-4%.

5.3.1.5 Photochemical ozone formation

Figure 5.6 represents a comparison between NMC333 and NMC622 on what proportion each component or process contributes to photochemical ozone formation. The cathode stands for the highest contribution to the impact category where the highest share is from the production of nickel sulfate. The results from the structural path analysis shows that the refining process for nickel accounts for around 18% for NMC333 and 27% for NMC622 of the total impact, which is mainly due to the emissions of sulfur dioxide. The anode has the second highest impact on photochemical ozone formation which is mostly due to the production of battery-grade graphite (7%) and transportation from China to Korea by ship (6%). The most noticeable difference between the batteries is on the cathode, where NMC622 has a higher impact since it consists of a higher share of nickel.
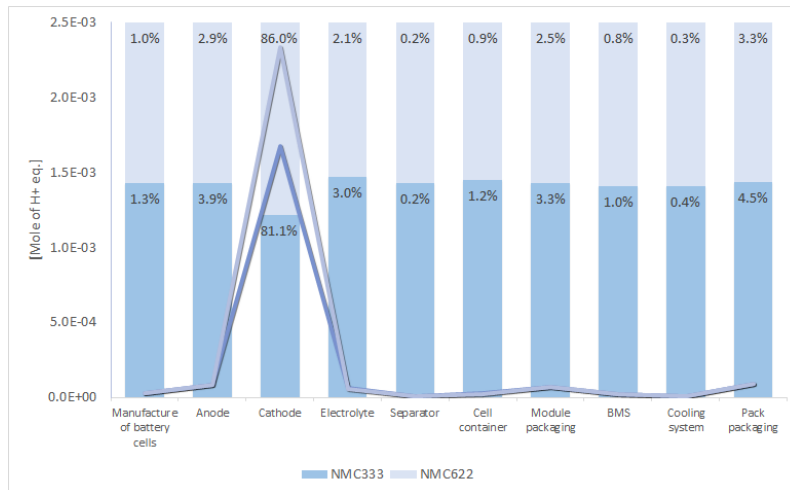
Figure 5.5: Contribution of different components and processes to the cradle-to-gate environmental impacts on acidification for NMC333 and NMC622. The right axis represents the absolute value whereas the left represents shares of the total impact on acidification.

5.3.1.6 Terrestrial eutrophication

Figure 5.8 represents a comparison between NMC333 and NMC622 on what component or process contributes to terrestrial eutrophication. The cathode stands for the highest contribution to terrestrial eutrophication where the highest share is from the transportation of from China to Korea by ship accounting for around 11% of the total impact. The second-highest share (9%) is from the use of the chemical sodium carbonate to produce the cathode. Furthermore, the anode has a relatively high contribution to terrestrial eutrophication with the same reasoning as the cathode, which is the transport from China to Korea with ship accounting for 8% of the total impact. The most noticeable difference between the batteries is on the cathode, where NMC3333 has a higher impact since it has a higher proportion of the amount of active cathode material.

5.3.1.7 Freshwater eutrophication

Figure 5.8 represents a comparison between NMC333 and NMC622 on the absolute and relative contribution to freshwater eutrophication from each component or process. The pack and module packaging stands for the highest contribution to freshwater eutrophication. The results of the structural pathway analysis point out that the electronic components stand for the highest share where module packaging and pack packaging accounts for around 32% and 30% respectively of the total impact. It should be noted that the results have a high uncertainty since it was not completely clear in the BatPac model what kind of electronic components that was supposed to be used on the batteries that were modelled. The datasets that were used for the electronic components are inspired by the LCA study by Ellingsen et al. (2014). Apart from the electronic components, the anode has a relatively high impact on freshwater eutrophication with a share of around 9%. No significant
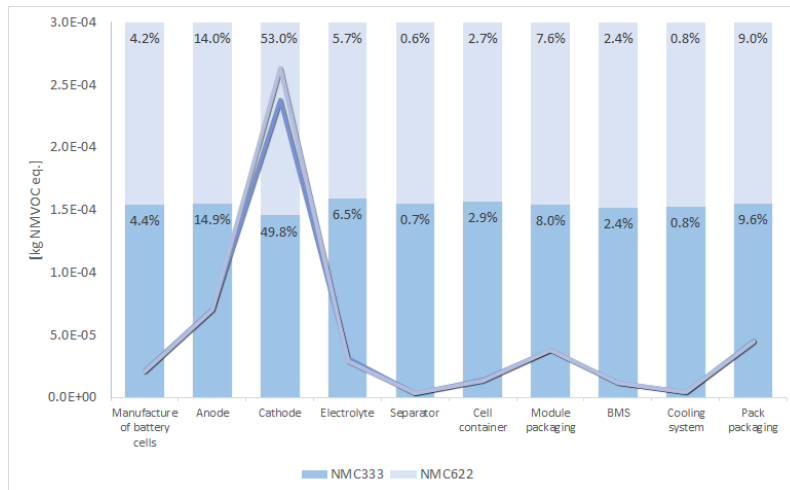
Figure 5.6: Contribution of different components and processes to the cradle-to-gate environmental impacts on photochemical ozone formation for NMC333 and NMC622. The right axis represents the absolute value whereas the left represents shares of the total impact on photochemical ozone formation.

differences between NMC333 and NMC622 were found on this impact category.

5.3.1.8 Marine eutrophication

Figure 5.8 represents a comparison between NMC333 and NMC622 on what component or process contributes to marine eutrophication. The cathode stands for the highest contribution to marine eutrophication where the highest share is from transportation from China to Korea by ship which is around 11%. The second-highest share (8%) is from the anode which is also due to the same transport as for the cathode.

In the same way as terrestrial eutrophication, the cathode has a high impact on marine eutrophication due to the intensive use of chemicals and energy during processing. Apart from the fact that NMC333 has a higher share of active cathode material and more material use in general, the NMC333 also has a higher impact on terrestrial and marine eutrophication since the production of cobalt sulfate has approximately 3% more impact than the production of nickel sulfate.

5.3.1.9 Ozone depletion

Figure 5.10 represents a comparison between NMC333 and NMC622 on what proportion each component or process contributes to ozone depletion. The cathode stands for the highest contribution to ozone depletion where the highest share is from the production of the binder used in battery cells. Likewise for anode, the binder has a high contribution to ozone depletion but also the production of graphite. The material used as a binder is polyvinylidene fluoride (PVDF) and the results from the structural path analysis show that the production of the polymer accounts for around 41-44% which is almost the entire impact from cathode. As for the anode, the polymer accounts for around 23-24% of the total impact. The noticeable differ-
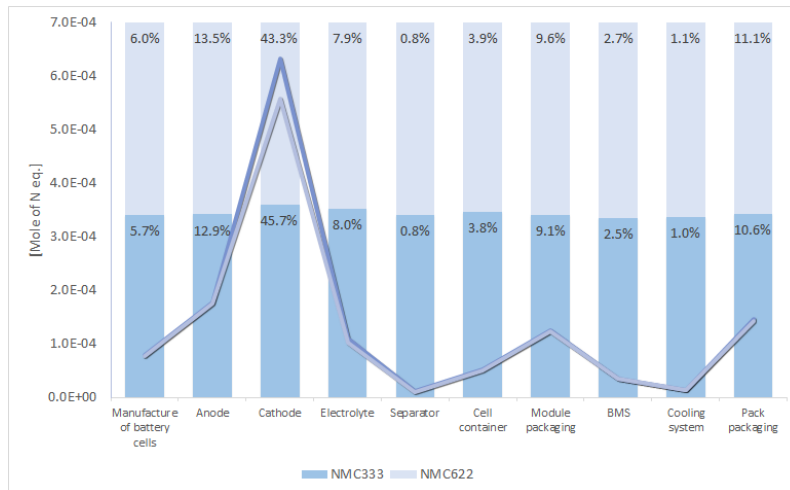
Figure 5.7: Contribution of different components and processes to the cradle-to-gate environmental impacts on terrestrial eutrophication for NMC333 and NMC622. The right axis represents the absolute value whereas the left represents shares of the total impact on terrestrial eutrophication.

ence between NMC333 and NMC622 is most likely due to the different proportion on the amount of active cathode material in the batteries. Apart from the cathode and anode, the electrolyte has a relatively high impact, where the production of lithium is almost entirely responsible. The most noticeable difference between the batteries is on the cathode, where NMC3333 has a higher impact since it has a higher proportion of the amount of active cathode material and thus, consists of more PVDF material.

5.3.1.10   Toxicity

Human toxicity and freshwater ecotoxicity were excluded in the normalization and weighting step since they were considered to have low quality level according to the ILCD handbook. The impact categories related to toxicity are thus described more broadly and similar figures presented for the previous impact categories are found in Appendix G. The results of the structural path analysis show that the module and pack packaging are the battery components contributing the most to the impact categories. The reason for this is that they consists of electronic components that accounts for more than half of the total impact. However, data on what type of electronics that were used was not found which results in higher uncertainty as more general datasets were used.

5.3.1.11   Resource depletion and land use

The impacts on resource depletion and land use were also excluded in the normalization and weighting step with the same reasons as for the ones related to toxicity. The impact categories will also be described more broadly and the figures representing the results from the contribution analysis are found in Appendix G. As for water scarcity, the component that contributes the most is cathode followed by the

Figure 5.8: Contribution of different components and processes to the cradle-to-gate environmental impacts on freshwater eutrophication for NMC333 and NMC622. The right axis represents the absolute value whereas the left represents shares of the total impact on freshwater eutrophication.

manufacturing of the battery cell. The results from the structural path analysis show that the impact from the production of the cathode and the manufacturing of battery cells is from the electricity usage.

The impact on depletion of metal, mineral, fossils and renewables is mostly from the module and pack packaging. The results from the structural path analysis show that more than half of the total impact is from electronic components.

The impact on land use is considered to be one of the most non-representative of all impact categories. Apart from the fact that the impact category is considered to have a low-quality level, the results are only based on background data on upstream processes. The results from the structural path analysis show that the module and pack packaging have the highest contribution, which is due to the content of electronic components.

5.3.2 Cobalt and nickel sulfate

From the contribution analysis on the production phase, it was concluded that the production of cobalt and nickel sulfate had a significant influence on the results. The reason for this is the due fact that NMC333 and NMC622 have a different share of cobalt and nickel in the active cathode material and that the involved production processes have a relatively high impact. In figure 5.11, shows the percentage each impact categories contributes to a total as well as the absolute value per kg cobalt or nickel.

As for the production of nickel sulfate, the refining process is identified as the hotspot in the production chain and has the highest contribution to the majority of the impact categories. Thereafter comes primary extraction as a second highest contributor to the majority of the impact categories while nickel ore preparation and ore mining
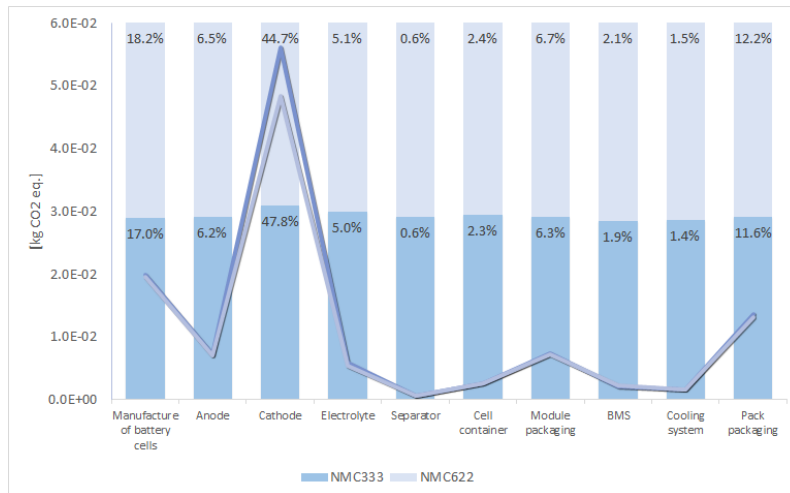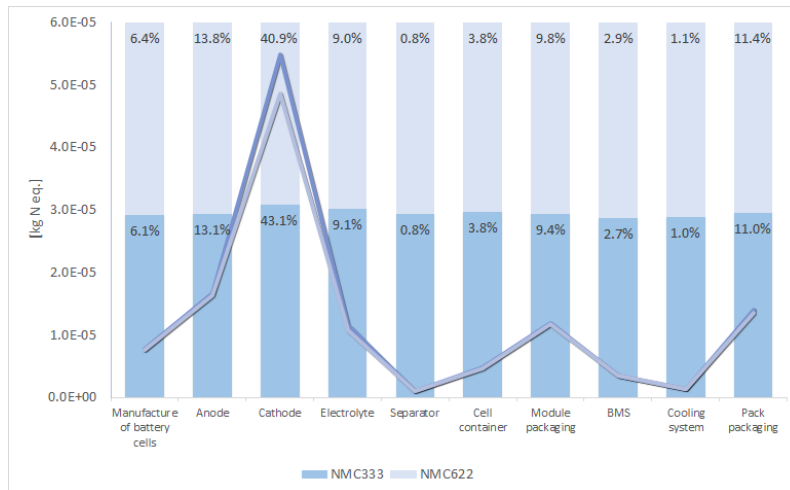
Figure 5.9: Contribution of different components and processes to the cradle-to-gate environmental impacts on marine eutrophication for NMC333 and NMC622. The right axis represents the absolute value whereas the left represents shares of the total impact on marine eutrophication.

is almost negligible compared to the other processing steps. See figure I.1 in appendix I for further information on the environmental impacts from the production of nickel sulfate.

In the case of the production of cobalt sulfate, the process involving the conversion of cobalt hydroxide to cobalt sulfate has the highest contribution to the majority of the impact categories. The cobalt ore processing is almost responsible for the entire impact on ozone depletion whereas cobalt mining has a relatively high impact on particulate matter. See figure I.1 in appendix I for further information on the environmental impacts from the production of cobalt sulfate.

5.3.3 Use phase

The LCIA results from the use phase are dependent on which electricity grid mix that is used as well as the energy density of the battery. The NMC622 has a plug-to-wheel energy consumption that is 2% lower than NMC333 due to having around 8% higher energy density. As the NMC333 weighs more, the total energy consumption will be higher, leading to lower environmental performance. It is assumed that the lifetime for both batteries is 180,000 km which results in total energy consumption of 43783 kWh and 42895 kWh for NMC333 respective NMC622. As described in the goal and scope, the LCIA results are converted to the functional unit by multiplying them with the reference flow that is calculated by dividing the battery weight with the total energy consumption over a battery lifetime. However, this results in the functional unit recommended by PEFCR being more beneficial for NMC333 as it consumes more energy per battery lifetime. The difference in battery weight between NMC622 and NMC333 is around 9% but by dividing it with the total energy consumption which differs around 2% between the batteries, the total difference is decreased to 7%. In the sensitivity analysis, the use-phase will be analyzed further
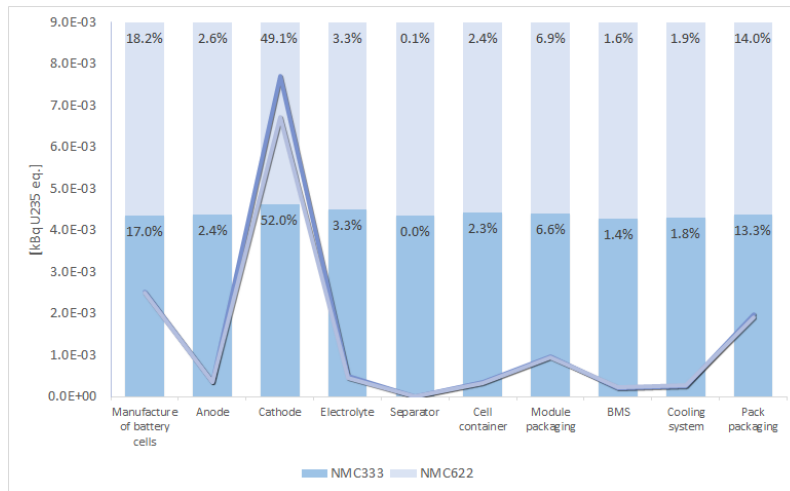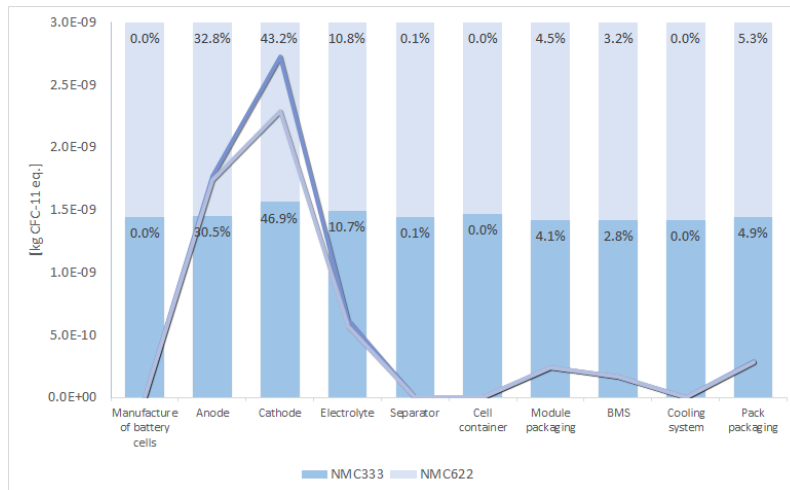
Figure 5.10: Contribution of different components and processes to the cradle-to-gate environmental impacts on ozone depletion for NMC333 and NMC622. The right axis represents the absolute value whereas the left represents shares of the total impact on ozone depletion.

by comparing LCIA results generated by different electricity grid mixes and also by using absolute values rather than the ones that are per kWh of the total energy provided over the service life by the battery system.

5.3.4 End-of-life phase

In the following section, the contribution to gate-to-grave impacts is analyzed. Figure 5.12 shows the total impact on each category for NMC333 and NMC622 from the end-of-life phase.The recycling of the batteries are divided into four parts: cell recycling, passive parts recycling, OEM parts recycling and unsorted battery fraction. Cell recycling includes all active materials that are directly linked to the electrochemical performance which are the cathode, anode, electrolyte and separator. The passive parts includes all packaging which are the cell container, module packaging and pack packaging. The OEM parts are the supportive systems to the battery including the battery management system and cooling system. Lastly, the unsorted battery fraction is the 5% share of the battery that end up in the landfill which may be due to the materials having been sorted incorrectly or not recoverable.

As seen in chapter 4, the total impact on each impact category from the end-of-life phase was low compared to the other life cycle stages and thus, the analysis of this life cycle stage will not be as comprehensive as the production phase. What can be seen in figure 5.12 is that NMC622 has a lower contribution to all impact categories in the four recycling parts which is mainly due to the fact that NMC333 weighs more than NMC622. Another reason is the difference in material composition, the NMC622 has, for example, around 1.2% less battery cell per kg battery than NMC333 which is the component that has a relatively high contribution to the majority of the impact categories when recycled. What more can be seen in figure 5.12 is that passive parts recycling has relatively high contribution on several
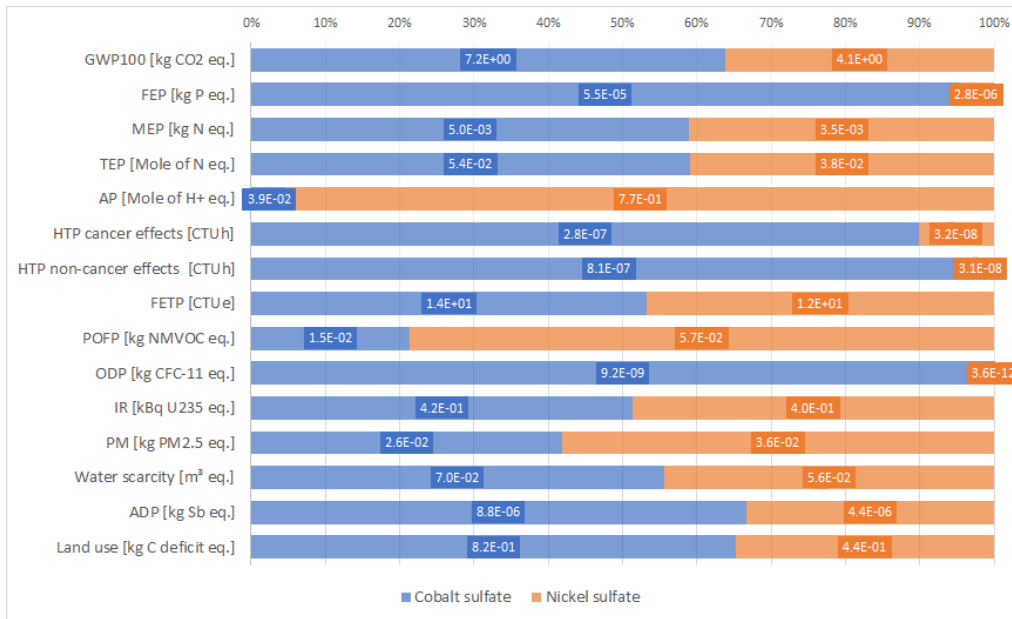
Figure 5.11: Contribution of cradle-to-grave impacts from production of cobalt and nickel sulfate. The stacked bars shows the percentage each impact categories contributes to a total and values represent the absolute per kg cobalt or nickel.

impact categories as well. By looking at the most important impact categories according to the weighting there were two processes that were responsible for the high contribution to the environmental impact from cell recycling: cell dismantling and metallic alloy treatment. In the case of cell dismantling, it was the electricity usage and process stream from natural gas that accounted for the highest shares. As for the metallic alloy treatment, it was the use of the chemicals sodium hydroxide and sulphuric acid. For passive parts recycling, the highest shares of the contribution to the most important impact categories were solely from the recycling of steel.

5.4 Sensitivity analysis

To test the robustness of the LCA results, sensitivity analyses have been conducted. The results of this analysis can be found below.

5.4.1 Functional unit

It was concluded in section 5.3.3 that the functional unit recommended by the PEFCR was more beneficial for NMC333 since the battery consume more kWh per battery lifetime. In the following sensitive analysis, the total weighted environmental impact will be investigated by changing the functional unit to see how crucial the choice of functional unit is. Table 5.7 shows the difference in percentage on how much NMC622 contributes to the weighted environmental impacts compared to NMC333 when using different functional units.

The results of the sensitivity analysis on the function unit show that NMC622 would
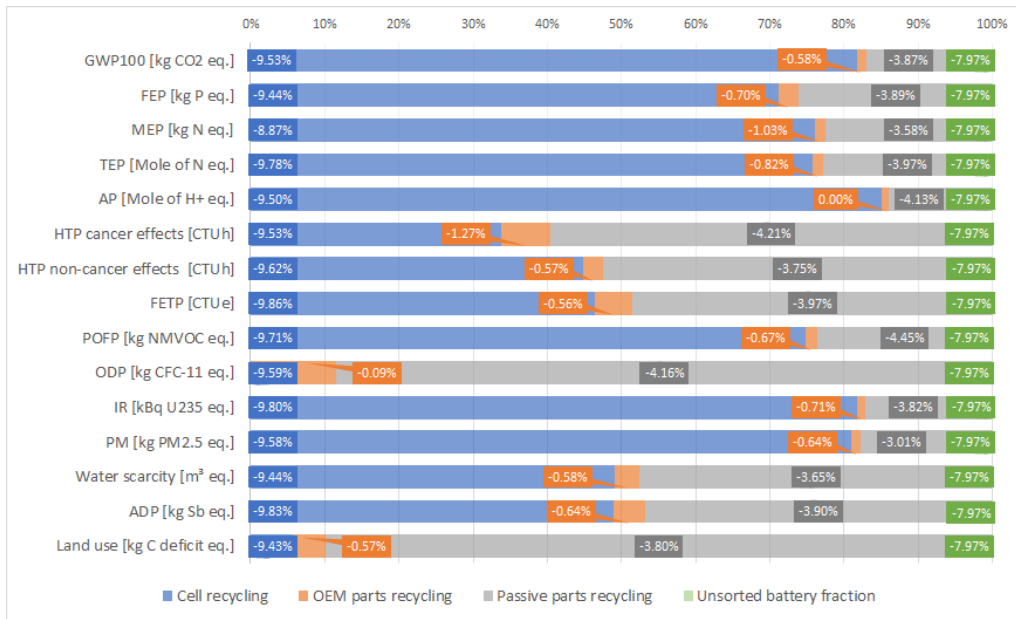
Figure 5.12: Contribution of gate-to-grave impacts from the end-of-life phase. The percentages represent the difference in values of NMC622 compared to NMC333

have even lower environmental performance than NMC333 if the functional unit was per kg battery pack instead of the baseline. The reason for this is due to the fact that the total weight of the battery is not considered which is more beneficial for NMC333 as it is heavier. The results does also indicate that the material composition of the NMC622 lead to a higher contribution to the total weighted environmental impact than NMC333. In the case of the functional unit per battery pack, the NMC622 has slightly higher environmental performance than NMC333 which is, as explained in section 5.3.3, due to not consider how much energy the batteries provides over their service life. In short, the reason for this is that NMC333 benefits from dividing the mass of the battery with the total energy provided over the service life as the battery need to produce more energy per km compared to NMC622.

5.4.2 Electricity grid mix

The following sensitivity analysis focuses on the choice of electricity grid mix in the use-phase. Around 80% of total energy usage is from when the batteries are used in a electric vehicle and thus, it is of interest to investigate how much the LCA results are affected by the choice of different electricity grid mixes. The country-specific electricity grid mixes that have been included in the sensitivity analysis is from the following countries: Germany (DE), Spain (ES) and Norway (NO). Figure 5.13 shows how the weighted environmental impacts of NMC622 vary when using different electricity grid mixes in the use-phase. Furthermore, the figure shows the difference in percentage on how much NMC622 contributes to the total weighted environmental impact compared to NMC333.

The sensitivity analysis indicates that the use of different electricity grid mix has a significant influence on the results of the weighted environmental impacts. For

Table 5.7: The difference in percentage on how much NMC622 contributes to the weighted environmental impacts compared to NMC333 with respect to different functional units. The baseline is 1 kWh of the total energy provided over the service life by the battery system.

NMC622 versus NMC333

Impact categories	Baseline (per kWh)	Per kg battery pack	Per battery pack
Climate change	-2.3%	5.5%	-4.1%
Ionising radiations	-0.6%	-1.6%	-5.6%
Particulate matter/ Respiratory Inorganics	2.3%	27%	15%
Acidification	18%	10%	0.5%
Photochemical ozone formation	-0.2%	7.3%	-2.4%
Eutrophication terrestrial	-3.3%	7.8%	-1.8%
Eutrophication freshwater	-0.1%	4.4%	-5.2%
Eutrophication marine	-3.1%	7.8%	-2.1%
Ozone depletion	-8.9%	4.6%	-5.0%
Total environmental impact	1.6%	9.7%	-0.3%

instance, if the vehicles were assumed to be used in Germany, the NMC622 would be considered to have better environmental performance than NMC333. The reason for this is that the production of electricity in Germany has a higher amount CO2-equivalents emissions compared to the other countries which in turn affect the results on climate change. This is beneficial for NMC622 as it has lower energy consumption per km than NMC333. Furthermore, it was concluded in section x that climate change has the highest share of the total weighted environmental impact which makes changes in climate change more sensitive than compared to the other impact categories. As for the electricity production in Spain and Norway, the total environmental impact is less compared to the European average and Germany. In addition, the NMC622 has a lower environmental performance compared to NMC333 in these two countries. The reason for this is that the impact categories, particulate matter, and acidification, has a higher share of the total environmental impact which is the two that NMC622 contributes to more than NMC333.

5.4.3 Cobalt and nickel sulfate

From the contribution analysis, it was clear that the production of cobalt and nickel sulfate is responsible for a large share of the total environmental impacts. Furthermore, a significant distinction from NMC622 and NMC333 is the cathode chemistry since they have a different proportion of cobalt and nickel. It is thus, interesting to
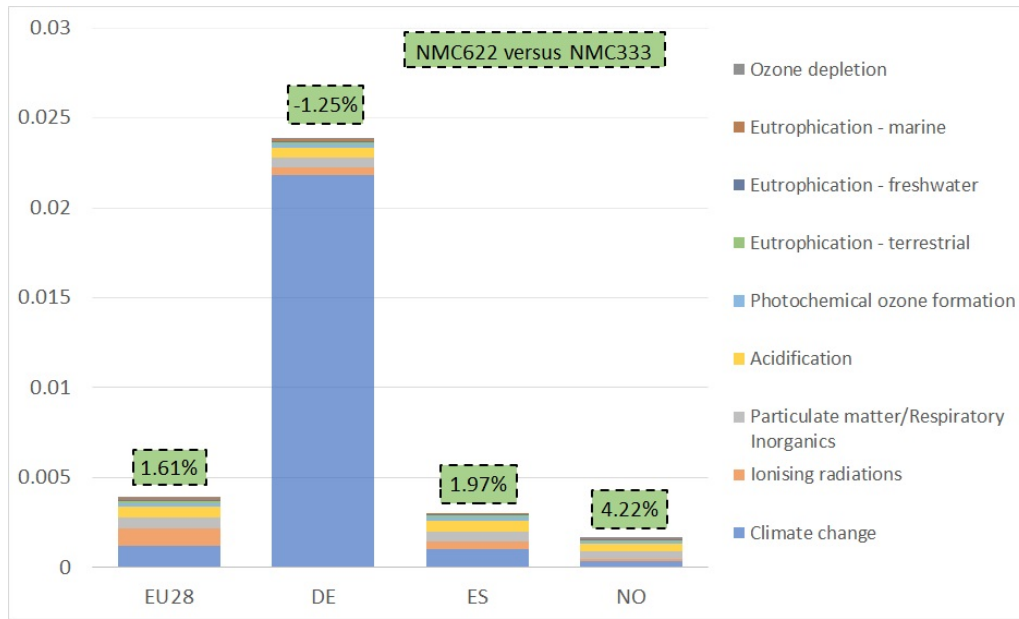
Figure 5.13: The results of the weighted environmental impact of NMC622 with the use of different electricity grid mix in the use-phase. The boxes with dashed outlines are representing a comparison of NMC622 with NMC333 with respect to the total weighted environmental impacts.

investigate how different datasets influence the total weighted environmental impact from these two batteries. The comparison of the production of nickel and cobalt is limited to the datasets provided by the PEFCR. Figure 5.14 shows how much the environmental impacts vary when the dataset on the production of cobalt from the PEFCR study is used instead. With the datasets from the PEFCR, the total weighted environmental impact slightly increased for both batteries. In addition, the difference in the total weighted environmental impact between the two batteries was reduced from 1.61% to 0.96%. However, the NMC622 has still lower environmental performance than NMC333 as in the baseline scenario.

Figure 5.14 shows how much the environmental impacts vary when the dataset on the production of nickel from the PEFCR study is used instead. With the datasets from the PEFCR, the total weighted environmental impact slightly decreased for both batteries. In addition, the difference in the total weighted environmental impact between the two batteries was reduced from 1.61% to 0.90%. The outcome is similar to the sensitivity analysis for cobalt in the sense that NMC622 still has lower environmental performance than NMC333 and that the difference between them was slightly reduced.
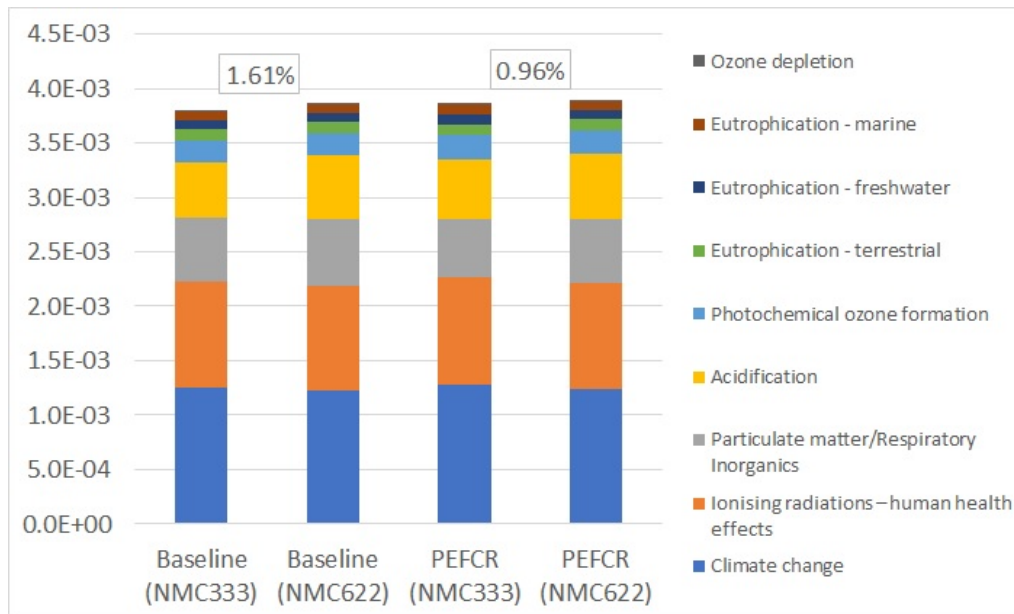
Figure 5.14: Sensitivity analysis on the production of cobalt and how it influence the weighted impact categories. The datasets used in this study , which is from Dai et al. (2018a), is compared with the datasets from the PEFCR (Siret et al., 2018).
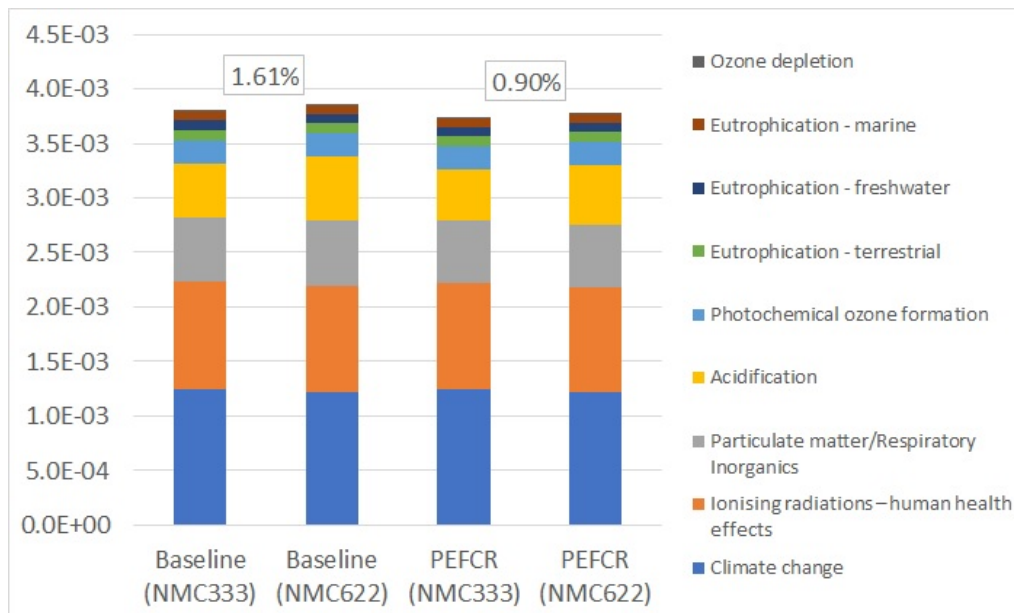
Figure 5.15: Sensitivity analysis on the production of nickel and how it influence the weighted impact categories. The datasets used in this study , which is from Dai et al. (2018a), is compared with the datasets from the PEFCR (Siret et al., 2018).

6

DISCUSSION

Key findings from the LCIA results include that the production and use phase is the life cycle stages with the highest environmental impacts and thus more relevant. However, in the use phase, the difference in percentage between the two batteries was relatively low in all impact categories which concludes that environmental impacts are more sensitive to changes in bill-of-materials than in mass of the battery. Furthermore, the screening by normalization and weighting shows that over 80% of the total environmental impact is from the following impact categories: climate change, ionizing radiations, particulate matter/respiratory inorganics and acidification. From these four, the impact on acidification and particulate matter was higher from NMC622 than NMC333. The difference in the impact on acidification was exceptional compared to the rest and became a crucial factor of the outcome in which NMC622 turn out to have a higher total environmental impact than NMC333. The main reason is that the production of nickel sulfate has a higher impact compared to cobalt sulfate due to relatively high emissions of sulfur dioxide. Overall, the results from the contribution analysis show that the cathode is the battery component that has the greatest impact and also the one that differs most between the two batteries.

The results from the LCA study shows that NMC622 has better environmental performance in all most representative impact categories except for acidification and particulate matter. It has lower energy consumption during use-phase and requires less material per kWh compared to NMC333. However, the higher proportion of nickel in the active cathode material causes NMC622 to perform worse than NMC333 in terms of the total environmental impact. Given the results, it is yet too early to prove which of the batteries has the best overall environmental impact since the difference in the results are marginal and due to uncertainties in the data. Instead, the results provide an early insight into which life cycle steps, components, processes and impact categories that are most relevant when comparing the cathode chemistries NMC622 and NMC333. The main stakeholders that the LCA study was intended for are those involved in the ALINE project. The fact that the difference in environmental performance between the batteries is marginal informs the actors that the battery lifetime may have a crucial role in an environmental perspective.

A methodological choice affecting the results in an LCA is the LCIA methods. The choice of methods was based on the recommendation from the PEFCR for High Specific Energy Rechargeable Batteries for Mobile Applications which is initiated by the European Commission to harmonize the LCA methodologies for specific product categories. By following specific guidelines on how to perform an LCA, the

comparability of products in the same category increases. In addition to the LCIA methods, the choice of functional unit is determined in the PEFCR. The sensitivity analysis of the functional unit shows how the results could vary and how it affects the comparability.

The uncertainties in the study that deserves attentions are the ones affecting the most relevant impact categories as well as the difference in results between the batteries. For example, uncertainty in the choice of electricity grid mix may not be as important as uncertainties in the production of the cathode as different material proportion is used for NMC622 and NMC333. One of the uncertainties is that the batteries are theoretically designed in a model provided by a single source. The credibility of the data on the characteristics of the batteries and the majority of the BOMs could have been strengthened if there were more models available. Even better would have been if there were data on actual batteries available for the chosen cathode chemistries. Other important uncertainties are the ones affecting the upstream data that account for a high share of the total contribution to the impact categories. The cathode has the highest contribution to the impact categories that accounts for more than 80% of the total environmental impact. Among the upstream data, the production of nickel and cobalt was often responsible for a relatively high share of the total environmental impact. The data on the production of nickel was not entirely transparent as only elementary flows were provided. If the information on the production processes was available, the LCA data could have been modeled with different datasets.

7

CONCLUSION

In the following chapter, the research questions presented in the goal and scope will be assessed.

> **Research question 1:** How is NMC622 performing environmentally compared with NMC333 throughout their life cycle?

When the LCIA results were normalized and weighted according to the PEFCR, the NMC622 turned out to have around 2% higher environmental impact than NMC333. When looking at the life cycle stages, it was only in the production phase that NMC622 had a higher environmental impact compared to NMC333 which was due to higher contribution to acidification and particulate matter. In the use-phase, the NMC622 had around 2% lower energy consumption than NMC333 due to higher energy density. As for the end-of-life phase, the NMC622 had a lower contribution to all impact categories which was mainly due to the fact that it has lower battery weight and consists of a smaller proportion of battery cells per kg battery than NMC333.

> **Research question 2:** Which are the hotspots in the life cycle and what influence does the configuration of the cathode chemistry have in relation to them?

The weighted LCIA results were mainly influenced by climate change followed by ionizing radiation, particulate matter, and acidification which accounted for over 80 % of the total environmental impact. However, even though climate change was responsible for a higher share of the total impact, the difference in the contribution to the impact categories between the batteries was greater for acidification. Furthermore, the highest share of the contribution to climate change as well as ionizing radiation was from the use phase and thereby less significant to the research question as the results are more dependent on the choice of the electricity mix in the use phase rather than the cathode chemistry configuration. The NMC622 had around 15% higher contribution to acidification compared to NMC333, which is a relatively large difference when compared to the other impact categories. The battery component that was mainly responsible for the increase in environmental impact of the NMC622 was the cathode. More specifically, it was the production of nickel sulfate that resulted in higher contribution to both acidification and particulate matter. The production process that accounted for the highest contribution to acidification and particulate matter was nickel refining and was mainly due to the air emission

of sulfur dioxide. For 1 kg of refined nickel produced, 1.04 kg of sulfur dioxide emissions is emitted into the air according to the nickel institute. As for climate change, the cathode was again the hotspot. However, in this case, NMC333 had a higher contribution to the impact category since the production of cobalt sulfate accounted for a larger share than nickel sulfate and also due to the fact that NMC622 has a smaller proportion of active cathode material per kg battery than NMC333. As for the ionizing radiation, it was the similar case as climate change where the production of cobalt sulfate accounted for a larger share than nickel sulfate and the fact that the proportion of active cathode material was less per kg battery for NMC622 than NMC333.

Apart from the production phase, the use phase was also considered as a hotspot as it accounted for around 62% of the total weighted environmental impact. However, the configuration of the cathode chemistry did not have as much influence on the environmental impact between NMC622 and NMC333 in the use phase compared to the production phase. This indicates that the change in the material composition may have a higher influence than the change in energy density.

References

An, S. J., Li, J., Du, Z., Daniel, C., & Wood III, D. L. (2017). Fast formation cycling for lithium ion batteries. *Journal of Power Sources*, *342*, 846–852.

Bauer, C., Hofer, J., Althaus, H.-J., Del Duce, A., & Simons, A. (2015). The environmental performance of current and future passenger vehicles: life cycle assessment based on a novel scenario analysis framework. *Applied energy*, *157*, 871–883.

Baumann, H., & Tillman, A.-M. (2004). *The hitchhiker's guide to lca : an orientation in life cycle assessment methodology and application.* Lund : Studentlitteratur, 2004. Retrieved from `http://proxy.lib.chalmers.se/` `login?url=http://search.ebscohost.com/login.aspx?direct=true&db=` `cat06296a&AN=clc.b1274116&lang=sv&site=eds-live&scope=site`

Bonell, M., Carrillo, V., Chanson, C., Ebert, T., Gediga, J., Mistry, M., . . . Yazicioglu, B. (2015). *Pef screening report on high specific energy rechargeable batteries for mobile applications.*

Bütler, T., & Winkler, H. (2013). Energy consumption of battery electric vehicles (bev). *EMPA Materials Science & Technology*.

Dai, Q., C., K., & Elgowainy, A. (2018a). *Cobalt life cycle analysis update for the greet model* (Tech. Rep.). Argonne, IL (United States): Argonne National Lab.(ANL).

Dai, Q., C., K., & Elgowainy, A. (2018b). *Update of bill-of-materials and cathode materials production for lithium-ion batteries in the greet model* (Tech. Rep.). Argonne, IL (United States): Argonne National Lab.(ANL).

Dai, Q., Dunn, J., Kelly, C., & Elgowainy, A. (2017). *Update of life cycle analysis of lithium-ion batteries in the greet* (Tech. Rep.). Argonne, IL (United States): Argonne National Lab.(ANL).

Del Duce, A., Egede, P., Öhlschläger, G., Dettmer, T., Althaus, H., Thomas Bütler, T., & Szczechowicz, E. (2013). *Guidelines for the lca of electric vehicles.* Brussels: European Union Seventh Framework Programme.

Deng, Y., Li, J., Li, T., Zhang, J., Yang, F., & Yuan, C. (2017a). Life cycle assessment of high capacity molybdenum disulfide lithium-ion battery for electric vehicles. *Energy*, *123*, 77–88.

References

Deng, Y., Li, J., Li, T., Zhang, J., Yang, F., & Yuan, C. (2017b). Life cycle assessment of lithium sulfur battery for electric vehicles. *Journal of Power Sources*, *343*, 284 - 295. Retrieved from `http://proxy.lib.chalmers.se/login?url=http://search.ebscohost.com/login.aspx?direct=true&db=edselp&AN=S0378775317300368&lang=sv&site=eds-live&scope=site`

Dunn, J. B., Gaines, L., Barnes, M., Sullivan, J. L., & Wang, M. (2014). *Material and energy flows in the materials production, assembly, and end-of-life stages of the automotive lithium-ion battery life cycle* (Tech. Rep.). Argonne, IL (United States): Argonne National Lab.(ANL).

Dunn, J. B., James, C., Gaines, L., Gallagher, K., Dai, Q., & Kelly, J. C. (2015). *Material and energy flows in the production of cathode and anode materials for lithium ion batteries* (Tech. Rep.). Argonne, IL (United States): Argonne National Lab.(ANL), Argonne, IL (United States).

Ellingsen, L. A., Majeau-Bettez, G., Singh, B., Srivastava, A. K., Valen, L. O., & Strmman, A. H. (2014). Life cycle assessment of a lithium-ion battery vehicle pack. *JOURNAL OF INDUSTRIAL ECOLOGY*(1), 113. Retrieved from `http://proxy.lib.chalmers.se/login?url=http://search.ebscohost.com/login.aspx?direct=true&db=edsbl&AN=RN347818239&lang=sv&site=eds-live&scope=site`

Elwert, T., Goldmann, D., Römer, F., Buchert, M., Merz, C., Schueler, D., & Sutter, J. (2015). Current developments and challenges in the recycling of key components of (hybrid) electric vehicles. *Recycling*, *1*(1), 25–60.

European Commission. (2017). *Guidance document, - guidance for the development of product environmental footprint category rules (pefcrs).*

European Commission-Joint Research Centre. (2011). Institute for environment and sustainability: International reference life cycle data system (ilcd) handbook-recommendations for life cycle impact assessment in the european context. *EUR 24571 EN. Luxemburg.*

European Joint Research Centre. (2010). International reference life cycle data system (ilcd) handbook e general guide for life cycle assessment e detailed guidance. *Institute for Environment and Sustainability.*

Fazio, S., Castellani, V., Sala, S., Schau, E., Secchi, M., Zampori, L., & Diaconu, E. (2018). Supporting information to the characterisation factors of recommended ef life cycle impact assessment methods. *New models and differences with ILCD. EUR*, *28888*.

Federal Highway Administration. (2018). *Average annual miles per driver by age group.* Retrieved 2018-10-22, from `https://www.fhwa.dot.gov/ohim/onh00/bar8.htm`

Frischknecht, R., Braunschweig, A., Hofstetter, P., & Suter, P. (2000). Human health damages due to ionising radiation in life cycle impact assessment. *Environmental impact assessment Review*, *20*(2), 159–189.

Gediga, J., Sandilands, J., Roomanay, N., & Boonzaier, S. (2015). *Life cycle assessment of nickel products.*

Hofer, J. (2014). *Sustainability assessment of passenger vehicles: Analysis of past trends and future impacts of electric powertrains* (Unpublished doctoral dissertation). ETH Zurich.

Jing, L., Downie, L. E., Lin, M., Wenda, Q., & Dahn, J. R. (2015). Study of the failure mechanisms of lini0.8mn0.1co0.1o2 cathode material for lithium ion batteries. *Journal of the Electrochemical Society*, *162*(7), A1401. Retrieved from `http://proxy.lib.chalmers.se/login?url=http://search.ebscohost.com.proxy.lib.chalmers.se/login.aspx?direct=true&db=edb&AN=103137209&lang=sv&site=eds-live&scope=site`

Jung, R., Morasch, R., Karayaylali, P., Phillips, K., Maglia, F., Stinner, C., ... Gasteiger, H. A. (2018). Effect of ambient storage on the degradation of ni-rich positive electrode materials (nmc811) for li-ion batteries. *Journal of the Electrochemical Society*, *165*(2), A132. Retrieved from `http://proxy.lib.chalmers.se/login?url=http://search.ebscohost.com/login.aspx?direct=true&db=edo&AN=128012397&lang=sv&site=eds-live&scope=site`

Li, W., Song, B., & Manthiram, A. (2017). High-voltage positive electrode materials for lithium-ion batteries. *CHEMICAL SOCIETY REVIEWS*(10), 3006. Retrieved from `http://proxy.lib.chalmers.se/login?url=http://search.ebscohost.com.proxy.lib.chalmers.se/login.aspx?direct=true&db=edsbl&AN=RN384681231&lang=sv&site=eds-live&scope=site`

Ma, L., Self, J., Nie, M., Glazier, S., Wang, D. Y., Lin, Y. S., & Dahn, J. R. (2015). A systematic study of some promising electrolyte additives in li[ni1/3mn1/3co1/3]o2/graphite, li[ni0.5mn0.3co0.2]/graphite and li[ni0.6mn0.2co0.2]/graphite pouch cells. *JOURNAL OF POWER SOURCES*, 130. Retrieved from `http://proxy.lib.chalmers.se/login?url=http://search.ebscohost.com/login.aspx?direct=true&db=edsbl&AN=RN372419086&lang=sv&site=eds-live&scope=site`

Masoni, P. (2016). Lca compendium—the complete world of life cycle assessment (book series) series editors: Walter klöpffer and mary ann curran. *INTERNATIONAL JOURNAL OF LIFE CYCLE ASSESSMENT*(4), 595. Retrieved from `http://proxy.lib.chalmers.se/login?url=http://search.ebscohost.com/login.aspx?direct=true&db=edsbl&AN=RN376638170&lang=sv&site=eds-live&scope=site`

Nelson, P., Gallagher, K., Bloom, I., Dees, D., & Ahmed, S. (2018). *Batpac: A lithium-ion battery performance and cost model for electric-drive vehicles (version 3.1-28june2018) [computer software].* Retrieved 2018-10-08, from `http://www.cse.anl.gov/batpac/index.html`

Olofsson, Y., & Romare, M. (2013). *Life cycle assessment of lithium-ion batteries for plug-in hybrid buses* [Master's thesis]. Chalmers University of Technology.

Retrieved from `http://publications.lib.chalmers.se/records/fulltext/180166/180166.pdf`

Pachauri, R. K., Allen, M. R., Barros, V. R., Broome, J., Cramer, W., Christ, R., ... others (2014). *Climate change 2014: synthesis report. contribution of working groups i, ii and iii to the fifth assessment report of the intergovernmental panel on climate change.* Ipcc.

Pistoia, G., & Liaw, B. (2018). *Behaviour of lithium-ion batteries in electric vehicles. [electronic resource] : Battery health, performance, safety, and cost.* Cham : Springer International Publishing : Imprint: Springer, 2018. Retrieved from `http://proxy.lib.chalmers.se/login?url=http://search.ebscohost.com/login.aspx?direct=true&db=cat06296a&AN=clc.b2503480&lang=sv&site=eds-live&scope=site`

Romare, M., & Dahllöf, L. (2017). *The life cycle energy consumption and greenhouse gas emissions from lithium-ion batteries. a study with focus on current technology and batteries for light-duty vehicle.* IVL Swedish Environmental Research Institute Stockholm, Sweden.

Sims R., R., Schaeffer, F., Creutzig, X., Cruz-nunez, M., D'Agosto, D., Dimitriu, M., ... Tiwari (2014). *Transport. in: Climate change 2014: Mitigation of climate change. contribution of working group iii to the fifth assessment report of the intergovern- mental panel on climate change* (R. Edenhofer O. et al., Eds.). United Kingdom and New York, NY, USA: Cambridge University Press.

Siret, C., Tytgat, J., Ebert, T., Mistry, M., Thirlaway, C., Schutz, B., ... Carrillo, V. (2018). *Pefcr - product environmental footprint category rules for high specific energy rechargeable batteries for mobile application.* European Commission.

Stocker, T. (2013). *Climate change 2013 : the physical science basis : Working group i contribution to the fifth assessment report of the intergovernmental panel on climate change.* Cambridge : Cambridge University Press, 2013. Retrieved from `http://proxy.lib.chalmers.se/login?url=http://search.ebscohost.com/login.aspx?direct=true&db=cat06296a&AN=clc.b1765952&lang=sv&site=eds-live&scope=site`

Tank, A. K., Wijngaard, J., Können, G., Böhm, R., Demarée, G., Gocheva, A., ... others (2002). Daily dataset of 20th-century surface air temperature and precipitation series for the european climate assessment. *International journal of climatology*, *22*(12), 1441–1453.

Tutuianu, M., Marotta, A., Steven, H., Ericsson, E., Haniu, T., Ichikawa, N., & Ishii, H. (2013). Development of a world-wide worldwide harmonized light duty driving test cycle (wltc). *Draft Technical Report, DHC subgroup, GRPE-67-03*.

Tytgat, J. (2013). The recycling efficiency of li-ion ev batteries according to the european commission regulation, and the relation with the end-of-life vehicles directive recycling rate. *2013 World Electric Vehicle Symposium & Exhibition (EVS27)*, 1. Retrieved from `http://proxy.lib.chalmers.se/login?url=http://`

`search.ebscohost.com.proxy.lib.chalmers.se/login.aspx?direct=`
`true&db=edb&AN=99489156&lang=sv&site=eds-live&scope=site`

Van Oers, L., de Koning, A., Guinée & G, J., & Huppes, G. (2002). *Abiotic resource depletion in lca.* Road and Hydraulic Engineering Institute.

Wang, M., Elgowainy, A., Benavides, P., Burnham, A., Cai, H., Dai, Q., . . . L., O. (2018). *The greenhouse gases, regulated emissions, and energy use in transportation model.* Retrieved 2018-10-29, from `https://greet.es.anl.gov`

Zubi, G., Dufo-López, R., Carvalho, M., & Pasaoglu, G. (2018). The lithium-ion battery: State of the art and future perspectives. *Renewable and Sustainable Energy Reviews*, *89*, 292 - 308. Retrieved from `http://proxy.lib.chalmers.se/` `login?url=http://search.ebscohost.com/login.aspx?direct=true&db=` `edselp&AN=S1364032118300728&lang=sv&site=eds-live&scope=site`

References

A
Battery model

A.1 BOMs derivations

The following equations are either found from the report by Dunn et al. (2014) or by backtracking existing equations in the BatPac model. The validity of all equations have been tested with help of the latest report on the update of BOMs in the GREET Model (Dai et al., 2018b). The choice of materials for each component has also been inspired by the report.

A.1.1 Current collectors

Mass calculation of aluminium current collector per unit cell. The thickness and area are assumed to be 15 μm respective 2.1 m^2.

$$m_{Al\_foil} = A_{Al\_foil} \times \delta_{Al\_foil} \times \rho_{Al} \qquad \text{(A.1)}$$

Where:

$$m_{Al\_foil} : \text{the mass of the aluminium foil (g):}$$
$$A_{Al\_foil} : \text{the area of the aluminum foil (cm}^2\text{):}$$
$$\delta_{Al\_foil} : \text{the thickness of the aluminum foil (cm); and}$$
$$\rho_{Al} : \text{the density of aluminum (2.7 g/cm}^3\text{).}$$

mass calculation of copper current collector per unit cell. The thickness and area is assumed to be 10 μm respective 2.2 m^2.

$$m_{Cu\_foil} = A_{Cu\_foil} \times \delta_{Cu\_foil} \times \rho_{Cu} \qquad \text{(A.2)}$$

Where:

$$m_{Cu\_foil} : \text{the mass of the copper foil (g):}$$
$$A_{Cu\_foil} : \text{the area of the copper foil (cm}^2\text{):}$$
$$\delta_{Cu\_foil} : \text{the thickness of the copper foil (cm); and}$$
$$\rho_{Cu} : \text{the density of copper (8.92 g/cm}^3\text{).}$$

A.1.2 Separator

Mass calculation of separator per unit cell. The thickness and area are assumed to be 15 μm respective 4.1 m^2. The outer layer consisting of PP is assumed to be 80% of the total mass whereas the inner layer consisting of PE is assumed to be 20% of the total mass.

$$m_{Sep} = \delta_{Sep} \times A_{Sep} \times \rho_{Sep} \tag{A.3}$$

Where:

$$m_{Sep} : \text{the mass of the separator (g);}$$
$$\delta_{Sep} : \text{the thickness of the separator (cm);}$$
$$A_{Sep} : \text{the area of the seperator (cm}^2\text{); and}$$
$$\rho_{Sep} : \text{the density of the separator (0.46 g/cm}^3\text{).}$$

A.1.3 Electrolyte

Mass calculation of the salt LiPF$_6$ per unit cell. The volume and concentration are assumed to be 0.2 liters respective 1.2 mol/l.

$$m_{LiPF6} = V_{elec} \times c_{LiPF6} \times M_{LiPF6} \tag{A.4}$$

Where:

$$m_{LiPF6} : \text{the mass of the LiPF}_6\text{ (g);}$$
$$V_{elec} : \text{the volume of the electrolyte (l);}$$
$$c_{LiPF6} : \text{the concentration of the LiPF}_6\text{ (mol/l); and}$$
$$M_{LiPF6} : \text{the molar mass of the LiPF}_6\text{ (151.91 g/mol).}$$

Mass calculation of ethylene and dimethyl carbonate per unit cell. The mass is calculated by subtracting the mass of the salt with the remaining mass of the electrolyte.

$$m_{EC\&DMC} = \frac{(\rho_{elec} \times 1000 \times V_{elec}) - m_{LiPF6}}{2} \tag{A.5}$$

Where:

$$m_{EC\&DMC} : \text{the mass of the ethylene and dimethyl carbonate (g);}$$
$$\rho_{elec} : \text{the electrolyte density (l);}$$
$$V_{elec} : \text{the volume of the electrolyte (l); and}$$
$$m_{LiPF6} : \text{the mass of the LiPF}_6\text{ (g).}$$

A.1.4   Cell container

Mass calculation of aluminium multilayer film per unit cell. The cell dimensions are the following: 342mm length, 106 mm width and 20 mm thick. The thickness of the aluminium layer is assumed to be 100 μm.

$$m_{alu.layer} = (W_{cell} + 2 \times \delta_{cell} + 6) \times (L_{cell} - 6) \times \delta_{alu.layer} \times \frac{2}{1000} \times \frac{\rho_{alu}}{1000} \quad (A.6)$$

Where:

$$
\begin{aligned}
m_{alu.layer} &: \text{the mass of the aluminium multilayer film (g);} \\
W_{cell} &: \text{the width of the cell (cm);} \\
\delta_{cell} &: \text{the thickness of the cell (cm);} \\
L_{cell} &: \text{the length of the cell (cm);} \\
\delta_{alu.layer} &: \text{the thickness of the aluminium layer (cm); and} \\
\rho_{cell} &: \text{the density of aluminium (2.7 g/cm}^3\text{).}
\end{aligned}
$$

Mass calculation of PET multilayer film per unit cell. The thickness of the aluminium layer is assumed to be 30 μm.

$$m_{PET.layer} = (W_{cell} + 2 \times \delta_{cell} + 6) \times (L_{cell} - 6) \times \delta_{PET.layer} \times \frac{2}{1000} \times \frac{\rho_{PET}}{1000} \quad (A.7)$$

Where:

$$
\begin{aligned}
m_{alu.layer} &: \text{the mass of the aluminium multilayer film (g);} \\
W_{cell} &: \text{the width of the cell (cm);} \\
\delta_{cell} &: \text{the thickness of the cell (cm);} \\
L_{cell} &: \text{the length of the cell (cm);} \\
\delta_{alu.layer} &: \text{the thickness of the aluminium layer (cm); and} \\
\rho_{cell} &: \text{the density of PET (1.4 g/cm}^3\text{).}
\end{aligned}
$$

Mass calculation of PP multilayer film per unit cell. The thickness of the aluminium layer is assumed to be 20 μm.

$$m_{PET.layer} = (W_{cell} + 2 \times \delta_{cell} + 6) \times (L_{cell} - 6) \times \delta_{PP.layer} \times \frac{2}{1000} \times \frac{\rho_{PP}}{1000} \quad (A.8)$$

Where:

$$
\begin{aligned}
m_{alu.layer} &: \text{the mass of the aluminium multilayer film (g);} \\
W_{cell} &: \text{the width of the cell (cm);} \\
\delta_{cell} &: \text{the thickness of the cell (cm);} \\
L_{cell} &: \text{the length of the cell (cm);} \\
\delta_{alu.layer} &: \text{the thickness of the aluminium layer (cm); and} \\
\rho_{cell} &: \text{the density of PET (0.9 g/cm}^3\text{).}
\end{aligned}
$$

A.1.5 Module packaging

The mass of the components in the module package was calculated by multiplying by the number of modules in the battery pack which was assumed to be 12. The mass of the module terminals is assumed to consists of 80% of copper and the rest is for thermal insulation which is made of fiberglass.

A.1.6 Pack packaging

Mass calculation of aluminium battery jacket per unit battery pack. The area of the battery jacket is assumed to be 45,971 cm^2. In equation A.9, the insulation in the battery jacket is subtracted where the thickness of the insulation in the battery pack is assumed to be 10mm.

$$m_{j.alu} = (A_{j.alu} \times \tau) - (\frac{A_{j.alu} \times \delta_{j.ins} \times \rho_{j.ins}}{10}) \tag{A.9}$$

Where:

$m_{j.alu}$: the mass of the aluminium battery jacket (g);
$A_{j.alu}$: the area of the aluminium battery jacket (cm^2);
τ : the battery jacket weight parameter (1.11 g/cm^2);
$\delta_{j.ins}$: the thickness of the insulation layer in the jacket (cm); and
$\rho_{j.ins}$: the insulation density (0.032 g/cm^3).

Mass calculation of fiberglass thermal insulation per unit battery pack. The terminals of the battery pack consists of 75% copper and 25% ceramic. The ceramic work as insulator but in this study it has been simplified by assuming it is also made of fiberglass.

$$m_{b.ins} = (\frac{A_{j.alu} \times \delta_{j.ins} \times \rho_{j.ins}}{10}) + m_{term} \times 0.25 \tag{A.10}$$

Where:

$m_{b.ins}$: the mass of the fiberglass insulation in the battery pack (g);
$A_{j.alu}$: the area of the aluminium battery jacket (cm^2);
$\delta_{j.ins}$: the thickness of the insulation layer in the jacket (cm);
$\rho_{j.ins}$: the insulation density (0.032 g/cm^3); and
m_{term} : the mass of the terminals in the battery pack (g).

Mass calculation of each module inter-connect per unit battery pack. The total mass of the electronic parts are calculated by multiplying it with the number of modules in the battery pack which is assumed to be 20.

$$m_{tot.ic} = m_{.ic} \times (n_{mod} + 1) \tag{A.11}$$

Where:

$m_{tot.ic}$: the total mass of module inter-connect (g);
m_{ic} : the mass of each module inter-connect (g); and
n_{mod} : the number of modules in a battery pack.

A.2 Battery parameters

Table A.1 represents battery parameters on each level: battery system parameters, battery pack parameters and battery cell parameters. Complete information is found in the BatPac model provided by Nelson et al. (2018).

A.3 Battery model layout

Figure A.1 represents a screenshot on an excel spreadsheet where NMC333 and NMC622 was configured. The worksheet uses macros to change the cell chemistry and the material composition on BOMs for components that are influenced by the choice.

Table A.1: Battery parameters from the BatPac model.

Battery characteristics		
Battery System Parameters		
Number of packs per vehicle (parallel or series)	1.00	
Battery Pack Parameters		
Vehicle type (microHEV, HEV-HP, PHEV, EV)	EV	
Pack heat transfer fluid (EG-W, CA, CoolA)	EG-W	
Target battery pack power, kW	147.00	
Number of cells per module	12.00	
Number of cells in parallel	1.00	
Number of modules in row	5.00	
Number of rows of modules per pack	4.00	
Number of modules per battery pack	20.00	
Number of modules in parallel	1.00	
Cells per battery pack	240.00	
Total cells per battery system	240.00	
Battery Cell Parameters		
Cell chemistry	NMC333-G	NMC622-G
Active material molecular weight	93.88	94.39
Active material capacity, mAh/g:	155.00	180
Open circuit voltage at 20% SOC, V	3.52	3.565
Open circuit voltage at 50% SOC, V	3.67	3.75
Open circuit voltage at 80% SOC (mid SOC-HP), V	3.90	4
Open circuit voltage at 100% SOC, V	4.10	4.2
Positive electrode, g Li/g active material	0.078	0.077
Nickel, g/g active material	0.208	0.373
Cobalt, g/g active material	0.209	0.125
Manganese, g/g active material	0.195	0.116
Available battery energy, % of total	0.85	0.85
Battery lifetime, km	180000	180000
Driving distance, km	350	350
Calculated parameters		
Battery mass, kg	520	472
Battery pack energy, kWh	85.1	83.4
Energy consumption, MJ/km	0.74	0.73

Battery simulation	
Battery System Parameters	
Number of packs per vehicle (parallel or series)	1.00
Parallel packs (P) or series (S)	
Battery Pack Parameters	
Vehicle type (microHEV, HEV-HP, PHEV, EV)	EV
Pack heat transfer fluid (EG-W, CA, CoolA)	EG-W
Target battery pack power, kW	147.00
Number of cells per module	12.00
Number of cells in parallel	1.00
Number of modules in row	5.00
Number of rows of modules per pack	4.00
Number of modules per battery pack	20.00
Number of modules in parallel	1.00
Cells per battery pack	240.00
Total cells per battery system	240.00
Battery Cell Parameters	
Cell chemistry	NMC622-G
Active material molecular weight	94.39
Active material capacity, mAh/g:	180.00
Open circuit voltage at 20% SOC, V	3.57
Open circuit voltage at 50% SOC, V	3.75
Open circuit voltage at 80% SOC (mid SOC-HP), V	4.00
Open circuit voltage at 100% SOC, V	4.20
Positive electrode, g Li/g active material	0.077
Nickel, g/g active material	0.373
Cobalt, g/g active material	0.125
Manganese, g/g active material	0.116
Available battery energy, % of total	0.85
Battery lifetime, km	180000
Results	
Battery mass (kg)	472
Battery pack energy (kWh)	83.4
Driving distance (km)	350
Energy consumption (MJ/km)	0.73

[NMC333] [NMC622] ← **Click to change cell chemistry**

What changes?
- Battery cell chemistry in worksheet "Cell chemistry"
- The material composition on the active cathode material in worksheet "Cathode"
- The material composition on the precursor in worksheet "Cathode"

Figure A.1: Screenshot on the layout of the excel spreadsheet where the batteries are configured. The teal colored cells are key input assumptions, the purple colored cells are cell chemistry inputs and the white colored cells are calculated values.

B

Vehicle model

Figure B.1 represents a screenshot on an excel spreadsheet where the mass of the electric vehicle and the energy consumption was calculated which subsequently determine the characteristics of the battery. The worksheet uses macros which can be used to calculate the required battery mass once the parameters are configured.

Vehicle mass simulation (kg) 2012					
	Glider	Transmission	Battery	Motor/Generator/Controller	Total weight
BEV-baseline (2012)	1295	86	448	147	1976
BEV	1281	59	472	132.3	1944
Peak power for powertrain, kW		147			
Mass coefficient of transmission, kg/kW		0.4			
Mass coefficient of motor, kg/kW		0.90			
Glider coefficient, change in kg/change in powertrain		0.79			

Vehicle energy consumption simulation 2012	
Plug-to-wheel consumption, Wh/km	233.78
Battery-to-Wheel consumption, Wh/km	202.56
Battery-to-Wheel consumption Wh/miles	325.99
Charging losses, Wh/km	31.23
Standstill losses, Wh/km	1.57
Auxiliares, Wh/km	2.35
Heating and air conditioning, Wh/km	55.96
Basic consumption, Wh/km	142.67
Average driving speed, km/h	46.51
Vehicle mass, kg	1944
Required battery mass, kg	472
Required battery energy storage, kWh	83.4067779673403000
Battery energy storage (BatPac) , kWh	83.4067779673403000
Driving distance, km	350
Driving distance, miles	217
Vehicle lifetime, km	180000
Drag coefficient	0.28
Cross section, m2	2.2
Rolling resistance	0.01
Capacity accessible ratio	0.85
Air density at 20 Celsius degrees	1.2041

2012

Click to calculate the required battery mass for scenario 2012

Figure B.1: Screenshot on the layout of the excel spreadsheet where the vehicle is configured. The vehicle is configured with respect to another electric vehicle as a baseline from the year 2012. The teal colored cells are key input assumptions, the purple colored cells are cell chemistry inputs, the yellow colored cells are default input values and the white colored cells are calculated values.

X

X

C

LCI data from literature and databases

The tables provide information on which flows that enter and leave the process, their size, and unit and which source the information was collected. In addition, there is information about the interconnection between flows and processes on the column named tracked flows.

C.1   Battery pack assembly

Table C.1: LCI data on battery pack assembly for NMC622. The data have been rounded to two value figures and if the values for NMC333 is different it is shown in parentheses.

Flow	Amount	Unit	Tracked flows	Source
INPUTS				
Battery cell	7.9E-01 (8.0E-01)	kg	Table C.2	(Nelson et al., 2018)
Module packaging	5.0E-02 (4.8E-02)	kg	Table C.37	(Nelson et al., 2018)
Pack packaging	1.2E-01 (1.1E-01)	kg	Table C.50	(Nelson et al., 2018)
BMS	8.5E-03 (7.7E-03)	kg	Table C.38	(Nelson et al., 2018)
Cooling system	4.0E-02 (3.8E-02)	kg	Table C.43	(Nelson et al., 2018)
OUTPUTS				
Battery pack	1.0E+00	kg	Table C.51	(Nelson et al., 2018)

C.2   Battery cell assembly

Table C.2: LCI data on battery cell assembly for NMC622. The data have been rounded to two value figures and if the values for NMC333 is different it is shown in parentheses.

Flow	Amount	Unit	Tracked flows	Source
		INPUTS		
Cathode	4.3E-01 (4.6E-01)	kg	Table C.9	(Nelson et al., 2018)
Anode	3.5E-01 (3.2E-01)	kg	Table C.5	(Nelson et al., 2018)
Electrolyte	1.5E-01	kg	Table C.31	(Nelson et al., 2018)
Separator	1.8E-02 (1.6E-02)	kg	Table C.35	(Nelson et al., 2018)
Cell container	5.4E-02 (5.2E-02)	kg	Table C.36	(Nelson et al., 2018))
Dry room maintenance	1.8E+01 (1.6E+01)	MJ	Table C.3	(Dai et al., 2017)
Electrode drying and NMP recovery	1.2E+01 (1.1E+01)	MJ	Table C.4	(Dai et al., 2017)
Water (process water)	5.7E+00 (5.3E+00)	kg	Table C.58	(Dai et al., 2017)
		OUTPUTS		
Battery cell	1.0E+00	kg	Table C.1	(Nelson et al., 2018)
Municipal waste water treatment	2.0E+00	kg	Table C.58	(Siret et al., 2018)

C.2.1   Dry room maintenance

Table C.3: LCI data on dry room maintenance for NMC622. The data have been rounded to two value figures and if the values for NMC333 is different it is shown in parentheses.

Flow	Amount	Unit	Tracked flows	Source
		INPUTS		
Electricity	3.0E-01	MJ	Table C.58	(Dai et al., 2017)
Natural gas	7.0E-01	MJ	Table C.58	(Dai et al., 2017)
		OUTPUTS		
Dry room maintenance	1.0E+00	MJ	Table C.2	(Dai et al., 2017)

C.2.2   Electrode drying and NMP recovery

Table C.4: LCI data on electrode drying and NMP recovery for NMC622. The data have been rounded to two value figures and if the values for NMC333 is different it is shown in parentheses.

Flow	Amount	Unit	Tracked flows	Source
		INPUTS		
Natural gas	1.0E+00	MJ	Table C.58	(Dai et al., 2017)
		OUTPUTS		
Electrode drying and NMP recovery	1.0E+00	MJ	Table C.2	(Dai et al., 2017)

C.3   Anode

Table C.5: LCI data on production of Anode for NMC622. The data have been rounded to two value figures and if the values for NMC333 is different it is shown in parentheses.

Flow	Amount	Unit	Tracked flows	Source
		INPUTS		
Negative electrode paste	6.5E-01	kg	Table C.6	(Nelson et al., 2018)
Negative current collector	3.5E-01	kg	Table C.8	(Nelson et al., 2018)
		OUTPUTS		
Anode	1.0	kg	Table C.2	(Nelson et al., 2018)

C.3.1   Negative electrode paste

Table C.6: LCI data on production of negative electrode paste for NMC622. The data have been rounded to two value figures and if the values for NMC333 is different it is shown in parentheses.

Flow	Amount	Unit	Tracked flows	Source
		INPUTS		
Synthetic graphite	9.5E-01	kg	Table C.7	(Nelson et al., 2018)
Binder (PVDF)	5.0E-02	kg	Table C.58	(Nelson et al., 2018)
		OUTPUTS		
Negative electrode paste	1.0E+00	kg	Table C.5	(Nelson et al., 2018)

C.3.2 Synthetic graphite

Table C.7: LCI data on production of synthetic graphite for NMC622. The data have been rounded to two value figures and if the values for NMC333 is different it is shown in parentheses.

Flow	Amount	Unit	Tracked flows	Source
INPUTS				
Petrol coke	9.5E-01	kg	Table C.58	(Dunn et al., 2015)
Coal tar pitch	2.4E-01	kg	Table C.58	(Dunn et al., 2015)
Natural gas	5.4E+00	MJ	Table C.58	(Dunn et al., 2015)
Electricity	1.5E+01	MJ	Table C.58	(Dunn et al., 2015)
OUTPUTS				
Synthetic graphite	1.0E+00	kg	Table C.6	(Dunn et al., 2015)
NOx	9.3E-03	kg		(Dunn et al., 2015)
PM10	4.1E-03	kg		(Dunn et al., 2015)
PM2.5	2.1E-03	kg		(Wang et al., 2018)
SOx	6.4E-02	kg		(Dunn et al., 2015)
CO2	4.4E-01	kg		(Dunn et al., 2015)

C.3.3 Negative current collector

Table C.8: LCI data on production of negative current collector for NMC622. The data have been rounded to two value figures and if the values for NMC333 is different it is shown in parentheses.

Flow	Amount	Unit	Tracked flows	Source
INPUTS				
Copper	1.0E+00	kg	Table C.58	(Nelson et al., 2018)
OUTPUTS				
Negative current collector	1.0E+00	kg	Table C.5	(Nelson et al., 2018)

C.4 Cathode

Table C.9: LCI data on production of cathode for NMC622.The data have been rounded to two value figures and if the values for NMC333 is different it is shown in parentheses.

Flow	Amount	Unit	Tracked flows	Source
INPUTS				
Positive electrode paste	8.8E-01 (8.9E-01)	kg	Table C.10	(Nelson et al., 2018)
Positive current collector	1.2E-01 (1.1E-01)	kg	Table C.30	(Nelson et al., 2018)
OUTPUTS				
Cathode	1.0E+00	kg	Table C.2	(Nelson et al., 2018)

C.4.1 Positive electrode paste

Table C.10: LCI data on production of the positive electrode paste for NMC622.The data have been rounded to two value figures and if the values for NMC333 is different it is shown in parentheses.

Flow	Amount	Unit	Tracked flows	Source
INPUTS				
Active cathode matetrial (Li-NMC)	8.9E-01	kg	Table C.11	(Nelson et al., 2018)
Binder (PVDF)	5.0E-02	kg	Table C.58	(Nelson et al., 2018)
Conductive additive (Carbon black)	6.0E-02	kg	Table C.58	(Nelson et al., 2018)
OUTPUTS				
Positive electrode paste	1.0E+00	kg	Table C.9	(Nelson et al., 2018)

C.4.2 Active cathode material

Table C.11: LCI data on production of the active cathode material for NMC622.The data have been rounded to two value figures and if the values for NMC333 is different it is shown in parentheses.

Flow	Amount	Unit	Tracked flows	Source
INPUTS				
Precursor	9.5E-01	kg	Table C.12	(Dai et al., 2018b)
Lithium carbonate	3.8E-01	kg	Table C.28	(Dai et al., 2018b)
Electricity	2.3E+01	MJ	Table C.58	(Dai et al., 2018b)
OUTPUTS				
Active cathode matetrial	1.0E+00	kg	Table C.10	(Dai et al., 2018b)
Carbon dioxide	2.1E-01	kg		(Dai et al., 2018b)

C.4.3 Precursor

Table C.12: LCI data on production of the precursor for NMC622.The data have been rounded to two value figures and if the values for NMC333 is different it is shown in parentheses.

Flow	Amount	Unit	Tracked flows	Source
		INPUTS		
Nickel sulfate	1.0E+00 (5.6E-01)	kg	Table C.13	(Dai et al., 2018b)
Manganese sulfate	3.4E-01 (5.6E-01)	kg	Table C.20	(Dai et al., 2018b)
Cobalt sulfate	3.3E-01 (5.5E-01)	kg	Table C.22	(Dai et al., 2018b)
Sodium hydroxide	8.9E-01	kg	Table C.58	(Dai et al., 2018b)
Ammonium hydroxide	1.2E-01	kg	Table C.58	(Dai et al., 2018b)
Water (process water)	1.7E+01	kg	Table C.58	(Dai et al., 2018b)
Natural gas	4.1E+01	MJ	Table C.58	(Dai et al., 2018b)
		OUTPUTS		
Precursor	1.0E+00	kg	Table C.11	(Dai et al., 2018b)

C.4.4 Nickel sulfate

Table C.13: LCI data on production of nickel sulfate for NMC622.The data have been rounded to two value figures and if the values for NMC333 is different it is shown in parentheses.

Flow	Amount	Unit	Tracked flows	Source
		INPUTS		
Nickel oxide class I	4.8E-01	kg	Table C.14	Stoichiometry
Sulfuric acid	6.3E-01	kg	Table C.58	Stoichiometry
Natural gas	7.0E-01	MJ	Table C.58	(Dunn et al., 2015)
		OUTPUTS		
Nickel sulfate	1.0E+00	kg	Table C.12	(Dunn et al., 2015)

C.4.4.1 Nickel refining

Table C.14: LCI data on nickel refining for NMC622.The data have been rounded to two value figures and if the values for NMC333 is different it is shown in parentheses.

Flow	Amount	Unit	Tracked flows	Source
		INPUTS		
Electricity	5.5E+00	MJ	Table C.58	(Gediga et al., 2015)
Nickel matte	1.5E+01	kg	Table C.15	(Gediga et al., 2015)
Crude oil	1.4E-01	kg	Table C.58	(Gediga et al., 2015)
Hard coal	2.4E-01	kg	Table C.58	(Gediga et al., 2015)
Natural gas	7.3E-01	kg	Table C.58	(Gediga et al., 2015)
		OUTPUTS		
Products				
Class 1 Nickel	1.0E+00	kg	Table C.13	(Gediga et al., 2015)
Emissions to air				
Chromium	2.1E-07	kg		(Gediga et al., 2015)
Cobalt	1.9E-05	kg		(Gediga et al., 2015)
Copper	4.5E-04	kg		(Gediga et al., 2015)
Nickel	4.1E-04	kg		(Gediga et al., 2015)
Carbon dioxide	2.9E+00	kg		(Gediga et al., 2015)
Carbon monoxide	4.0E-03	kg		(Gediga et al., 2015)
Nitrogen oxides	6.0E-03	kg		(Gediga et al., 2015)
Sulphur dioxide	1.1E+00	kg		(Gediga et al., 2015)
Volatile Organic Compounds	8.8E-04	kg		(Gediga et al., 2015)
Methane	5.8E-03	kg		(Gediga et al., 2015)
Particles	6.6E-03	kg		(Gediga et al., 2015)
Emissions to water				
Copper	2.3E-06	kg		(Gediga et al., 2015)
Iron	6.0E-04	kg		(Gediga et al., 2015)
Lead	4.7E-07	kg		(Gediga et al., 2015)
Nickel	5.9E-06	kg		(Gediga et al., 2015)
Chloride	5.3E-02	kg		(Gediga et al., 2015)
Sodium	1.8E-02	kg		(Gediga et al., 2015)
Sulphate	2.2E-03	kg		(Gediga et al., 2015)

C.4.4.2 Nickel primary extraction

Table C.15: LCI data on nickel primary extraction for NMC622.The data have been rounded to two value figures and if the values for NMC333 is different it is shown in parentheses.

Flow	Amount	Unit	Tracked flows	Source
		INPUTS		
Electricity	5.9E+00	MJ	Table C.58	(Gediga et al., 2015)
Nickel prepared ore (Oxidic)	4.0E+01	kg	Table C.18	(Gediga et al., 2015)
Nickel concentrate (Sulphidic)	3.4E+00	kg	Table C.18	(Gediga et al., 2015)
Crude oil	1.0E-01	kg	Table C.58	(Gediga et al., 2015)
Hard coal	1.5E-01	kg	Table C.58	(Gediga et al., 2015)
Natural gas	1.2E-01	kg	Table C.58	(Gediga et al., 2015)
		OUTPUTS		
Products				
Nickel matte	1.5E+01	kg	Table C.14	(Gediga et al., 2015)
Emissions to air				
Chromium	5.7E-07	kg		(Gediga et al., 2015)
Cobalt	7.4E-06	kg		(Gediga et al., 2015)
Copper	1.3E-04	kg		(Gediga et al., 2015)
Nickel	4.1E-04	kg		(Gediga et al., 2015)
Carbon dioxide	1.1E+00	kg		(Gediga et al., 2015)
Carbon monoxide	5.3E-04	kg		(Gediga et al., 2015)
Nitrogen oxides	2.9E-03	kg		(Gediga et al., 2015)
Sulphur dioxide	5.8E-02	kg		(Gediga et al., 2015)
Volatile Organic Compounds	3.6E-04	kg		(Gediga et al., 2015)
Methane	1.5E-03	kg		(Gediga et al., 2015)
Particles	5.5E-03	kg		(Gediga et al., 2015)
Emissions to water				
Copper	5.6E-07	kg		(Gediga et al., 2015)
Iron	2.6E-03	kg		(Gediga et al., 2015)
Lead	2.8E-07	kg		(Gediga et al., 2015)
Nickel	4.2E-06	kg		(Gediga et al., 2015)
Chloride	1.4E-02	kg		(Gediga et al., 2015)
Sodium	1.1E-03	kg		(Gediga et al., 2015)
Sulphate	2.3E-03	kg		(Gediga et al., 2015)

C.4.4.3 Nickel ore preparation

Table C.16: LCI data on nickel ore preparation for NMC622.The data have been rounded to two value figures and if the values for NMC333 is different it is shown in parentheses.

Flow	Amount	Unit	Tracked flows	Source
		INPUTS		
Electricity	3.0E-01	MJ	Table C.58	(Gediga et al., 2015)
Nickel ore (Oxidic)	7.6E+01	kg	Table C.18	(Gediga et al., 2015)
Crude oil	8.7E-04	kg	Table C.58	(Gediga et al., 2015)
Hard coal	2.1E-02	kg	Table C.58	(Gediga et al., 2015)
Natural gas	1.5E-02	kg	Table C.58	(Gediga et al., 2015)
		OUTPUTS		
Products				
Nickel prepared ore (Oxidic)	4.0E+01	kg	Table C.15	(Gediga et al., 2015)
Emissions to air				
Chromium	5.4E-08	kg		(Gediga et al., 2015)
Cobalt	2.2E-08	kg		(Gediga et al., 2015)
Copper	4.1E-08	kg		(Gediga et al., 2015)
Nickel	3.4E-08	kg		(Gediga et al., 2015)
Carbon dioxide	1.0E-01	kg		(Gediga et al., 2015)
Carbon monoxide	5.3E-05	kg		(Gediga et al., 2015)
Nitrogen oxides	2.3E-04	kg		(Gediga et al., 2015)
Sulphur dioxide	5.5E-04	kg		(Gediga et al., 2015)
Volatile Organic Compounds	2.5E-05	kg		(Gediga et al., 2015)
Methane	2.0E-04	kg		(Gediga et al., 2015)
Particles	6.1E-05	kg		(Gediga et al., 2015)
Emissions to water				
Copper	5.1E-09	kg		(Gediga et al., 2015)
Iron	7.2E-06	kg		(Gediga et al., 2015)
Lead	9.8E-09	kg		(Gediga et al., 2015)
Nickel	4.0E-09	kg		(Gediga et al., 2015)
Chloride	1.8E-04	kg		(Gediga et al., 2015)
Sodium	1.2E-05	kg		(Gediga et al., 2015)
Sulphate	4.0E-05	kg		(Gediga et al., 2015)

C.4.4.4 Nickel beneficiation

Table C.17: LCI data on nickel beneficiation for NMC622.The data have been rounded to two value figures and if the values for NMC333 is different it is shown in parentheses.

Flow	Amount	Unit	Tracked flows	Source
		INPUTS		
Electricity	2.8E+00	MJ	Table C.58	(Gediga et al., 2015)
Nickel ore (Sulphidic)	3.5E+01	kg	Table C.18	(Gediga et al., 2015)
Crude oil	7.5E-02	kg	C.58	(Gediga et al., 2015)
Hard coal	4.2E-02	kg	C.58	(Gediga et al., 2015)
Natural gas	9.3E-02	kg	C.58	(Gediga et al., 2015)
		OUTPUTS		
Products				
Nickel concentrate (Sulphidic)	3.4E+00	kg	Table C.15	(Gediga et al., 2015)
Emissions to air				
Chromium	2.7E-07	kg		(Gediga et al., 2015)
Cobalt	5.6E-07	kg		(Gediga et al., 2015)
Copper	1.0E-05	kg		(Gediga et al., 2015)
Nickel	3.5E-05	kg		(Gediga et al., 2015)
Carbon dioxide	6.5E-01	kg		(Gediga et al., 2015)
Carbon monoxide	6.2E-04	kg		(Gediga et al., 2015)
Nitrogen oxides	2.0E-03	kg		(Gediga et al., 2015)
Sulphur dioxide	1.0E-03	kg		(Gediga et al., 2015)
Volatile Organic Compounds	2.1E-04	kg		(Gediga et al., 2015)
Methane	8.1E-04	kg		(Gediga et al., 2015)
Particles	1.3E-03	kg		(Gediga et al., 2015)
Emissions to water				
Copper	7.6E-05	kg		(Gediga et al., 2015)
Iron	1.4E-03	kg		(Gediga et al., 2015)
Lead	1.3E-07	kg		(Gediga et al., 2015)
Nickel	7.6E-05	kg		(Gediga et al., 2015)
Chloride	9.6E-03	kg		(Gediga et al., 2015)
Sodium	1.1E-03	kg		(Gediga et al., 2015)
Sulphate	4.3E-04	kg		(Gediga et al., 2015)

C.4.4.5 Nickel mining

Table C.18: LCI data on nickel mining for NMC622.The data have been rounded to two value figures and if the values for NMC333 is different it is shown in parentheses.

Flow	Amount	Unit	Tracked flows	Source
		INPUTS		
Electricity	4.4E+00	MJ	Table C.58	(Gediga et al., 2015)
Crude oil	1.1E-01	kg	Table C.58	(Gediga et al., 2015)
Hard coal	5.0E-02	kg	Table C.58	(Gediga et al., 2015)
Natural gas	2.4E-01	kg	Table C.58	(Gediga et al., 2015)
		OUTPUTS		
Products				
Nickel ore (Oxidic)	4.4E+00	kg	Table C.16	(Gediga et al., 2015)
Nickel ore (Sulphidic)	6.3E+01	kg	Table C.17	(Gediga et al., 2015)
Emissions to air				
Chromium	5.6E-08	kg		(Gediga et al., 2015)
Cobalt	1.6E-08	kg		(Gediga et al., 2015)
Copper	6.6E-08	kg		(Gediga et al., 2015)
Nickel	2.5E-07	kg		(Gediga et al., 2015)
Carbon dioxide	1.3E+00	kg		(Gediga et al., 2015)
Carbon monoxide	1.9E-03	kg		(Gediga et al., 2015)
Nitrogen oxides	5.0E-03	kg		(Gediga et al., 2015)
Sulphur dioxide	1.7E-03	kg		(Gediga et al., 2015)
Volatile Organic Compounds	4.7E-04	kg		(Gediga et al., 2015)
Methane	2.1E-03	kg		(Gediga et al., 2015)
Particles	5.5E-04	kg		(Gediga et al., 2015)
Emissions to water				
Copper	5.9E-07	kg		(Gediga et al., 2015)
Iron	2.0E-03	kg		(Gediga et al., 2015)
Lead	1.8E-07	kg		(Gediga et al., 2015)
Nickel	3.4E-07	kg		(Gediga et al., 2015)
Chloride	7.8E-03	kg		(Gediga et al., 2015)
Sodium	3.5E-04	kg		(Gediga et al., 2015)
Sulphate	6.1E-04	kg		(Gediga et al., 2015)

C.4.4.6 Nickel routes

Table C.19: Different extraction routes depending on the type of ore and technology (Gediga et al., 2015).

Primary extraction routes by ore and technology type		
	Oxidic ore	Sulphidic ore
	Hydrometallurgy Pyrometallurgy	Pyrometallurgy
Class 1 nickel	12% 2%	86%

C.4.5   Manganese sulfate

Table C.20: LCI data on production of manganese sulfate for NMC622.The data have been rounded to two value figures and if the values for NMC333 is different it is shown in parentheses.

Flow	Amount	Unit	Tracked flows	Source
		INPUTS		
MnO	4.7E-01	kg	Table C.21	(Dunn et al., 2015)
Sulfuric acid	6.5E-01	kg	Table C.58	(Dunn et al., 2015)
		OUTPUTS		
Manganese sulfate	1.0E+00	kg	Table C.12	(Dunn et al., 2015)

C.4.5.1   Manganese oxide

Table C.21: LCI data on production of manganese oxide for NMC622.The data have been rounded to two value figures and if the values for NMC333 is different it is shown in parentheses.

Flow	Amount	Unit	Tracked flows	Source
		INPUTS		
Manganese	7.7E-01	kg		(Wang et al., 2018)
Diesel fuel	1.4E+00	MJ	Table C.58	(Wang et al., 2018)
Electricity	5.8E+00	MJ	Table C.58	(Wang et al., 2018)
		OUTPUTS		
Manganese oxide	1.0E+00	kg	Table C.20	(Wang et al., 2018)
PM10	3.0E-03	kg		(Wang et al., 2018)
PM2.5	1.5E-03	kg		(Wang et al., 2018)

C.4.6 Cobalt sulfate

Table C.22: LCI data on production of cobalt sulfate for NMC622.The data have been rounded to two value figures and if the values for NMC333 is different itis shown in parentheses.

Flow	Amount	Unit	Tracked flows	Source
INPUTS				
Crude Co(OH)2	6.0E-01	kg	Table C.23	(Dai et al., 2018a)
Limestone	2.1E-02	kg	Table C.58	(Dai et al., 2018a)
Calcium hydroxide	8.4E-03	kg	Table C.58	(Dai et al., 2018a)
Sodium hydroxide	1.0E+00	kg	Table C.58	(Dai et al., 2018a)
Sulfuric acid	9.8E-01	kg	Table C.58	(Dai et al., 2018a)
Hydrochloric acid	5.4E-01	kg	Table C.58	(Dai et al., 2018a)
Kerosene	1.8E-02	kg	Table C.58	(Dai et al., 2018a)
Sodium pyrosulphite	3.0E-02	kg	Table C.26	(Dai et al., 2018a)
Ammonium hydrogen carbonate	2.2E-01	kg	Table C.58	(Dai et al., 2018a)
Soda (sodium carbonate)	3.3E-02	kg	Table C.58	(Dai et al., 2018a)
Fresh water	1.3E+00	kg		(Dai et al., 2018a)
Natural gas	1.1E+01	MJ	Table C.58	(Dai et al., 2018a)
Electricity	4.2E+00	MJ	Table C.58	(Dai et al., 2018a)
OUTPUTS				
Cobalt sulfate	1.0E+00	kg	Table C.12	(Dai et al., 2018a)

C.4.6.1 Cobalt ore processing

Table C.23: LCI data on cobalt ore processing for NMC622.The data have been rounded to two value figures and if the values for NMC333 is different it is shown in parentheses.

Flow	Amount	Unit	Tracked flows	Source
INPUTS				
Cu-Co ores	1.3E+02	kg	Table C.24	(Dai et al., 2018a)
Sulfur	2.0E+00	kg	Table C.25	(Dai et al., 2018a)
Limestone	2.6E+00	kg	Table C.58	(Dai et al., 2018a)
Calcium hydroxide	9.5E-01	kg	Table C.58	(Dai et al., 2018a)
Sodium hydroxide	1.1E-01	kg	Table C.58	(Dai et al., 2018a)
Magnesium oxide	7.5E-01	kg	Table C.58	(Dai et al., 2018a)
Fresh water	6.6E+00	kg		(Dai et al., 2018a)
Electricity	2.0E+01	MJ	Table C.58	(Dai et al., 2018a)
OUTPUTS				
Crude Co(OH)2	1.0E+00	kg	Table C.22	(Dai et al., 2018a)
Sulfur dioxide	1.8E-02	kg		(Dai et al., 2018a)

C.4.6.2 Cobalt mining

Table C.24: LCI data on cobalt mining for NMC622.The data have been rounded to two value figures and if the values for NMC333 is different it is shown in parentheses.

Flow	Amount	Unit	Tracked flows	Source
INPUTS				
Cobalt [Non renewable elements]	4.7E-03	kg		(Dai et al., 2018a)
Fresh water	7.2E-03	kg		(Dai et al., 2018a)
Diesel fuel	3.5E-01	MJ	Table C.58	(Dai et al., 2018a)
OUTPUTS				
Cu-Co ores	1.0E+00	kg	Table C.23	(Dai et al., 2018a)
PM10	8.6E-04	kg		(Dai et al., 2018a)
PM2.5	8.9E-05	kg		(Dai et al., 2018a)

C.4.6.3 Sulfur

Table C.25: LCI data on production of sulfur for NMC622.The data have been rounded to two value figures and if the values for NMC333 is different it is shown in parentheses.

Flow	Amount	Unit	Tracked flows	Source
INPUTS				
Hard coal	9.2E-02	MJ	Table C.58	(Dai et al., 2018a)
Natural gas	2.1E-01	MJ	Table C.58	(Dai et al., 2018a)
Sulfur dioxide	2.0E+00	kg		(Dai et al., 2018a)
Water	4.7E-02	kg		(Dai et al., 2018a)
OUTPUTS				
Sulfur	1.0E+00	kg	Table C.23	(Dai et al., 2018a)

C.4.6.4 Sodium metabisulfite

Table C.26: LCI data on production of sodium metabisulfite for NMC622.The data have been rounded to two value figures and if the values for NMC333 is different it is shown in parentheses.

Flow	Amount	Unit	Tracked flows	Source
INPUTS				
Sodium hydroxide	4.2E-01	kg	Table C.58	(Dai et al., 2018a)
Sulfur dioxide	6.7E-01	kg		(Dai et al., 2018a)
OUTPUTS				
Sodium metabisulfite	1.0E+00	kg	Table C.22	(Dai et al., 2018a)

C.4.6.5 Ammonium bicarbonate

Table C.27: LCI data on production of ammonium bicarbonate for NMC622.The data have been rounded to two value figures and if the values for NMC333 is different it is shown in parentheses.

Flow	Amount	Unit	Tracked flows	Source
INPUTS				
Ammonia	2.2E-01	kg	Table C.58	(Dai et al., 2018a)
Carbon dioxide	5.6E-01	kg		(Dai et al., 2018a)
Water	1.4E-02	kg		(Dai et al., 2018a)
OUTPUTS				
Ammonium Bicarbonate	1.0E+00	kg	Table C.22	(Dai et al., 2018a)

C.4.7 Lithium carbonate

Table C.28: LCI data on production of ammonium bicarbonate for NMC622.The data have been rounded to two value figures and if the values for NMC333 is different it is shown in parentheses.

Flow	Amount	Unit	Tracked flows	Source
INPUTS				
Concentrated lithium brine (60,000 ppm)	5.5E+00	kg	Table C.29	(Dunn et al., 2014)
Soda ash (Na2CO3)	2.5E+00	kg	Table C.58	(Dunn et al., 2014)
Lime (CaO)	9.0E-02	kg	Table C.58	(Dunn et al., 2014)
Hydrochloric acid (HCl)	4.0E-02	kg	Table C.58	(Dunn et al., 2014)
Organic solvent	2.0E-02	kg	Table C.58	(Dunn et al., 2014)
Sulfuric acid (H2SO4)	5.0E-02	kg	Table C.58	(Dunn et al., 2014)
Alcohol	7.1E-04	kg	Table C.58	(Dunn et al., 2014)
Electricity	1.9E+00	MJ	Table C.58	(Dunn et al., 2014)
Natural gas	2.4E+00	MJ	Table C.58	(Dunn et al., 2014)
Diesel fuel	6.3E+00	MJ	Table C.58	(Dunn et al., 2014)
OUTPUTS				
Lithium carbonate	1.0E+00	kg	Table C.11	(Dunn et al., 2014)
PM10	5.8E-05	kg		(Dunn et al., 2014)

C.4.7.1 Concentrated lithium brine

Table C.29: LCI data on production of ammonium bicarbonate for NMC622.The data have been rounded to two value figures and if the values for NMC333 is different it is shown in parentheses.

Flow	Amount	Unit	Tracked flows	Source
		INPUTS		
Lithium [Non renewable elements]	6.0E-02	kg		(Dunn et al., 2014)
Diesel fuel	1.4E-01	MJ	Table C.58	(Dunn et al., 2014)
		OUTPUTS		
Concentrated Lithium Brine (60,000 ppm)	1.0E+00	kg	Table C.28	(Dunn et al., 2014)

C.4.8 Positive current collector

Table C.30: LCI data on production of a positive current collector for NMC622.The data have been rounded to two value figures and if the values for NMC333 is different it is shown in parentheses.

Flow	Amount	Unit	Tracked flows	Source
		INPUTS		
Aluminium	1.0E+00	kg	Table C.58	(Nelson et al., 2018)
		OUTPUTS		
Positive current collector	1.0E+00	kg	Table C.9	(Nelson et al., 2018)

C.5 Electrolyte

Table C.31: LCI data on production of electrolyte for NMC622.The data have been rounded to two value figures and if the values for NMC333 is different it is shown in parentheses.

Flow	Amount	Unit	Tracked flows	Source
		INPUTS		
Lithium hexafluorophosphate	1.5E-01	kg	Table C.58	(Nelson et al., 2018)
Ethylene carbonate	4.2E-01	kg	Table C.32	(Nelson et al., 2018)
Dimethyl carbonate	4.2E-01	kg	Table C.33	(Nelson et al., 2018)
		OUTPUTS		
Electrolyte	1.0E+00	kg	Table C.2	(Nelson et al., 2018)

C.5.1   Ethylene carbonate

Table C.32: LCI data on production of ethylene carbonate for NMC622.The data have been rounded to two value figures and if the values for NMC333 is different it is shown in parentheses.

Flow	Amount	Unit	Tracked flows	Source
		INPUTS		
Ethylene oxide	1.6E-01	kg	Table C.34	(Dunn et al., 2014)
Electricity	4.2E-02	MJ	Table C.58	(Dunn et al., 2014)
Natural gas	2.3E-01	MJ	Table C.58	(Dunn et al., 2014)
		OUTPUTS		
Ethylene carbonate	1.0E+00	kg	Table C.31	(Dunn et al., 2014)

C.5.2   Dimethyl carbonate

Table C.33: LCI data on production of dimethyl carbonate for NMC622.The data have been rounded to two value figures and if the values for NMC333 is different it is shown in parentheses.

Flow	Amount	Unit	Tracked flows	Source
		INPUTS		
Ethylene oxide	5.8E-01	kg	Table C.34	(Dunn et al., 2014)
Electricity	9.2E-02	MJ	Table C.58	(Dunn et al., 2014)
Natural gas	1.3E+00	MJ	Table C.58	(Dunn et al., 2014)
		OUTPUTS		
Dimethyl carbonate	1.0E+00	kg	Table C.31	(Dunn et al., 2014)

C.5.3   Ethylene oxide

Table C.34: LCI data on the production of ethylene oxide for NMC622.The data have been rounded to two value figures and if the values for NMC333 is different it is shown in parentheses.

Flow	Amount	Unit	Tracked flows	Source
		INPUTS		
Ethylene	7.9E-01	kg	Table C.58	(Dunn et al., 2014)
Electricity	7.3E-01	MJ	Table C.58	(Dunn et al., 2014)
Natural gas	3.4E+00	MJ	Table C.58	(Dunn et al., 2014)
		OUTPUTS		
Ethylene oxide	1.0E+00	kg	Table C.32 & C.33	(Dunn et al., 2014)

C.6 Separator

Table C.35: LCI data on the production of separator for NMC622. The data have been rounded to two value figures and if the values for NMC333 is different it is shown in parentheses.

Flow	Amount	Unit	Tracked flows	Source
INPUTS				
Polypropylene	8.0E-01	kg	Table C.58	(Nelson et al., 2018)
Polyethylene	2.0E-01	kg	Table C.58	(Nelson et al., 2018)
OUTPUTS				
Separator	1.0E+00	kg	Table C.2	(Nelson et al., 2018)

C.7 Cell container

Table C.36: LCI data on the production of a cell container for NMC622. The data have been rounded to two value figures and if the values for NMC333 is different it is shown in parentheses.

Flow	Amount	Unit	Tracked flows	Source
INPUTS				
Multilayer film (Aluminium)	3.0E-01 (3.1E-01)	kg	Table C.58	(Nelson et al., 2018)
Multilayer film (PET)	4.7E-02 (4.8E-02)	kg	Table C.58	(Nelson et al., 2018)
Multilayer film (PP)	2.0E-02 (2.1E-02)	kg	Table C.58	(Nelson et al., 2018)
Positive terminal (Aluminium)	1.5E-01 (1.4E-01)	kg	Table C.58	(Nelson et al., 2018)
Negative terminals (Copper)	4.8E-01	kg	Table C.58	(Nelson et al., 2018)
OUTPUTS				
Cell container	1.0E+00	kg	Table C.2	(Nelson et al., 2018)

C.8 Module packaging

Table C.37: LCI data on the production of a module packaging for NMC622. The data have been rounded to two value figures and if the values for NMC333 is different it is shown in parentheses.

Flow	Amount	Unit	Tracked flows	Source
INPUTS				
Module state-of-charge regulator assembly	8.2E-02 (7.7E-02)	kg	Table C.58	(Nelson et al., 2018)
Module thermal conductor (Aluminium)	5.0E-01 (5.1E-01)	kg	Table C.58	(Nelson et al., 2018)
Module terminals (Copper)	4.8E-02 (4.7E-02)	kg	Table C.58	(Nelson et al., 2018)
Thermal Inslutation (Fiberglass)	1.2E-02	kg	Table C.58	(Nelson et al., 2018)
Module closure (Aluminium)	3.5E-01	kg	Table C.58	(Nelson et al., 2018)
Module spacer (PE)	1.3E-02 (1.2E-02)	kg	Table C.58	(Nelson et al., 2018)
OUTPUTS				
Module packaging	1.0E+00	kg	Table C.1	(Nelson et al., 2018)

C.9 Battery Pack Assembly

Table C.38: LCI data on the production of a BMS for NMC622. The data have been rounded to two value figures and if the values for NMC333 is different it is shown in parentheses.

Flow	Amount	Unit	Tracked flows	Source
INPUTS				
BMB (printed wiring board)	8.9E-02	kg	Table C.58	(Ellingsen et al., 2014)
IBIS	4.8E-01	kg	Table C.39	(Ellingsen et al., 2014)
IBIS fasteners	3.0E-03	kg	Table C.40	(Ellingsen et al., 2014)
High Voltage system	3.0E-01	kg	Table C.41	(Ellingsen et al., 2014)
Low Voltage system	1.3E-01	kg	Table C.42	(Ellingsen et al., 2014)
OUTPUTS				
BMS	1.0E+00	kg	Table C.1	(Ellingsen et al., 2014)

C.9.1 IBIS

Table C.39: LCI data on the production of an Integrated Battery Interface System for NMC622. The data have been rounded to two value figures and if the values for NMC333 is different it is shown in parentheses.

Flow	Amount	Unit	Tracked flows	Source
			INPUTS	
BMS_GLAND _O-RING (ABS)	2.0E-04	kg	Table C.58	(Ellingsen et al., 2014)
BMS printed circuit board	1.1E-01	kg	Table C.58	(Ellingsen et al., 2014)
BMS_FIRMWARE (Integrated circuit)	1.7E-05	kg	Table C.58	(Ellingsen et al., 2014)
Components (steel)	8.5E-01	kg	Table C.58	(Ellingsen et al., 2014)
Connectors (clamp connection)	2.1E-02	kg	Table C.58	(Ellingsen et al., 2014)
Crimp housing (PET)	6.8E-03	kg	Table C.58	(Ellingsen et al., 2014)
Standoffs, nylon part (nylon 6)	1.9E-03	kg	Table C.58	(Ellingsen et al., 2014)
Standoffs brass part (brass)	5.7E-03	kg	Table C.58	(Ellingsen et al., 2014)
			OUTPUTS	
IBIS	1.0E+00	kg	Table C.38	(Ellingsen et al., 2014)

C.9.2 IBIS fasteners

Table C.40: LCI data on the production of IBIS fasteners for NMC622. The data have been rounded to two value figures and if the values for NMC333 is different it is shown in parentheses.

Flow	Amount	Unit	Tracked flows	Source
			INPUTS	
Fixings (steel)	1.0E+00	kg	Table C.58	(Ellingsen et al., 2014)
			OUTPUTS	
IBIS fasteners	1.0E+00	kg	Table C.38	(Ellingsen et al., 2014)

XXX

C.9.3 High voltage system

Table C.41: LCI data on the production of a high voltage system for NMC622. The data have been rounded to two value figures and if the values for NMC333 is different it is shown in parentheses.

Flow	Amount	Unit	Tracked flows	Source
		INPUTS		
Steel products	1.4E-03	kg	Table C.58	(Ellingsen et al., 2014)
HVC and lid (aluminium)	1.2E-01	kg	Table C.58	(Ellingsen et al., 2014)
Clips & fasteners (nylon 66)	4.4E-02	kg	Table C.58	(Ellingsen et al., 2014)
Neoprene gasket (synthetic rubber)	3.6E-03	kg	Table C.58	(Ellingsen et al., 2014)
Plastic (PET)	5.7E-02	kg	Table C.58	(Ellingsen et al., 2014)
Intermodule Fuse (copper)	2.7E-01	kg	Table C.58	(Ellingsen et al., 2014)
Intermodule Fuse (polyphenylene sulfide)	3.2E-02	kg	Table C.58	(Ellingsen et al., 2014)
Intermodule Fuse (tin)	1.6E-02	kg	Table C.58	(Ellingsen et al., 2014)
Cables (ribbon cable)	4.5E-01	kg	Table C.58	(Ellingsen et al., 2014)
		OUTPUTS		
High voltage system	1.0E+00	kg	Table C.38	(Ellingsen et al., 2014)

C.9.4 Low voltage system

Table C.42: LCI data on the production of a low voltage system for NMC622. The data have been rounded to two value figures and if the values for NMC333 is different it is shown in parentheses.

Flow	Amount	Unit	Tracked flows	Source
		INPUTS		
Clips (nylon 66)	2.9E-02	kg	Table C.58	(Ellingsen et al., 2014)
Harnesses (electronic component)	9.7E-01	kg	Table C.58	(Ellingsen et al., 2014)
		OUTPUTS		
Low Voltage system	1.0E+00	kg	Table C.38	(Ellingsen et al., 2014)

C.10 Cooling system

Table C.43: LCI data on the production of a cooling system for NMC622. The data have been rounded to two value figures and if the values for NMC333 is different it is shown in parentheses.

Flow	Factor	Unit	Tracked flows	Source
		INPUTS		
Cooling System Exterior	3.7E-01 (3.6E-01)	kg	Table C.44	(Nelson et al., 2018)
Coolant (Ethylene glycol)	6.3E-01 (6.4E-01)	kg	Table C.58	(Nelson et al., 2018)
		OUTPUTS		
Cooling System	1.0E+00	kg	Table C.1	(Nelson et al., 2018)

C.10.1 Cooling system exterior

Table C.44: LCI data on the production of a cooling system exterior for NMC622. The data have been rounded to two value figures and if the values for NMC333 is different it is shown in parentheses.

Flow	Amount	Unit	Tracked flows	Source
		INPUTS		
Radiator	9.1E-01	kg	Table C.45	(Ellingsen et al., 2014)
Manifolds	4.0E-02	kg	Table C.46	(Ellingsen et al., 2014)
Clamps & fasteners	2.4E-02	kg	Table C.47	(Ellingsen et al., 2014)
Pipe fitting	1.0E-03	kg	Table C.48	(Ellingsen et al., 2014)
Thermal pad	2.1E-02	kg	Table C.49	(Ellingsen et al., 2014)
		OUTPUTS		
Cooling System Exterior	1.0E+00	kg	Table C.44	(Ellingsen et al., 2014)

C.10.1.1 Radiator

Table C.45: LCI data on the production of a radiator for NMC622. The data have been rounded to two value figures and if the values for NMC333 is different it is shown in parentheses.

Flow	Amount	Unit	Tracked flows	Source
		INPUTS		
Aluminium	1.0E+00	kg	Table C.58	(Ellingsen et al., 2014)
		OUTPUTS		
Radiator	1.0E+00	kg	Table C.44	(Ellingsen et al., 2014)

C.10.1.2 Manifolds

Table C.46: LCI data on the production of a manifolds for NMC622. The data have been rounded to two value figures and if the values for NMC333 is different it is shown in parentheses.

Flow	Amount	Unit	Tracked flows	Source
			INPUTS	
Aluminium	1.0E+00	kg	Table C.58	(Ellingsen et al., 2014)
			OUTPUTS	
Manifolds	1.0E+00	kg	Table C.44	(Ellingsen et al., 2014)

C.10.1.3 Clamps & fasteners

Table C.47: LCI data on the production of a clamps and fasteners for NMC622. The data have been rounded to two value figures and if the values for NMC333 is different it is shown in parentheses.

Flow	Amount	Unit	Tracked flows	Source
			INPUTS	
Steel	1.0E+00	kg	Table C.58	(Ellingsen et al., 2014)
			OUTPUTS	
Clamps & fasteners	1.0E+00	kg	Table C.44	(Ellingsen et al., 2014)

C.10.1.4 Pipe fitting

Table C.48: LCI data on the production of pipe fitting for NMC622. The data have been rounded to two value figures and if the values for NMC333 is different it is shown in parentheses.

Flow	Amount	Unit	Tracked flows	Source
			INPUTS	
Pipe fitting plastic (polyvinylchloride)	7.5E-01	kg	Table C.58	(Ellingsen et al., 2014)
Pipe fitting rubber (synthetic rubber)	2.5E-01	kg	Table C.58	(Ellingsen et al., 2014)
			OUTPUTS	
Pipe fitting	1.0E+00	kg	Table C.44	(Ellingsen et al., 2014)

C.10.1.5 Thermal pad

Table C.49: LCI data on the production of a thermal pad for NMC622. The data have been rounded to two value figures and if the values for NMC333 is different it is shown in parentheses.

Flow	Amount	Unit	Tracked flows	Source
			INPUTS	
Thermal pad (glass fibre)	1.0E-01	kg	Table C.58	(Ellingsen et al., 2014)
Thermal pad (silicon)	3.0E-01	kg	Table C.58	(Ellingsen et al., 2014)
Thermal pad (ABS)	6.0E-01	kg	Table C.58	(Ellingsen et al., 2014)
			OUTPUTS	
Thermal pad	1.0E+00	kg	Table C.44	(Ellingsen et al., 2014)

C.11 Pack packaging

Table C.50: LCI data on the production of the pack packaging for NMC622. The data have been rounded to two value figures and if the values for NMC333 is different it is shown in parentheses.

Flow	Amount	Unit	Tracked flows	Source
			INPUTS	
Battery jacket (Aluminium)	8.7E-01	kg	Table C.58	(Nelson et al., 2018)
Thermal Insulation (Fiberglass)	2.6E-02	kg	Table C.58	(Nelson et al., 2018)
Battery pack heaters (electronic comp.)	7.4E-03 (7.0E-03)	kg	Table C.58	(Nelson et al., 2018)
Battery pack terminals (Copper)	2.2E-03	kg	Table C.58	(Nelson et al., 2018)
Module inter-connect (electronic comp.)	3.2E-02	kg	Table C.58	(Nelson et al., 2018)
Module compression plates and steel straps	6.4E-02 (6.6E-02)	kg	Table C.58	(Nelson et al., 2018)
			OUTPUTS	
Pack packaging	1.0E+00	kg	Table C.1	(Nelson et al., 2018)

C.12   Use phase

Table C.51: LCI data on the use phase for NMC622. The data have been rounded to two value figures and if the values for NMC333 is different it is shown in parentheses.

Flow	Amount	Unit	Tracked flows
	INPUTS		
Battery pack	1.0	kg	Table C.1
Basic consumption	196 (183)	MJ	Table C.58
Heating and air conditioning	77 (70)	MJ	Table C.58
Auxiliares	3.0	MJ	Table C.58
Standstill losses	2.0	MJ	Table C.58
Charging losses	43 (40)	MJ	Table C.58
	OUTPUTS		
Battery pack	1.0	kg	Table C.52

C.13   Battery pack dissembling

Table C.52: LCI data on battery pack dissembling for NMC622. The data have been rounded to two value figures and if the values for NMC333 is different it is shown in parentheses.

Flow	Amount	Unit	Tracked flows	Source
		INPUTS		
Battery pack	1.0E+00	kg	Table C.51	(Nelson et al., 2018)
		OUTPUTS		
Battery cell	7.3E-01 (7.4E-01)	kg	Table C.53	(Nelson et al., 2018)
Passive parts	2.0E-01	kg	Table C.55	(Nelson et al., 2018)
OEM parts	4.8E-02 (4.5E-02)	kg	Table C.56	(Nelson et al., 2018)
Unsorted battery fraction	1.7E-02	kg	Table C.57	(Nelson et al., 2018)

C.13.1 Cell recycling

Table C.53: LCI data on cell recycling for NMC622. The data have been rounded to two value figures and if the values for NMC333 is different it is shown in parentheses.

Flow	Amount	Unit	Tracked flows	Source
INPUTS				
Battery cell	1.0E+00	kg	Table C.52	(Siret et al., 2018)
Lime (CaO)	2.0E-02	kg	Table C.58	(Siret et al., 2018)
Hard coal mix	1.0E-02	kg	Table C.58	(Siret et al., 2018)
Electricity	3.0E-01	MJ	Table C.58	(Siret et al., 2018)
Process steam from natural gas 90%	2.8E+00	MJ	Table C.58	(Siret et al., 2018)
OUTPUTS				
Metallic alloy	4.8E-01	kg	Table C.54	(Siret et al., 2018)
Slag	2.5E-01	kg		(Siret et al., 2018)

C.13.1.1 Metallic alloy treatment

Table C.54: LCI data on metallic alloy treatment for NMC622. The data have been rounded to two value figures and if the values for NMC333 is different it is shown in parentheses.

Flow	Amount	Unit	Tracked flows	Source
INPUTS				
Metalic alloy	1.0E+00	kg	Table C.53	(Siret et al., 2018)
Sodium hydroxide	8.0E-02	kg	Table C.58	(Siret et al., 2018)
Sulphuric acid (96%)	2.8E-01	kg	Table C.58	(Siret et al., 2018)
Thermal energy from natural gas	9.0E-01	MJ	Table C.58	(Siret et al., 2018)
Tap water	3.3E+00	kg	Table C.58	(Siret et al., 2018)
OUTPUTS				
Landfill for inert matter (Steel)	3.0E-02	kg	Table C.58	(Siret et al., 2018)
Municipal waste water treatment	3.6E+00	kg	Table C.58	(Siret et al., 2018)

C.13.2 Passive parts recycling

Table C.55: LCI data on passive parts recycling for NMC622. The data have been rounded to two value figures and if the values for NMC333 is different it is shown in parentheses.

Flow	Amount	Unit	Tracked flows	Source
INPUTS				
Passive parts	1.0E+00	kg	Table C.58	(Siret et al., 2018)
EAF Steel billet / Slab / Bloom	4.7E-01	kg	Table C.58	(Siret et al., 2018)
Aluminium recycling	7.0E-02	kg	Table C.58	(Siret et al., 2018)
Recycling of copper from electronic scrap	1.0E-02	kg	Table C.58	(Siret et al., 2018)
Plastic granulate secondary	1.0E-01	kg	Table C.58	(Siret et al., 2018)
OUTPUTS				

C.13.3 OEM parts recycling

Table C.56: LCI data on OEM parts recycling for NMC622. The data have been rounded to two value figures and if the values for NMC333 is different it is shown in parentheses.

Flow	Amount	Unit	Tracked flows	Source
INPUTS				
OEM parts	1.0E+00	kg	Table C.52	(Siret et al., 2018)
Aluminium recycling	4.0E-02	kg	Table C.58	(Siret et al., 2018)
EAF Steel billet / Slab / Bloom	9.9E-02	kg	Table C.58	(Siret et al., 2018)
Plastic granulate secondary	5.3E-02	kg	Table C.58	(Siret et al., 2018)
Recycling of copper from electronic scrap	1.0E-09	kg	Table C.58	(Siret et al., 2018)
Recycling of gold from electronic scrap	2.5E-16	kg	Table C.58	(Siret et al., 2018)
Recycling of palladium from electronic scrap	1.1E-16	kg	Table C.58	(Siret et al., 2018)
Recycling of silver from electronic scrap	1.5E-13	kg	Table C.58	(Siret et al., 2018)
OUTPUTS				

C.13.4   Treatment of unsorted battery fraction

Table C.57: LCI data on treatment of unsorted battery fraction for NMC622. The data have been rounded to two value figures and if the values for NMC333 is different it is shown in parentheses.

Flow	Amount	Unit	Tracked flows	Source
INPUTS				
Unsorted battery fraction	1.0E+00	kg	Table C.52	(Siret et al., 2018)
OUTPUTS				
Landfill for inert matter	6.3E-02	kg	Table C.58	(Siret et al., 2018)

C.14   LCI data from databases

Table C.58: LCI data from databases.

Component/Process	Flow	Source
Battery cell assembly	EU-28: Process water ts	GaBi 6 ts
Battery cell assembly	EU-28+EFTA: Treatment of residential wastewater, large plant	PEF/OEF data
Anode/Negative electrode paste	EU-28+EFTA: Injection moulding	PEF/OEF data
Anode/Negative electrode paste	World: Polyvinylidene fluoride (PVDF)	PEF/OEF data
Anode/Negative current collector	EU-28: Copper Sheet Mix DKI/ECI	GaBi 6 ts
Cathode/Positive current collector	EU-28: Aluminium sheet ts <p-agg>	GaBi 6 ts
Cathode/Positive current collector	EU-28: Aluminium ingot mix ts	GaBi 6 ts
Cathode/Positive electrode paste	EU-28+EFTA: Injection moulding	PEF/OEF data
Cathode/Positive electrode paste	World: Polyvinylidene fluoride (PVDF)	PEF/OEF data
Cathode/Positive electrode paste	DE: Carbon black (furnace black; general purpose) ts	GaBi 6 ts
Cathode/.../Active cathode material	EU-28: Electricity grid mix 1kV-60kV ts	GaBi 6 ts
Cathode/.../Precursor	Sodium hydroxide (caustic soda) mix (100%)	GaBi 6 ts
Cathode/.../Precursor	RoW: market for ammonia, liquid ecoinvent 3.4	ecoinvent 3.4
		Continued on next page

Table C.58 – continued from previous page

Component/Process	Flow	Source
Cathode/.../Precursor	EU-28: Thermal energy from natural gas ts	GaBi 6 ts
Cathode/.../Precursor	EU-28: Process water ts	GaBi 6 ts
Cathode/.../Lithium carbonate	BR: Thermal energy from light fuel oil (LFO) ts	GaBi 6 ts
Cathode/.../Lithium carbonate	DE: Soda (Na2CO3) ts	GaBi 6 ts
Cathode/.../Lithium carbonate	DE: Lime (CaO; quick-lime lumpy) ts	GaBi 6 ts
Cathode/.../Lithium carbonate	DE: Hydrochloric acid mix (100%) ts	GaBi 6 ts
Cathode/.../Lithium carbonate	GLO: market for methanol ecoinvent 3.4	ecoinvent 3.4
Cathode/.../Lithium carbonate	GLO: market for solvent, organic ecoinvent 3.4	ecoinvent 3.4
Cathode/.../Lithium carbonate	EU-28: Sulphuric acid (96%) ts	GaBi 6 ts
Cathode/.../Lithium carbonate	BR: Electricity grid mix 1kV-60kV ts	GaBi 6 ts
Cathode/.../Lithium carbonate	BR: Thermal energy from natural gas ts	GaBi 6 ts
Cathode/.../Lithium carbonate	BR: Thermal energy from light fuel oil (LFO) ts	GaBi 6 ts
Cathode/.../Nickel sulfate	EU-28: Thermal energy from natural gas ts	GaBi 6 ts
Cathode/.../Nickel sulfate	EU-28: Sulphuric acid (96%) ts	GaBi 6 ts
Cathode/.../Nickel sulfate/Nickel refining	EU-28: Natural gas mix ts	GaBi 6 ts
Cathode/.../Nickel sulfate/Nickel refining	EU-28: Electricity grid mix 1kV-60kV ts	GaBi 6 ts
Cathode/.../Nickel sulfate/Nickel refining	DE: Crude oil mix ts	GaBi 6 ts
Cathode/.../Nickel sulfate/Nickel refining	EU-28: Hard coal mix ts	GaBi 6 ts
Cathode/.../Nickel sulfate/.../Nickel primary extraction	EU-28: Natural gas mix ts	GaBi 6 ts
Cathode/.../Nickel sulfate/.../Nickel primary extraction	EU-28: Electricity grid mix 1kV-60kV ts	GaBi 6 ts
Cathode/.../Nickel sulfate/.../Nickel primary extraction	DE: Crude oil mix ts	GaBi 6 ts
		Continued on next page

Table C.58 – continued from previous page

Component/Process	Flow	Source
Cathode/.../Nickel sulfate/.../Nickel primary extraction	EU-28: Hard coal mix ts	GaBi 6 ts
Cathode/.../Nickel sulfate/.../Nickel beneficiation	EU-28: Natural gas mix ts	GaBi 6 ts
Cathode/.../Nickel sulfate/.../Nickel beneficiation	EU-28: Electricity grid mix 1kV-60kV ts	GaBi 6 ts
Cathode/.../Nickel sulfate/.../Nickel beneficiation	DE: Crude oil mix ts	GaBi 6 ts
Cathode/.../Nickel sulfate/.../Nickel beneficiation	EU-28: Hard coal mix ts	GaBi 6 ts
Cathode/.../Nickel sulfate/.../Nickel ore preparation	EU-28: Natural gas mix ts	GaBi 6 ts
Cathode/.../Nickel sulfate/.../Nickel ore preparation	EU-28: Electricity grid mix 1kV-60kV ts	GaBi 6 ts
Cathode/.../Nickel sulfate/.../Nickel ore preparation	DE: Crude oil mix ts	GaBi 6 ts
Cathode/.../Nickel sulfate/.../Nickel ore preparation	EU-28: Hard coal mix ts	GaBi 6 ts
Cathode/.../Nickel sulfate/.../Nickel mining	EU-28: Natural gas mix ts	GaBi 6 ts
Cathode/.../Nickel sulfate/.../Nickel mining	EU-28: Electricity grid mix 1kV-60kV ts	GaBi 6 ts
Cathode/.../Nickel sulfate/.../Nickel mining	DE: Crude oil mix ts	GaBi 6 ts
Cathode/.../Nickel sulfate/.../Nickel mining	EU-28: Hard coal mix ts	GaBi 6 ts
Cathode/.../Manganese sulfate	EU-28: Sulphuric acid (96%) ts	GaBi 6 ts
Cathode/.../Manganese sulfate/Manganese oxide	EU-28: Thermal energy from light fuel oil (LFO) ts	GaBi 6 ts
Cathode/.../Manganese sulfate/Manganese oxide	EU-28: Electricity grid mix 1kV-60kV ts	GaBi 6 ts
Cathode/.../Cobalt sulfate	Limestone flour, average (0.1-5 mm) (DE)	GaBi 6 ts
		Continued on next page

Table C.58 – continued from previous page

Component/Process	Flow	Source
Cathode/…/Cobalt sulfate	DE: Calcium hydroxide (Ca(OH)2; dry; slaked lime)	GaBi 6 ts
Cathode/…/Cobalt sulfate	EU-28: Sodium hydroxide (caustic soda) mix (100%) ts	GaBi 6 ts
Cathode/…/Cobalt sulfate	DE: Hydrochloric acid mix (100%) ts	GaBi 6 ts
Cathode/…/Cobalt sulfate	CN: Kerosene / Jet A1 at refinery ts	GaBi 6 ts
Cathode/…/Cobalt sulfate	EU-28: Sodium hydroxide (caustic soda) mix (100%) ts	GaBi 6 ts
Cathode/…/Cobalt sulfate	EU-28: Soda (Na2CO3) ts	GaBi 6 ts
Cathode/…/Cobalt sulfate	CN: Thermal energy from natural gas ts	GaBi 6 ts
Cathode/…/Cobalt sulfate	CN: Electricity grid mix 1kV-60kV ts	GaBi 6 ts
Cathode/…/Cobalt sulfate	EU-28: Sulphuric acid (96%) ts	GaBi 6 ts
Cathode/…/Cobalt sulfate	EU-28: Ammonia mix (NH3) ts	GaBi 6 ts
Cathode/…/Cobalt sulfate/Cobalt ore processing	Limestone flour, average (0.1-5 mm)	GaBi 6 ts
Cathode/…/Cobalt sulfate/Cobalt ore processing	DE: Calcium hydroxide (Ca(OH)2; dry; slaked lime)	GaBi 6 ts
Cathode/…/Cobalt sulfate/Cobalt ore processing	EU-28: Sodium hydroxide (caustic soda) mix (100%) ts	GaBi 6 ts
Cathode/…/Cobalt sulfate/Cobalt ore processing	GLO: market for magnesium oxide ecoinvent 3.4	ecoinvent 3.4
Cathode/…/Cobalt sulfate/Cobalt ore processing	RAF: Electricity from hydro power	GaBi 6 ts
Cathode/…/Cobalt sulfate/…/Cobalt mining	EU-28: Thermal energy from light fuel oil (LFO) ts	GaBi 6 ts
Cathode/…/Cobalt sulfate/…/Sulfur	CN: Thermal energy from natural gas ts	GaBi 6 ts
Cathode/…/Cobalt sulfate/…/Sulfur	CN: Thermal energy from hard coal ts	GaBi 6 ts

Table C.58 – continued from previous page

Component/Process	Flow	Source
Electrolyte	GLO: market for lithium hexafluorophosphate ecoinvent 3.4	ecoinvent 3.4
Electrolyte/Ethylene carbonate	EU-28: Electricity grid mix 1kV-60kV ts	GaBi 6 ts
Electrolyte/Ethylene carbonate	EU-28: Thermal energy from natural gas ts	GaBi 6 ts
Electrolyte/Dimethyl carbonate	EU-28: Electricity grid mix 1kV-60kV ts	GaBi 6 ts
Electrolyte/Dimethyl carbonate	EU-28: Thermal energy from natural gas ts	GaBi 6 ts
Electrolyte/.../Ethylene oxide	EU-28: Ethene (ethylene) ts	GaBi 6 ts
Electrolyte/.../Ethylene oxide	EU-28: Electricity grid mix 1kV-60kV ts	GaBi 6 ts
Electrolyte/.../Ethylene oxide	EU-28: Thermal energy from natural gas ts	GaBi 6 ts
Separator	Polypropylene injection moulding part (PP) (RER)	PlasticEurope/IVL
Separator	EU-28+EFTA: Injection moulding	PEF/OEF data
Separator	RER: Polyethylene high density granulate (PE-HD)	PlasticEurope/IVL
Cell container	EU-28: Aluminium ingot mix ts	GaBi 6 ts
Cell container	EU-28: Aluminium sheet ts	GaBi 6 ts
Cell container	EU-28: Polyethylene terephthalate bottle grade granulate (PET)	GaBi 6 ts
Cell container	EU-28+EFTA: Injection moulding	PEF/OEF data
Cell container	Polypropylene injection moulding part (PP) (RER)	PlasticEurope/IVL
Cell container	EU-28: Copper Sheet Mix DKI/ECI	GaBi 6 ts
Module packaging	GLO: market for electronic component, passive, unspecified ecoinvent 3.4	ecoinvent 3.4
Module packaging	EU-28: Aluminium ingot mix ts	GaBi 6 ts
Module packaging	EU-28: Aluminium sheet ts	GaBi 6 ts

Table C.58 – continued from previous page

Component/Process	Flow	Source
Module packaging	EU-28: Copper Sheet Mix DKI/ECI	GaBi 6 ts
Module packaging	DE: Glass fibres ts	GaBi 6 ts
Module packaging	EU-28+EFTA: Injection moulding	PEF/OEF data
Module packaging	RER: Polyethylene high density granulate (PE-HD)	PlasticEurope/IVL
BMS	GLO: market for printed wiring board, through-hole mounted, unspecified, Pb free ecoinvent 3.4	ecoinvent 3.4
BMS/IBIS	EU-28: Acrylonitrile butadiene styrene (ABS) PlasticsEurope	PlasticEurope
BMS/IBIS	RER: injection moulding ecoinvent 3.4	ecoinvent 3.4
BMS/IBIS	GLO: market for printed wiring board, through-hole mounted, unspecified, Pb free ecoinvent 3.4	ecoinvent 3.4
BMS/IBIS	GLO: market for integrated circuit, logic type ecoinvent 3.4	ecoinvent 3.4
BMS/IBIS	EU: Steel finished cold rolled coil worldsteel	Worldsteel
BMS/IBIS	RER: metal working, average for steel product manufacturing ecoinvent 3.4	ecoinvent 3.4
BMS/IBIS	GLO: market for electric connector, wire clamp ecoinvent 3.4	ecoinvent 3.4
BMS/IBIS	EU-28: Polyethylene terephthalate bottle grade granulate (PET) via PTA ts	GaBi 6 ts
BMS/IBIS	EU-28+EFTA: Injection moulding	PEF/OEF data
BMS/IBIS	DE: Polyamide 6 Granulate (PA 6) Mix ts	GaBi 6 ts
BMS/IBIS	EU-28: Brass (CuZn20) ts	GaBi 6 ts
BMS/IBIS	GLO: market for casting, brass ecoinvent 3.4	ecoinvent 3.4
BMS/IBIS fasteners	EU: Steel finished cold rolled coil worldsteel	Worldsteel

Table C.58 – continued from previous page

Component/Process	Flow	Source
BMS/IBIS fasteners	RER: metal working, average for steel product manufacturing ecoinvent 3.4	ecoinvent 3.4
BMS/High voltage system	EU: Steel finished cold rolled coil worldsteel	Worldsteel
BMS/High voltage system	RER: metal working, average for steel product manufacturing ecoinvent 3.4	ecoinvent 3.4
BMS/High voltage system	EU-28: Aluminium ingot mix ts	GaBi 6 ts
BMS/High voltage system	RER: metal working, average for aluminium product manufacturing ecoinvent 3.4	ecoinvent 3.4
BMS/High voltage system	DE: Polyamide 6.6 Granulate (PA 6.6) Mix ts	GaBi 6 ts
BMS/High voltage system	RER: injection moulding ecoinvent 3.4	ecoinvent 3.4
BMS/High voltage system	DE: Styrene-Butadiene Rubber (SBR) Mix ts	GaBi 6 ts
BMS/High voltage system	EU-28: Polyethylene terephthalate bottle grade granulate (PET)	GaBi 6 ts
BMS/High voltage system	EU-28+EFTA: Injection moulding	PEF/OEF data
BMS/High voltage system	EU-28: Copper Wire Mix DKI/ECI	GaBi 6 ts
BMS/High voltage system	RER: metal working, average for copper product manufacturing ecoinvent 3.4	ecoinvent 3.4
BMS/High voltage system	DE: Polyphenylene sulfide granulate (PPS) ts	GaBi 6 ts
BMS/High voltage system	GLO: market for tin ecoinvent 3.4	ecoinvent 3.4
BMS/High voltage system	RER: metal working, average for metal product manufacturing ecoinvent 3.4	ecoinvent 3.4
BMS/High voltage system	GLO: market for cable, ribbon cable, 20-pin, with plugs ecoinvent 3.4	ecoinvent 3.4
BMS/Low voltage system	DE: Polyamide 6.6 Granulate (PA 6.6) Mix ts	GaBi 6 ts

Table C.58 – continued from previous page

Component/Process	Flow	Source
BMS/Low voltage system	GLO: market for electronic component, passive, unspecified ecoinvent 3.4	ecoinvent 3.4
Cooling system	EU-28: Ethylene glycol ts	GaBi 6 ts
Cooling system/.../Radiator	EU-28: Aluminium ingot mix ts	GaBi 6 ts
Cooling system/.../Radiator	EU-28: Aluminium sheet ts	GaBi 6 ts
Cooling system/.../Manifolds	EU-28: Aluminium ingot mix ts	GaBi 6 ts
Cooling system/.../Manifolds	RER: metal working, average for aluminium product manufacturing ecoinvent 3.4	ecoinvent 3.4
Cooling system/.../Clamps & fasteners	EU: Steel finished cold rolled coil worldsteel	Worldsteel
Cooling system/.../Clamps & fasteners	RER: metal working, average for steel product manufacturing ecoinvent 3.4	ecoinvent 3.4
Cooling system/.../Pipe fittning	DE: Polyvinyl chloride granulate (Suspension, S-PVC) ts	GaBi 6 ts
Cooling system/.../Pipe fittning	RER: injection moulding ecoinvent 3.4	ecoinvent 3.4
Cooling system/.../Pipe fittning	DE: Styrene-Butadiene Rubber (SBR) Mix ts	GaBi 6 ts
Cooling system/.../Thermal pad	DE: Glass fibres ts	GaBi 6 ts
Cooling system/.../Thermal pad	RER: injection moulding ecoinvent 3.4	ecoinvent 3.4
Cooling system/.../Thermal pad	GLO: Silicon mix (99%) ts	GaBi 6 ts
Cooling system/.../Thermal pad	EU-28: Acrylonitrile butadiene styrene (ABS) PlasticsEurope	PlasticEurope
Pack packaging	EU-28: Aluminium ingot mix ts	GaBi 6 ts
Pack packaging	EU-28: Aluminium sheet ts	GaBi 6 ts
Pack packaging	DE: Glass fibres ts	GaBi 6 ts
Pack packaging	RER: injection moulding ecoinvent 3.4	ecoinvent 3.4
		Continued on next page

<div align="center">Table C.58 – continued from previous page</div>

Component/Process	Flow	Source
Pack packaging	GLO: market for electronic component, passive, unspecified ecoinvent 3.4	ecoinvent 3.4
Pack packaging	EU-28: Copper Sheet Mix DKI/ECI	GaBi 6 ts
Pack packaging	Steel cold rolled coil (Worldsteel 2014, EU)	Worldsteel
Pack packaging	RER: metal working, average for steel product manufacturing ecoinvent 3.4	GaBi 6 ts
Transport of active material	GLO: Truck-trailer, Euro 4, 34 - 40t gross weight / 27t payload capacity ts	GaBi 6 ts
Transport of active material	EU-28: Diesel mix at refinery ts	GaBi 6 ts
Transport of active material	GLO: Rail transport cargo - average, average train, gross tonne weight 1000t / 726t payload capacity ts	GaBi 6 ts
Transport of active material	EU-28: Electricity grid mix 1kV-60kV ts	GaBi 6 ts
Transport of active material	EU-28: Diesel mix at refinery ts	GaBi 6 ts
Transport of active material	GLO: Bulk commodity carrier, average, ocean going ts	GaBi 6 ts
Transport of active material	EU-28: Heavy fuel oil at refinery (1.0wt.% S) ts	GaBi 6 ts
Transport of passive material	GLO: Truck-trailer, Euro 4, 34 - 40t gross weight / 27t payload capacity ts	GaBi 6 ts
Transport of passive material	EU-28: Diesel mix at refinery ts	GaBi 6 ts
Transport of passive material	GLO: Rail transport cargo - average, average train, gross tonne weight 1000t / 726t payload capacity ts	GaBi 6 ts
Transport of passive material	EU-28: Electricity grid mix 1kV-60kV ts	GaBi 6 ts
Transport of passive material	EU-28: Diesel mix at refinery ts	GaBi 6 ts

Table C.58 – continued from previous page

Component/Process	Flow	Source
Transport of passive material	GLO: Bulk commodity carrier, average, ocean going ts	GaBi 6 ts
Transport of passive material	EU-28: Heavy fuel oil at refinery (1.0wt.% S) ts	GaBi 6 ts
Transport of cell from China, Korea or Japan to Europe	GLO: Truck-trailer, Euro 4, 34 - 40t gross weight / 27t payload capacity ts	GaBi 6 ts
Transport of cell from China, Korea or Japan to Europe	EU-28: Diesel mix at refinery ts	GaBi 6 ts
Transport of cell from China, Korea or Japan to Europe	GLO: Rail transport cargo - average, average train, gross tonne weight 1000t / 726t payload capacity ts	GaBi 6 ts
Transport of cell from China, Korea or Japan to Europe	EU-28: Electricity grid mix 1kV-60kV ts	GaBi 6 ts
Transport of cell from China, Korea or Japan to Europe	EU-28: Diesel mix at refinery ts	GaBi 6 ts
Transport of cell from China, Korea or Japan to Europe	GLO: Bulk commodity carrier, average, ocean going ts	GaBi 6 ts
Transport of cell from China, Korea or Japan to Europe	EU-28: Heavy fuel oil at refinery (1.0wt.% S) ts	GaBi 6 ts
Transport of components from supplier to OEM factory in Europe	GLO: Truck, Euro 5, 28 - 32t gross weight / 22t payload capacity ts	GaBi 6 ts
Transport of components from supplier to OEM factory in Europe	EU-28: Diesel mix at refinery ts	GaBi 6 ts
Transport of components from supplier to OEM factory in Europe	GLO: Rail transport cargo - average, average train, gross tonne weight 1000t / 726t payload capacity ts	GaBi 6 ts
Transport of components from supplier to OEM factory in Europe	EU-28: Electricity grid mix 1kV-60kV ts	GaBi 6 ts
Transport of components from supplier to OEM factory in Europe	EU-28: Diesel mix at refinery ts	GaBi 6 ts

Table C.58 – continued from previous page

Component/Process	Flow	Source
Transport of components from supplier to OEM factory in Europe	GLO: Average ship, 1500t payload capacity/ canal ts	GaBi 6 ts
Transport of components from supplier to OEM factory in Europe	EU-28: Diesel mix at refinery ts	GaBi 6 ts
Use-phase/Basic consumption	EU-28: Electricity grid mix 1kV-60kV ts	GaBi 6 ts
Use-phase/Heating and air conditioning	EU-28: Electricity grid mix 1kV-60kV ts	GaBi 6 ts
Use-phase/Auxiliares	EU-28: Electricity grid mix 1kV-60kV ts	GaBi 6 ts
Use-phase/Standstill losses	EU-28: Electricity grid mix 1kV-60kV ts	GaBi 6 ts
Use-phase/Charging losses	EU-28: Electricity grid mix 1kV-60kV ts	GaBi 6 ts
Battery pack dissembling/Cell recycling	EU-28: Electricity grid mix 1kV-60kV ts	GaBi 6 ts
Battery pack dissembling/Cell recycling	EU-28: Hard coal mix ts	GaBi 6 ts
Battery pack dissembling/Cell recycling	DE: Lime (CaO; quick-lime lumpy) ts	GaBi 6 ts
Battery pack dissembling/Cell recycling	EU-28: Process steam from natural gas 90% ts	GaBi 6 ts
Battery pack dissembling/.../Metallic aloy treatment	EU-28: Sodium hydroxide (caustic soda) mix (100%) ts	GaBi 6 ts
Battery pack dissembling/.../Metallic aloy treatment	EU-28: Sulphuric acid (96%) ts	GaBi 6 ts
Battery pack dissembling/.../Metallic aloy treatment	EU-28: Tap water ts	GaBi 6 ts
Battery pack dissembling/.../Metallic aloy treatment	EU-28: Thermal energy from natural gas ts	GaBi 6 ts
Battery pack dissembling/.../Metallic aloy treatment	EU-28+EFTA: Landfill of inert (steel)	PEF/OEF data
Battery pack dissembling/.../Metallic aloy treatment	EU-28+EFTA: Treatment of residential wastewater, large plant	PEF/OEF data
Battery pack dissembling/Passive parts recycling	EU-28: Aluminium recycling (2010)	GaBi 6 ts

Table C.58 – continued from previous page

Component/Process	Flow	Source
Battery pack dissembling/Passive parts recycling	DE: EAF Steel billet / Slab / Bloom ts	GaBi 6 ts
Battery pack dissembling/Passive parts recycling	US: Recycling of polypropylene (PP) plastic	PEF/OEF data
Battery pack dissembling/Passive parts recycling	EU-28+EFTA: Recycling of copper from electronic and electric waste	PEF/OEF data
Battery pack dissembling/OEM parts recycling	EU-28: Aluminium recycling (2010) EAA	GaBi 6 ts
Battery pack dissembling/OEM parts recycling	DE: EAF Steel billet / Slab / Bloom ts	GaBi 6 ts
Battery pack dissembling/OEM parts recycling	US: Recycling of polypropylene (PP) plastic	PEF/OEF data
Battery pack dissembling/OEM parts recycling	EU-28+EFTA: Recycling of copper from electronic and electric waste	PEF/OEF data
Battery pack dissembling/OEM parts recycling	EU-28+EFTA: Recycling of gold from electronic and electric scrap	PEF/OEF data
Battery pack dissembling/OEM parts recycling	EU-28+EFTA: Recycling of palladium, from electronic and electric scrap	PEF/OEF data
Battery pack dissembling/OEM parts recycling	EU-28+EFTA: Recycling of silver, from electronic and electric scrap	PEF/OEF data
Battery pack dissembling/Treatment of unsorted battery	EU-28+EFTA: Landfill of inert material (other materials)	PEF/OEF data
Transport from OEM factory to user	GLO: Truck, Euro 5, 28 - 32t gross weight / 22t payload capacity ts	GaBi 6 ts
Transport from OEM factory to user	EU-28: Diesel mix at refinery ts	GaBi 6 ts
Transport to the EoL recycling	GLO: Truck, Euro 5, 28 - 32t gross weight / 22t payload capacity ts	GaBi 6 ts
Transport to the EoL recycling	EU-28: Diesel mix at refinery ts	GaBi 6 ts

L

D

LCIA results

D.1 Climate change

Table D.1: Results on climate change throughout the life cycle on NMC333 and NMC622 batteries

Climate change [kg CO2 eq/fu]	NMC333	NMC622
Production phase	1.2E-01	1.1E-01
Use phase	3.9E-01	3.9E-01
End-of-Life phase	4.0E-03	3.7E-03
Transports	3.5E-04	3.3E-04
SUM	5.2E-01	5.1E-01

D.2 Eutrophication

Table D.2: Results on eutrophication freshwater throughout the life cycle on NMC333 and NMC622 batteries

Eutrophication freshwater [kg P eq/fu]	NMC333	NMC622
Production phase	4.0E-05	4.0E-05
Use phase	1.1E-06	1.1E-06
End-of-Life phase	3.7E-08	3.4E-08
Transports	1.8E-09	1.6E-09
SUM	4.1E-05	4.1E-05

Table D.3: Results on eutrophication marine throughout the life cycle on NMC333 and NMC622 batteries

Eutrophication marine [kg N eq/fu]	NMC333	NMC622
Production phase	1.9E-04	1.8E-04
Use phase	2.4E-04	2.4E-04
End-of-Life phase	1.9E-06	1.7E-06
Transports	5.4E-07	5.0E-07
SUM	4.4E-04	4.2E-04

Table D.4: Results on eutrophication terrestrial throughout the life cycle on NMC333 and NMC622 batteries

Eutrophication terrestrial [Mole of N eq/fu]	NMC333	NMC622
Production phase	2.1E-03	1.9E-03
Use phase	2.5E-03	2.5E-03
End-of-Life phase	1.9E-05	1.8E-05
Transports	5.8E-06	5.4E-06
SUM	4.6E-03	4.4E-03

D.3 Acidification

Table D.5: Results on acidification throughout the life cycle on NMC333 and NMC622 batteries

Acidification [Mole of H+ eq/fu]	NMC333	NMC622
Production phase	2.3E-03	2.9E-03
Use phase	1.2E-03	1.2E-03
End-of-Life phase	1.4E-05	1.3E-05
Transports	1.2E-06	1.1E-06
SUM	3.5E-03	4.2E-03

D.4 Human toxicity

Table D.6: Results on human toxicity with non-cancer effects throughout the life cycle on NMC333 and NMC622 batteries

Human toxicity, non-cancer effects [CTUh/fu]	NMC333	NMC622
Production phase	7.1E-08	7.0E-08
Use phase	5.3E-11	5.3E-11
End-of-Life phase	1.2E-10	1.2E-10
Transports	2.5E-11	2.3E-11
SUM	7.1E-08	7.0E-08

Table D.7: Results on human toxicity with cancer effects throughout the life cycle on NMC333 and NMC622 batteries

Human toxicity, cancer effects [CTUh/fu]	NMC333	NMC622
Production phase	4.1E-09	3.9E-09
Use phase	3.2E-10	3.2E-10
End-of-Life phase	2.2E-11	2.1E-11
Transports	2.2E-12	2.0E-12
SUM	4.5E-09	4.2E-09

Table D.8: Results on ecotoxicity freshwater throughout the life cycle on NMC333 and NMC622 batteries

Ecotoxicity freshwater [CTUe/fu]	NMC333	NMC622
Production phase	1.6E+00	1.6E+00
Use phase	1.2E-02	1.2E-02
End-of-Life phase	4.5E-04	4.2E-04
Transports	5.4E-05	5.0E-05
SUM	1.6E+00	1.6E+00

D.5 Freshwater ecotoxicity

D.6 Photochemical ozone formation

D.7 Ozone depletion

D.8 Ionizing radiation

D.9 Particulate matter

D.10 Resource depletion

D.11 Land use

Table D.9: Results on photochemical ozone formation throughout the life cycle on NMC333 and NMC622 batteries

Photochemical ozone formation [kg NMVOC/fu]	NMC333	NMC622
Production phase	6.5E-04	6.5E-04
Use phase	6.4E-04	6.4E-04
End-of-Life phase	6.0E-06	5.5E-06
Transports	1.0E-06	9.3E-07
SUM	1.3E-03	1.3E-03

Table D.10: Results on ozone depletion throughout the life cycle on NMC333 and NMC622 batteries

Ozone depletion [kg CFC-11 eq/fu]	NMC333	NMC622
Production phase	3.3E-09	3.2E-09
Use phase	1.7E-12	1.7E-12
End-of-Life phase	1.3E-12	1.3E-12
Transports	9.5E-18	8.8E-18
SUM	3.3E-09	3.2E-09

Table D.11: Results on ionizing radiation throughout the life cycle on NMC333 and NMC622 batteries

Ionizing radiation [kg kBq U235 eq/fu]	NMC333	NMC622
Production phase	1.49E-02	1.38E-02
Use phase	1.90E-01	1.90E-01
End-of-Life phase	3.47E-04	3.20E-04
Transports	9.58E-07	8.87E-07
SUM	2.05E-01	2.05E-01

Table D.12: Results on particulate matter throughout the life cycle on NMC333 and NMC622 batteries

Particulate matter/Respiratory inorganics [kg PM2.5 eq/fu]	NMC333	NMC622
Production phase	1.7E-04	1.8E-04
Use phase	5.9E-05	5.9E-05
End-of-Life phase	7.0E-07	6.4E-07
Transports	3.3E-08	3.1E-08
SUM	2.3E-04	2.4E-04

Table D.13: Results on resource depletion mineral, fossils and renewables throughout the life cycle on NMC333 and NMC622 batteries

Resource depletion, mineral, fossils and renewables [kg Sb eq/fu]	NMC333	NMC622
Production phase	6.6E-05	6.5E-05
Use phase	1.8E-06	1.8E-06
End-of-Life phase	7.1E-09	6.7E-09
Transports	1.3E-10	1.2E-10
SUM	6.8E-05	6.6E-05

Table D.14: Results on resource depletion water throughout the life cycle on NMC333 and NMC622 batteries

Resource depletion water [m3 eq/fu]	NMC333	NMC622
Production phase	2.3E-03	2.1E-03
Use phase	2.6E-02	2.6E-02
End-of-Life phase	9.0E-05	8.4E-05
Transports	4.1E-07	3.8E-07
SUM	2.9E-02	2.8E-02

Table D.15: Results on land use throughout the life cycle on NMC333 and NMC622 batteries

Land use [kg C deficit eq]	NMC333	NMC622
Production phase	5.0E-02	4.8E-02
Use phase	2.0E-01	2.0E-01
End-of-Life phase	6.3E-03	6.0E-03
Transports	2.6E-04	2.4E-04
SUM	2.6E-01	2.6E-01

LVI

E

Normalization

E.1 ILCD classification of impact categories

The impact categories are classified according to the ILCD Handbook where the quality levels are described as follow:

- Level "I": Recommended and satisfactory

- Level "II": Recommended but in need of some improvements

- Level "III": Recommended, but to be applied with caution

Table E.1: ILCD classification of the recommended impact categories with three different quality levels The ranking is determined by the ILCD Handbook and facilitate the understanding of the importance of each impact category,

ILCD classification	Impact cateogies	Unit
I	Climate change, excl biogenic carbon	DPE
I	Climate change, incl biogenic carbon	DPE
I	Particulate matter/Respiratory inorganics	DPE
I	Ozone depletion	DPE
II	Acidification	DPE
II	Ionizing radiation	DPE
II	Photochemical ozone formation	DPE
II	Terrestrial eutrophication	DPE
II	Marine eutrophication	DPE
II/III	Human toxicity non-canc. effects	DPE
II/III	Human toxicity cancer effects	DPE
II/III	Ecotoxicity for aquatic fresh water	DPE
III	Resource depletion water	DPE
III	Land use	DPE

E.2   Normalisation factors

Table E.2: Normalization factors per person according to the ILCD-compliant normalization reference EC-JRC EU27.

Impact category	Normalisation Factor per Person
Climate change	9.2E+03
Ozone depletion	2.2E-02
Human toxicity - cancer effects	3.7E-05
Human toxicity - non-cancer effects	5.3E-04
Acidification	4.7E+01
Particulate matter/Respiratory Inorganics	3.8E+00
Ecotoxicity for aquatic fresh water	8.7E+03
Ionising radiations – human health effects	1.1E+03
Photochemical ozone formation	3.2E+01
Eutrophication - terrestrial	1.8E+02
Eutrophication - freshwater	1.5E+00
Eutrophication - marine	1.7E+01
Land use	7.5E+04
Resource depletion - water	8.1E+01
Resource depletion - mineral, fossil & renewable	1.0E-01

E.3 Complete list on the normalization

Table E.3: Complete list of results on the normalization of the cradle-to-grave impacts. The normalization factors that were used are recommended by the PEFCR and are expressed as impact per person within EU.

Impact category	NMC333	NMC622
Climate change	5.6E-05	5.5E-05
Ozone depletion	1.5E-07	1.5E-07
Human toxicity - cancer effects	1.2E-04	1.1E-04
Human toxicity - non-cancer effects	1.3E-04	1.3E-04
Acidification	7.5E-05	8.8E-05
Particulate matter/Respiratory Inorganics	6.1E-05	6.3E-05
Ecotoxicity for aquatic fresh water	1.8E-04	1.8E-04
Ionising radiations – human health effects	1.8E-04	1.8E-04
Photochemical ozone formation	4.1E-05	4.1E-05
Eutrophication - terrestrial	2.6E-05	2.5E-05
Eutrophication - freshwater	2.8E-05	2.8E-05
Eutrophication - marine	2.6E-05	2.5E-05
Land use	3.5E-06	3.5E-06
Resource depletion - water	3.5E-04	3.5E-04
Resource depletion - mineral, fossil & renewable	6.7E-04	6.6E-04

F
Weighting

F.1 Weighting factors

Table F.1: Weighting factors for each impact category recommended by the PE-FCR (Siret et al., 2018)

Impact categories	Weighting factors
Climate change	22.19
Ozone depletion	6.75
Acidification	6.64
Particulate matter/Respiratory Inorganics	9.54
Ionising radiations – human health effects	5.37
Photochemical ozone formation	5.1
Eutrophication - terrestrial	3.91
Eutrophication - freshwater	2.95
Eutrophication - marine	3.12

F.2 Complete list on the weighting

Table F.2: Complete list of LCIA results of the cradle-to-grave impact after normalization and weighting. The weighting factors that were used are recommended by the PEFCR and are derived from an aggregated weighting set and robustness factors.

Impact categories	NMC333	NMC622
Climate change	1.2E-03	1.2E-03
Ozone depletion	9.6E-07	9.2E-07
Human toxicity - cancer effects	2.6E-04	2.4E-04
Human toxicity - non-cancer effects	2.5E-04	2.4E-04
Acidification	4.6E-04	5.5E-04
Particulate matter/ Respiratory Inorganics	5.5E-04	5.6E-04
Ecotoxicity for aquatic fresh water	3.5E-04	3.5E-04
Ionising radiations	9.1E-04	9.1E-04
Photochemical ozone formation	2.0E-04	2.0E-04
Eutrophication - terrestrial	9.6E-05	9.3E-05
Eutrophication - freshwater	7.7E-05	7.7E-05
Eutrophication - marine	7.6E-05	7.4E-05
Land use	2.8E-05	2.7E-05
Resource depletion - water	3.0E-03	3.0E-03
Resource depletion - mineral, fossil & renewable	5.0E-03	5.0E-03
SUM	1.2E-02	1.2E-02

G

Contribution analysis

G.1 Toxicity
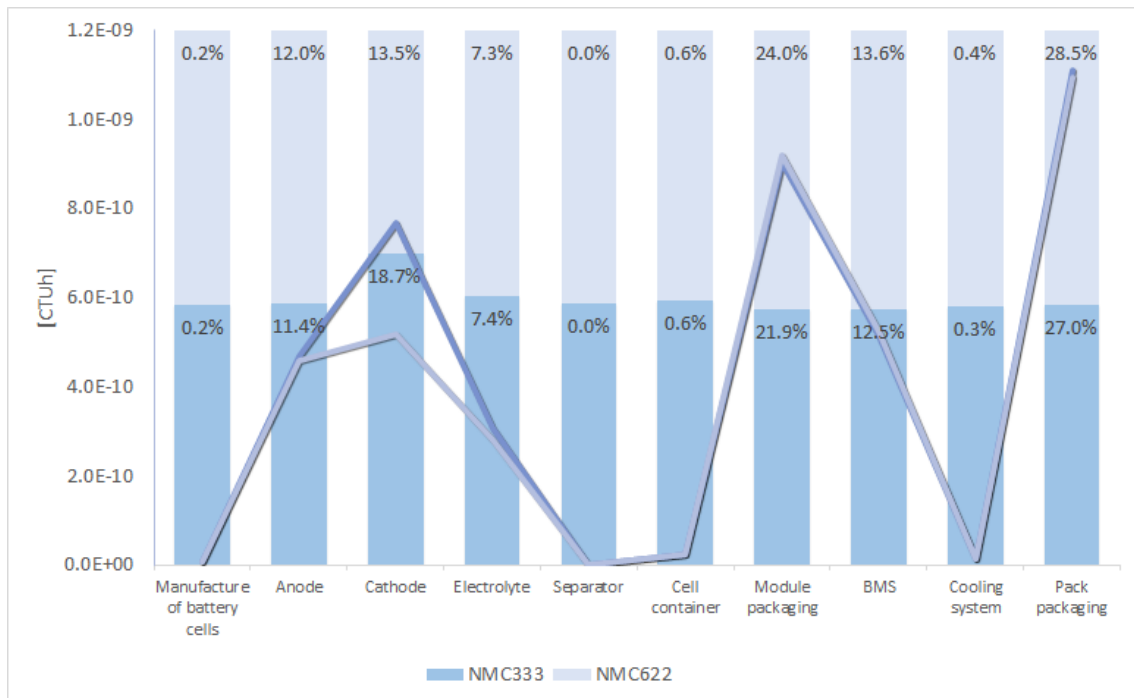
Figure G.1: Contribution of different components and processes to the cradle-to-gate environmental impacts on human toxicity with cancer effects for NMC333 and NMC622. The right axis represents the absolute value whereas the left represents shares of the total impact on human toxicity with cancer effects.

G.2 Resource depletion and land use
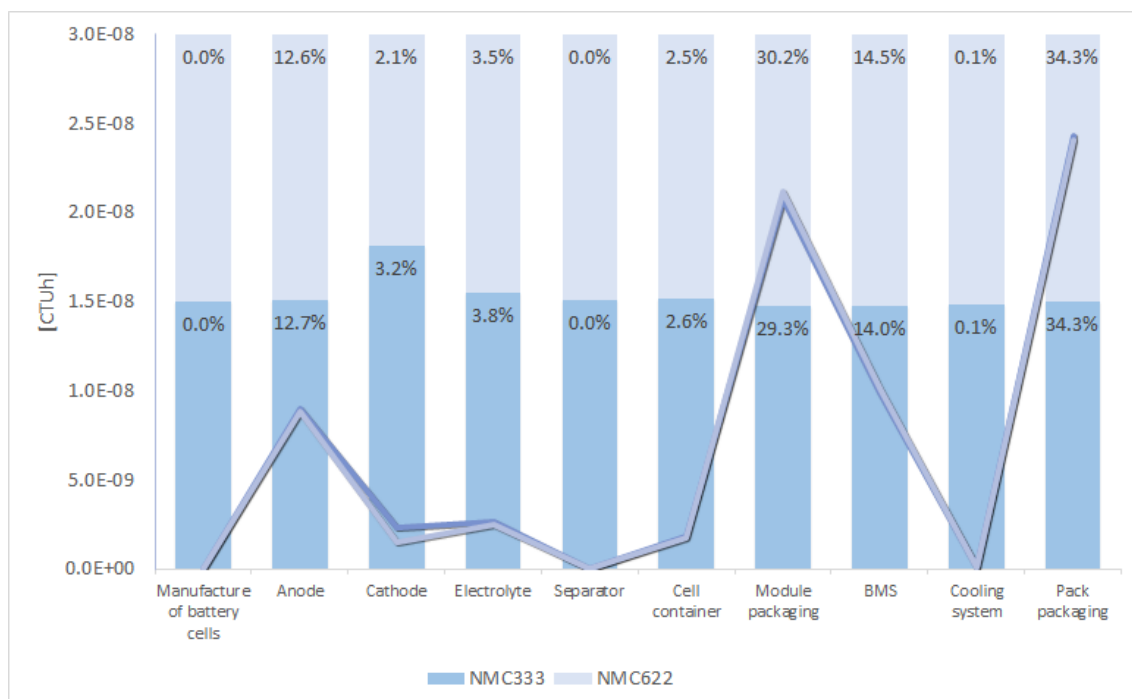
Figure G.2: Contribution of different components and processes to the cradle-to-gate environmental impacts on human toxicity with non-cancer effects for NMC333 and NMC622. The right axis represents the absolute value whereas the left represents shares of the total impact on human toxicity with non-cancer effects.
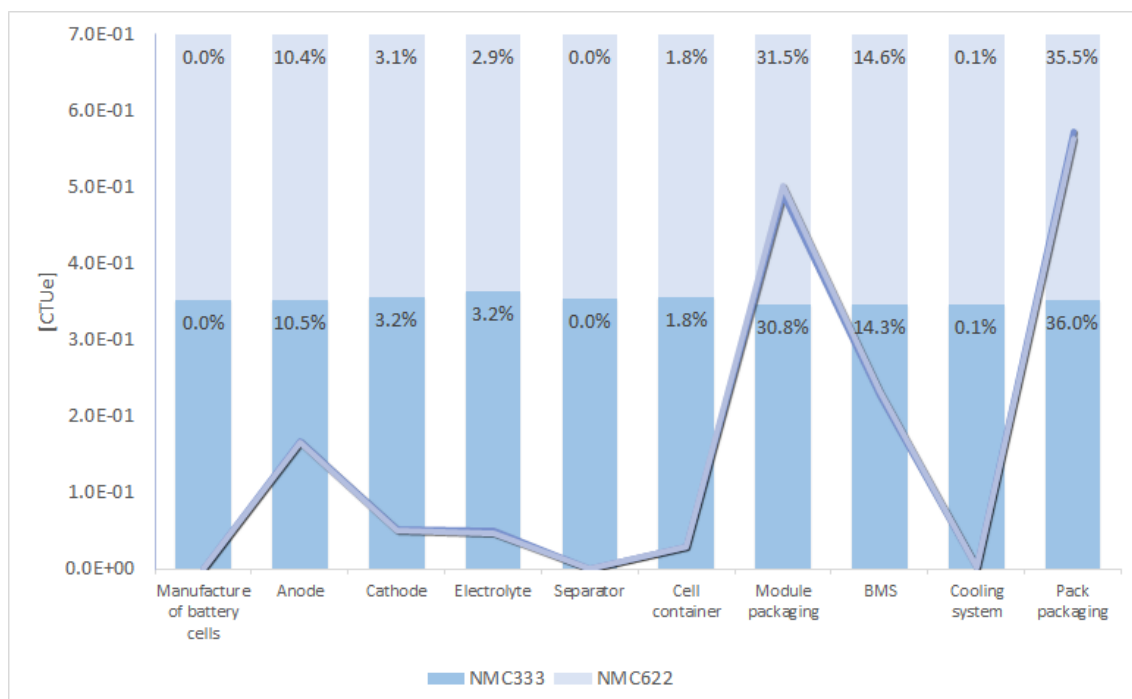
Figure G.3: Contribution of different components and processes to the cradle-to-gate environmental impacts on freshwater ecotoxicity for NMC333 and NMC622. The right axis represents the absolute value whereas the left represents shares of the total impact on freshwater ecotoxicity.
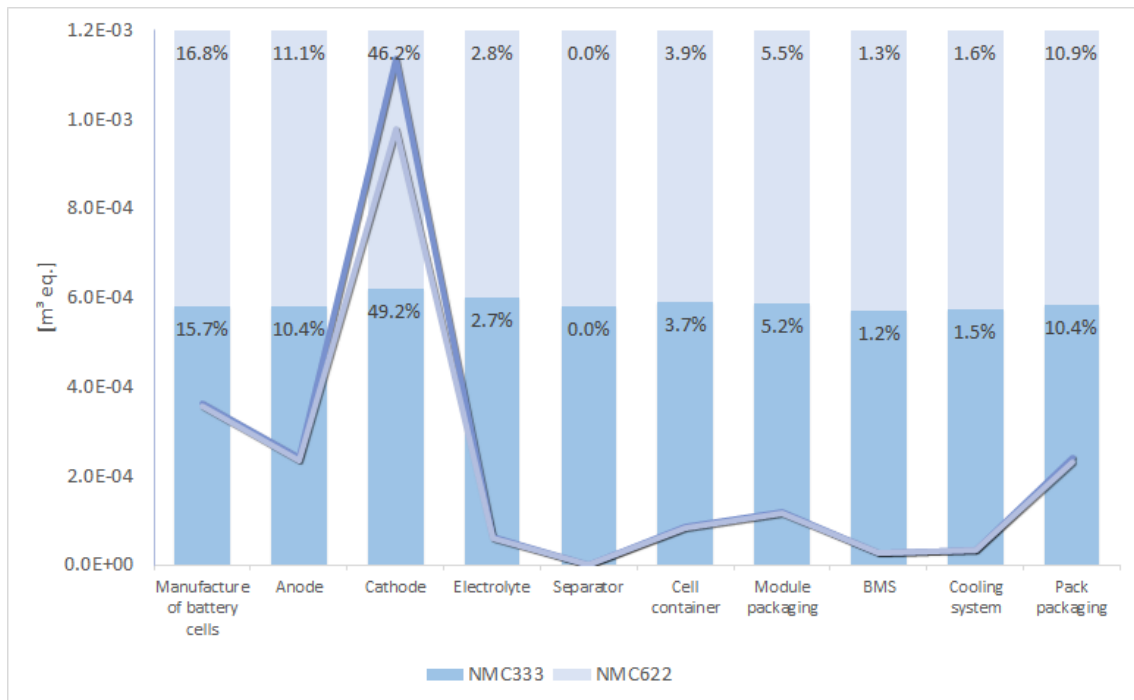
Figure G.4: Contribution of different components and processes to the cradle-to-gate environmental impacts on water scarcity for NMC333 and NMC622. The right axis represents the absolute value whereas the left represents shares of the total impact on water scarcity.
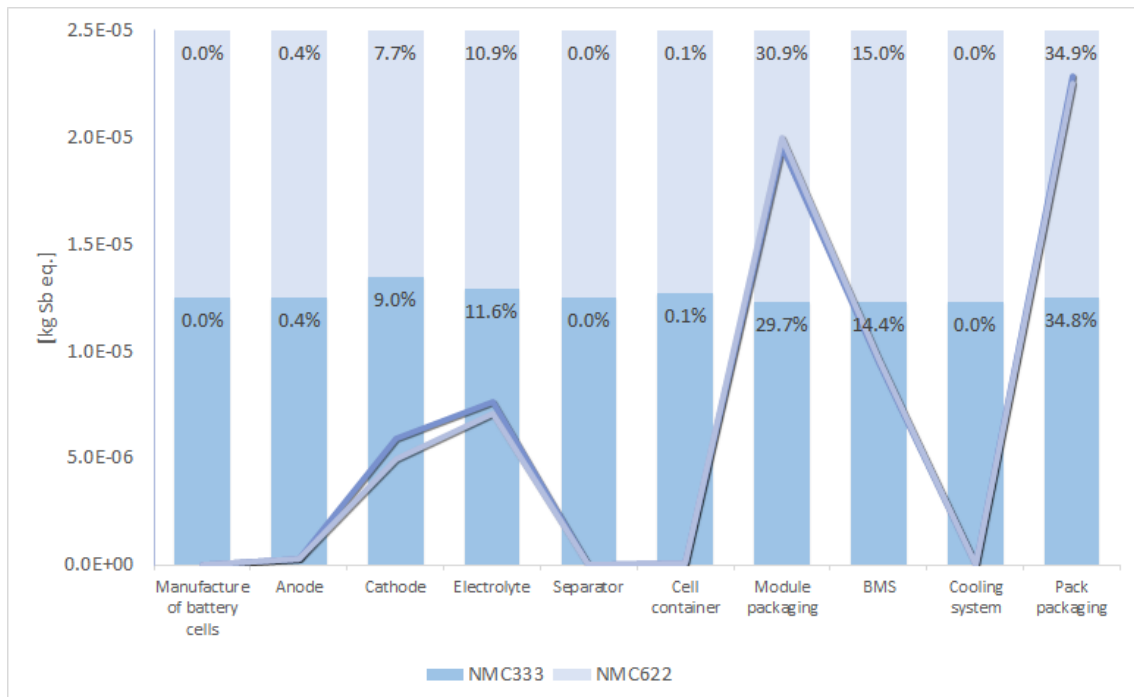
Figure G.5: Contribution of different components and processes to the cradle-to-gate environmental impacts on abiotic resource depletion for NMC333 and NMC622. The right axis represents the absolute value whereas the left represents shares of the total impact on abiotic resource depletion.
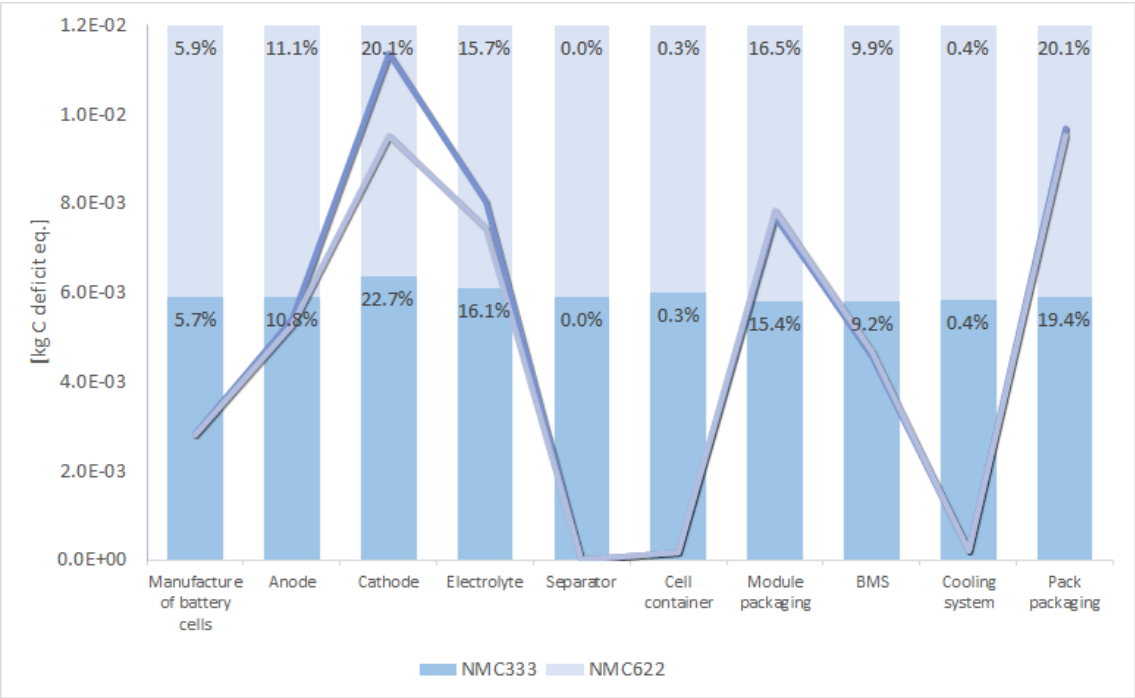
Figure G.6: Contribution of different components and processes to the cradle-to-gate environmental impacts on land use for NMC333 and NMC622. The right axis represents the absolute value whereas the left represents shares of the total impact on land use.

H
Structural path analysis

H.1 Global warming potential

Table H.1: The most important paths for global warming impacts of the NMC333 battery manufacturing

Absolute [kg CO2 eq.]	Relative	Cumulative			
9.4E-03	8.0%	8.0%	Pack packaging	EU-28: Aluminium ingot mix ts	
8.8E-03	7.5%	16%	Cathode	Precursor, NMC333 <u-so>	EU-28: Thermal energy from natural gas ts
8.6E-03	7.4%	23%	Cathode	Active cathode material, NMC333 <u-so>	EU-28: Electricity grid mix 1kV-60kV ts
7.2E-03	6.1%	29%	Manufacture of battery cells	Electrode drying & NMP recovery	EU-28: Thermal energy from natural gas ts
7.2E-03	6.1%	35%	Manufacture of battery cells	Dry room maintenance	EU-28: Thermal energy from natural gas ts
5.1E-03	4.4%	39%	Manufacture of battery cells	Dry room maintenance	EU-28: Electricity grid mix 1kV-60kV ts
4.7E-03	4.0%	44%	Cathode	Lithium carbonate	DE: Soda (Na2CO3) ts
4.6E-03	4.0%	47%	Electrolyte	GLO: market for lithium hexafluorophosphate ecoinvent 3.4	
4.3E-03	3.7%	51%	Cathode	Cobalt sulfate <LC>	EU-28: Thermal energy from light fuel oil (LFO) ts
3.9E-03	3.3%	55%	Cathode	Positive current collector	EU-28: Aluminium ingot mix ts
3.8E-03	3.2%	58%	Anode	GLO: market for graphite, battery grade ecoinvent 3.4	
2.8E-03	2.3%	60%	Cathode	Precursor	EU-28: Sodium hydroxide (caustic soda) mix (100%) ts
2.7E-03	2.3%	62%	Cathode	Nickel sulfate <LC>	Nickel refining (Ni institute) <u-so>
2.7E-03	2.3%	65%	Module packaging	GLO: market for electronic component, passive, unspecified ecoinvent 3.4	
2.6E-03	2.2%	67%	Pack packaging	GLO: market for electronic component, passive, unspecified ecoinvent 3.4	
2.4E-03	2.0%	69%	Module packaging	EU-28: Aluminium ingot mix ts	
1.8E-03	1.5%	70%	Cathode	Cobalt sulfate <LC>	EU-28: Sodium hydroxide (caustic soda) mix (100%) ts
1.7E-03	1.5%	72%	Cathode	Cobalt sulfate <LC>	CN: Electricity grid mix 1kV-60kV ts
1.6E-03	1.4%	73%	Module packaging	EU-28: Aluminium ingot mix ts	
1.4E-03	1.2%	75%	Cathode	Cobalt sulfate <LC>	CN: Thermal energy from natural gas ts
1.4E-03	1.2%	76%	Cathode	Transport of active material <LC>	GLO: Bulk commodity carrier, average, ocean going ts <u-so>
1.3E-03	1.1%	77%	Anode	EU-28: Copper Sheet Mix DKI/ECI	
1.3E-03	1.1%	78%	Cell container	EU-28: Aluminium ingot mix ts	
1.2E-03	1.0%	79%	Cooling system	EU-28: Aluminium ingot mix ts	
1.0E-03	0.9%	80%	Cathode	Nickel sulfate <LC>	Nickel primary extraction (Ni institute) <u-so>
9.9E-04	0.8%	81%	Anode	Transport of active material <LC>	GLO: Bulk commodity carrier, average, ocean going ts <u-so>

Table H.2: The most important paths for global warming impacts of the NMC622 battery manufacturing

Absolute [kg CO2 eq.]	Relative	Cumulative			
9.1E-03	8.5%	8.5%	Pack packaging	EU-28: Aluminium ingot mix ts	
7.4E-03	6.9%	15%	Cathode	EU-28: Thermal energy from natural gas ts	
7.3E-03	6.8%	22%	Cathode	EU-28: Electricity grid mix 1kV-60kV ts	
7.1E-03	6.6%	29%	Manufacture of battery cells	Dry room maintenance	EU-28: Thermal energy from natural gas ts
7.1E-03	6.6%	35%	Manufacture of battery cells	Electrode drying & NMP recovery	EU-28: Thermal energy from natural gas ts
5.0E-03	4.7%	40%	Manufacture of battery cells	Dry room maintenance	EU-28: Electricity grid mix 1kV-60kV ts
4.3E-03	4.0%	44%	Electrolyte	GLO: market for lithium hexafluorophosphate ecoinvent 3.4	
4.1E-03	3.8%	48%	Cathode	Nickel sulfate <LC>	Nickel refining (Ni institute) <u-so>
4.0E-03	3.7%	52%	Cathode	Lithium carbonate	DE: Soda (Na2CO3) ts
3.8E-03	3.6%	55%	Cathode	Positive current collector	EU-28: Aluminium ingot mix ts
3.7E-03	3.5%	59%	Anode	GLO: market for graphite, battery grade ecoinvent 3.4	
2.7E-03	2.5%	61%	Module packaging	GLO: market for electronic component, passive, unspecified ecoinvent 3.4	
2.5E-03	2.3%	63%	Pack packaging	GLO: market for electronic component, passive, unspecified ecoinvent 3.4	
2.3E-03	2.2%	66%	Cathode	Precursor	EU-28: Sodium hydroxide (caustic soda) mix (100%) ts
2.3E-03	2.1%	68%	Module packaging	EU-28: Aluminium ingot mix ts	
2.2E-03	2.0%	70%	Cathode	Cobalt sulfate <LC>	EU-28: Thermal energy from light fuel oil (LFO) ts
1.6E-03	1.5%	71%	Cathode	Nickel sulfate <LC>	Nickel primary extraction (Ni institute) <u-so>
1.6E-03	1.5%	73%	Module packaging	EU-28: Aluminium ingot mix ts	
1.3E-03	1.2%	74%	Anode	EU-28: Copper Sheet Mix DKI/ECI	
1.2E-03	1.1%	75%	Cooling system	EU-28: Aluminium ingot mix ts	
1.2E-03	1.1%	76%	Cathode	Transport of active material <LC>	GLO: Bulk commodity carrier, average, ocean going ts <u-so>
1.2E-03	1.1%	77%	Cell container	EU-28: Aluminium ingot mix ts	
9.8E-04	0.9%	78%	Anode	Transport of active material <LC>	GLO: Bulk commodity carrier, average, ocean going ts <u-so>
9.1E-04	0.8%	79%	Cathode	Nickel sulfate <LC>	Nickel mining (Sulphidic) <u-so>
9.0E-04	0.8%	80%	Cathode	Nickel sulfate <LC>	Nickel beneficiation (Sulphidic path) <u-so>
8.9E-04	0.8%	81%	Cathode	Cobalt sulfate <LC>	EU-28: Sodium hydroxide (caustic soda) mix (100%) ts

H.2   Eutrophication freshwater

Table H.3: The most important paths for eutrophication freshwater impacts of the NMC333 battery manufacturing

Absolute [kg P eq.]	Relative	Cumulative		
1.3E-05	32%	32%	Module packaging	GLO: market for electronic component, passive, unspecified ecoinvent 3.4
1.2E-05	31%	62%	Pack packaging	GLO: market for electronic component, passive, unspecified ecoinvent 3.4
3.7E-06	9.2%	72%	Anode	GLO: market for graphite, battery grade ecoinvent 3.4
3.3E-06	8.4%	80%	BMS	GLO: market for electronic component, passive, unspecified ecoinvent 3.4

Table H.4: The most important paths for eutrophication freshwater impacts of the NMC622 battery manufacturing

Absolute [kg CO2 eq.]	Relative	Cumulative		
1.3E-05	33%	33%	Module packaging	GLO: market for electronic component, passive, unspecified ecoinvent 3.4
1.2E-05	30%	63%	Pack packaging	GLO: market for electronic component, passive, unspecified ecoinvent 3.4
3.6E-06	9.0%	72%	Anode	GLO: market for graphite, battery grade ecoinvent 3.4
3.4E-06	8.6%	80%	BMS	GLO: market for electronic component, passive, unspecified ecoinvent 3.4

H.3   Eutrophication marine

Table H.5: The most important paths for eutrophication marine impacts of the NMC333 battery manufacturing

Absolute [kg N eq.]	Relative	Cumulative			
1.4E-05	11%	11%	Cathode	Transport of active material <LC>	GLO: Bulk commodity carrier, average, ocean going ts <u-so>
1.0E-05	8.0%	19%	Anode	Transport of active material <LC>	GLO: Bulk commodity carrier, average, ocean going ts <u-so>
8.0E-06	6.3%	26%	Cathode	Lithium carbonate	DE: Soda (Na2CO3) ts
7.1E-06	5.6%	31%	Pack packaging	EU-28: Aluminium ingot mix ts	
6.3E-06	5.0%	36%	Electrolyte	GLO: market for lithium hexafluorophosphate ecoinvent 3.4	
5.4E-06	4.3%	40%	Cathode	EU-28: Electricity grid mix 1kV-60kV ts	
5.1E-06	4.0%	45%	Module packaging	GLO: market for electronic component, passive, unspecified ecoinvent 3.4	
4.9E-06	3.9%	48%	Pack packaging	GLO: market for electronic component, passive, unspecified ecoinvent 3.4	
4.7E-06	3.7%	52%	Electrolyte	Transport of active material <LC>	GLO: Bulk commodity carrier, average, ocean going ts <u-so>
4.1E-06	3.2%	55%	Anode	GLO: market for graphite, battery grade ecoinvent 3.4	
3.4E-06	2.7%	58%	Module packaging	Transport of cell from China, Korea or Japan to Europe <LC>	GLO: Bulk commodity carrier, average, ocean going ts <u-so>
3.2E-06	2.5%	60%	Manufacture of battery cells	Dry room maintenance	EU-28: Electricity grid mix 1kV-60kV ts
2.9E-06	2.3%	63%	Cathode	EU-28: Aluminium ingot mix ts	
2.9E-06	2.3%	65%	Cell container	Transport of passive material <LC>	GLO: Bulk commodity carrier, average, ocean going ts <u-so>
2.6E-06	2.0%	67%	Cathode	EU-28: Sodium hydroxide (caustic soda) mix (100%) ts	
2.5E-06	2.0%	69%	Cathode	EU-28: Thermal energy from natural gas ts	
2.5E-06	2.0%	71%	Cathode	Cobalt sulfate <LC>	EU-28: Thermal energy from light fuel oil (LFO) ts
2.1E-06	1.6%	73%	Manufacture of battery cells	Dry room maintenance	EU-28: Thermal energy from natural gas ts
2.1E-06	1.6%	74%	Manufacture of battery cells	Electrode drying & NMP recovery	EU-28: Thermal energy from natural gas ts
2.1E-06	1.6%	76%	Cathode	Nickel sulfate <LC>	Nickel refining (Ni institute) <u-so>
1.8E-06	1.4%	77%	Module packaging	EU-28: Aluminium ingot mix ts	
1.7E-06	1.3%	79%	Cathode	Cobalt sulfate <LC>	EU-28: Sodium hydroxide (caustic soda) mix (100%) ts
1.4E-06	1.1%	80%	Cathode	Cobalt sulfate <LC>	CN: Electricity grid mix 1kV-60kV ts

Table H.6: The most important paths for eutrophication marine impacts of the NMC622 battery manufacturing

Absolute [kg N eq.]	Relative	Cumulative		
1.2E-05	11%	11%	Cathode	Transport of active material <LC>	GLO: Bulk commodity carrier, average, ocean going ts <u-so>
1.0E-05	9%	19%	Anode	Transport of active material <LC>	GLO: Bulk commodity carrier, average, ocean going ts <u-so>
6.9E-06	5.9%	25%	Pack packaging	EU-28: Aluminium ingot mix ts	
6.7E-06	5.8%	31%	Cathode	DE: Soda (Na2CO3) ts	
5.8E-06	5.0%	36%	Electrolyte	GLO: market for lithium hexafluorophosphate ecoinvent 3.4	
5.2E-06	4.5%	41%	Module packaging	GLO: market for electronic component, passive, unspecified ecoinvent 3.4	
4.8E-06	4.2%	45%	Pack packaging	GLO: market for electronic component, passive, unspecified ecoinvent 3.4	
4.6E-06	4.0%	49%	Cathode	EU-28: Electricity grid mix 1kV-60kV ts	
4.3E-06	3.7%	52%	Electrolyte	Transport of active material <LC>	GLO: Bulk commodity carrier, average, ocean going ts <u-so>
4.0E-06	3.4%	56%	Anode	GLO: market for graphite, battery grade ecoinvent 3.4	
3.3E-06	2.8%	59%	Module packaging	Transport of cell from China, Korea or Japan to Europe <LC>	GLO: Bulk commodity carrier, average, ocean going ts <u-so>
3.2E-06	2.7%	61%	Manufacture of battery cells	Dry room maintenance	EU-28: Electricity grid mix 1kV-60kV ts
3.1E-06	2.7%	64%	Cathode	Nickel sulfate <LC>	Nickel refining (Ni institute) <u-so>
2.9E-06	2.5%	67%	Cathode	EU-28: Aluminium ingot mix ts	
2.2E-06	1.9%	69%	Cathode	EU-28: Sodium hydroxide (caustic soda) mix (100%) ts	
2.1E-06	1.8%	70%	Cathode	EU-28: Thermal energy from natural gas ts	
2.0E-06	1.8%	72%	Manufacture of battery cells	Dry room maintenance	EU-28: Thermal energy from natural gas ts
2.0E-06	1.8%	74%	Manufacture of battery cells	Electrode drying & NMP recovery	EU-28: Thermal energy from natural gas ts
1.7E-06	1.5%	75%	Module packaging	EU-28: Aluminium ingot mix ts	
1.5E-06	1.3%	77%	Cathode	Nickel sulfate <LC>	Nickel primary extraction (Ni institute) <u-so>
1.4E-06	1.2%	78%	BMS	GLO: market for electronic component, passive, unspecified ecoinvent 3.4	
1.3E-06	1.1%	79%	Cathode	Cobalt sulfate <LC>	EU-28: Thermal energy from light fuel oil (LFO) ts
1.3E-06	1.1%	80%	Cathode	Nickel sulfate <LC>	Nickel mining (Sulphidic) <u-so>

H.4 Eutrophication terrestrial

Table H.7: The most important paths for eutrophication terrestrial impacts of the NMC333 battery manufacturing

Absolute [Mole of N eq.]	Relative	Cumulative			
1.6E-04	11%	11%	Cathode	Transport of active material <LC>	GLO: Bulk commodity carrier, average, ocean going ts <u-so>
1.3E-04	9.3%	21%	Cathode	DE: Soda (Na2CO3) ts	
1.1E-04	8.1%	29%	Anode	Transport of active material <LC>	GLO: Bulk commodity carrier, average, ocean going ts <u-so>
7.7E-05	5.6%	34%	Pack packaging	EU-28: Aluminium ingot mix ts	
5.5E-05	4.0%	38%	Cathode	EU-28: Electricity grid mix 1kV-60kV ts	
5.3E-05	3.8%	42%	Electrolyte	GLO: market for lithium hexafluorophosphate ecoinvent 3.4	
5.2E-05	3.8%	46%	Module packaging	GLO: market for electronic component, passive, unspecified ecoinvent 3.4	
5.1E-05	3.7%	50%	Electrolyte	Transport of active material <LC>	GLO: Bulk commodity carrier, average, ocean going ts <u-so>
5.0E-05	3.6%	53%	Pack packaging	GLO: market for electronic component, passive, unspecified ecoinvent 3.4	
3.9E-05	2.9%	56%	Anode	GLO: market for graphite, battery grade ecoinvent 3.4	
3.7E-05	2.7%	59%	Module packaging	Transport of cell from China, Korea or Japan to Europe <LC>	GLO: Bulk commodity carrier, average, ocean going ts <u-so>
3.2E-05	2.3%	61%	Manufacture of battery cells	Dry room maintenance	EU-28: Electricity grid mix 1kV-60kV ts
3.2E-05	2.3%	63%	Cell container	Transport of passive material <LC>	GLO: Bulk commodity carrier, average, ocean going ts <u-so>
3.2E-05	2.3%	66%	Cathode	EU-28: Aluminium ingot mix ts	
2.8E-05	2.1%	68%	Cathode	EU-28: Sodium hydroxide (caustic soda) mix (100%) ts	
2.8E-05	2.0%	70%	Cathode	EU-28: Thermal energy from natural gas ts	
2.8E-05	2.0%	72%	Cathode	Cobalt sulfate <LC>	EU-28: Thermal energy from light fuel oil (LFO) ts
2.3E-05	1.7%	73%	Manufacture of battery cells	Dry room maintenance	EU-28: Thermal energy from natural gas ts
2.3E-05	1.7%	75%	Manufacture of battery cells	Electrode drying & NMP recovery	EU-28: Thermal energy from natural gas ts
2.3E-05	1.6%	77%	Cathode	Nickel sulfate <LC>	Nickel refining (Ni institute) <u-so>
2.0E-05	1.4%	78%	Module packaging	EU-28: Aluminium ingot mix ts	
1.8E-05	1.3%	80%	Cathode	Cobalt sulfate <LC>	EU-28: Sodium hydroxide (caustic soda) mix (100%) ts
1.6E-05	1.1%	81%	Cathode	Cobalt sulfate <LC>	CN: Electricity grid mix 1kV-60kV ts

Table H.8: The most important paths for eutrophication terrestrial impacts of the NMC622 battery manufacturing

Absolute [Mole of N eq.]	Relative	Cumulative			
1.3E-04	11%	11%	Cathode	Transport of active material <LC>	GLO: Bulk commodity carrier, average, ocean going ts <u-so>
1.1E-04	8.7%	19%	Anode	Transport of active material <LC>	GLO: Bulk commodity carrier, average, ocean going ts <u-so>
1.1E-04	8.6%	28%	Cathode	DE: Soda (Na2CO3) ts	
7.4E-05	5.9%	34%	Pack packaging	EU-28: Aluminium ingot mix ts	
5.3E-05	4.2%	38%	Module packaging	GLO: market for electronic component, passive, unspecified ecoinvent 3.4	
4.9E-05	3.9%	42%	Electrolyte	GLO: market for lithium hexafluorophosphate ecoinvent 3.4	
4.9E-05	3.9%	46%	Pack packaging	GLO: market for electronic component, passive, unspecified ecoinvent 3.4	
4.8E-05	3.8%	50%	Electrolyte	Transport of active material <LC>	GLO: Bulk commodity carrier, average, ocean going ts <u-so>
4.6E-05	3.7%	54%	Cathode	EU-28: Electricity grid mix 1kV-60kV ts	
3.9E-05	3.1%	57%	Anode	GLO: market for graphite, battery grade ecoinvent 3.4	
3.6E-05	2.8%	59%	Module packaging	Transport of cell from China, Korea or Japan to Europe <LC>	GLO: Bulk commodity carrier, average, ocean going ts <u-so>
3.4E-05	2.7%	62%	Cathode	Nickel sulfate <LC>	Nickel refining (Ni institute) <u-so>
3.2E-05	2.6%	65%	Manufacture of battery cells	Dry room maintenance	EU-28: Electricity grid mix 1kV-60kV ts
3.1E-05	2.5%	67%	Cathode	EU-28: Aluminium ingot mix ts	
2.4E-05	1.9%	69%	Cathode	EU-28: Sodium hydroxide (caustic soda) mix (100%) ts	
2.4E-05	1.9%	71%	Cathode	EU-28: Thermal energy from natural gas ts	
2.3E-05	1.8%	73%	Manufacture of battery cells	Dry room maintenance	EU-28: Thermal energy from natural gas ts
2.3E-05	1.8%	75%	Manufacture of battery cells	Electrode drying & NMP recovery	EU-28: Thermal energy from natural gas ts
1.8E-05	1.5%	76%	Module packaging	EU-28: Aluminium ingot mix ts	
1.7E-05	1.3%	77%	Cathode	Nickel sulfate <LC>	Nickel primary extraction (Ni institute) <u-so>
1.4E-05	1.1%	79%	BMS	GLO: market for electronic component, passive, unspecified ecoinvent 3.4	
1.4E-05	1.1%	80%	Cathode	Cobalt sulfate <LC>	EU-28: Thermal energy from light fuel oil (LFO) ts
1.4E-05	1.1%	81%	Cathode	Nickel sulfate <LC>	Nickel mining (Sulphidic) <u-so>

H.5   Acidification

Table H.9: The most important paths for acidification impacts of the NMC333 battery manufacturing

Absolute [Mole of H+ eq.]	Relative	Cumulative			
1.3E-03	64%	64%	Cathode	Nickel sulfate <LC>	Nickel refining (Ni institute) <u-so>
6.9E-05	3.4%	68%	Cathode	Nickel sulfate <LC>	Nickel primary extraction (Ni institute) <u-so>
5.8E-05	2.8%	71%	Cathode	Transport of active material <LC>	GLO: Bulk commodity carrier, average, ocean going ts <u-so>
5.2E-05	2.5%	73%	Pack packaging	EU-28: Aluminium ingot mix ts	
4.1E-05	2.0%	75%	Anode	Transport of active material <LC>	GLO: Bulk commodity carrier, average, ocean going ts <u-so>
4.1E-05	2.0%	77%	Electrolyte	GLO: market for lithium hexafluorophosphate ecoinvent 3.4	
3.6E-05	1.7%	79%	Cathode	DE: Soda (Na2CO3) ts	
3.2E-05	1.5%	80%	Module packaging	GLO: market for electronic component, passive, unspecified ecoinvent 3.4	

Table H.10: The most important paths for acidification impacts of the NMC622 battery manufacturing

Absolute [Mole of H+ eq.]	Relative	Cumulative			
2.0E-03	74%	74%	Cathode	Nickel sulfate <LC>	Nickel refining (Ni institute) <u-so>
1.0E-04	3.9%	78%	Cathode	Nickel sulfate <LC>	Nickel primary extraction (Ni institute) <u-so>
5.0E-05	1.9%	80%	Pack packaging	EU-28: Aluminium ingot mix ts	

H.6 Human toxicity cancer effects

Table H.11: The most important paths for human toxicity cancer effects impacts of the NMC333 battery manufacturing

Absolute [CTUh]	Relative	Cumulative			
8.9E-10	22%	22%	Module packaging	GLO: market for electronic component, passive, unspecified ecoinvent 3.4	
8.5E-10	21%	42%	Pack packaging	GLO: market for electronic component, passive, unspecified ecoinvent 3.4	
3.7E-10	9.0%	51%	Anode	GLO: market for graphite, battery grade ecoinvent 3.4	
2.9E-10	7.1%	58%	Electrolyte	GLO: market for lithium hexafluorophosphate ecoinvent 3.4	
2.6E-10	6.3%	65%	Cathode	Cobalt sulfate <LC>	CN: Thermal energy from natural gas ts
2.3E-10	5.7%	70%	BMS	GLO: market for electronic component, passive, unspecified ecoinvent 3.4	
1.9E-10	4.5%	75%	Pack packaging	GLO: market for electronic component, passive, unspecified ecoinvent 3.4	
1.8E-10	4.3%	79%	Cathode	Cobalt sulfate <LC>	GLO: market for magnesium oxide ecoinvent 3.4
1.3E-10	3.1%	82%	Cathode	RER: Polyvinylchloride injection moulding part (PVC) PlasticsEurope	

Table H.12: The most important paths for human toxicity cancer effects impacts of the NMC622 battery manufacturing

Absolute [CTUh]	Relative	Cumulative			
9.1E-10	24%	24%	Module packaging	GLO: market for electronic component, passive, unspecified ecoinvent 3.4	
8.3E-10	22%	45%	Pack packaging	GLO: market for electronic component, passive, unspecified ecoinvent 3.4	
3.6E-10	9.4%	55%	Anode	GLO: market for graphite, battery grade ecoinvent 3.4	
2.7E-10	7.1%	62%	Electrolyte	GLO: market for lithium hexafluorophosphate ecoinvent 3.4	
2.4E-10	6.2%	68%	BMS	GLO: market for electronic component, passive, unspecified ecoinvent 3.4	
1.9E-10	4.9%	73%	Pack packaging	GLO: market for electronic component, passive, unspecified ecoinvent 3.4	
1.3E-10	3.4%	76%	Cathode	Cobalt sulfate <LC>	CN: Thermal energy from natural gas ts
1.2E-10	3.2%	80%	BMS	GLO: market for printed wiring board, through-hole mounted, unspecified, Pb free ecoinvent 3.4	

H.7 Human toxicity non-cancer effects

Table H.13: The most important paths for human toxicity non-cancer effects impacts of the NMC333 battery manufacturing

Absolute [CTUh]	Relative	Cumulative		
2.0E-08	29%	29%	Module packaging	GLO: market for electronic component, passive, unspecified ecoinvent 3.4
1.9E-08	27%	56%	Pack packaging	GLO: market for electronic component, passive, unspecified ecoinvent 3.4
7.8E-09	11%	67%	Anode	EU-28: Copper Sheet Mix DKI/ECI
5.3E-09	7.5%	75%	BMS	GLO: market for electronic component, passive, unspecified ecoinvent 3.4
4.2E-09	6.0%	81%	Pack packaging	GLO: market for electronic component, passive, unspecified ecoinvent 3.4

Table H.14: The most important paths for human toxicity non-cancer effects impacts of the NMC622 battery manufacturing

Absolute [CTUh]	Relative	Cumulative		
2.1E-08	30%	30%	Module packaging	GLO: market for electronic component, passive, unspecified ecoinvent 3.4
1.9E-08	27%	57%	Pack packaging	GLO: market for electronic component, passive, unspecified ecoinvent 3.4
7.7E-09	11%	68%	Anode	EU-28: Copper Sheet Mix DKI/ECI
5.5E-09	7.8%	76%	BMS	GLO: market for electronic component, passive, unspecified ecoinvent 3.4
4.3E-09	6.2%	82%	Pack packaging	GLO: market for electronic component, passive, unspecified ecoinvent 3.4

H.8   Ecotoxicity freshwater

Table H.15: The most important paths for ecotoxicity freshwater impacts of the NMC333 battery manufacturing

Absolute [CTUe]	Relative	Cumulative		
4.9E-01	31%	31%	Module packaging	GLO: market for electronic component, passive, unspecified ecoinvent 3.4
4.7E-01	29%	60%	Pack packaging	GLO: market for electronic component, passive, unspecified ecoinvent 3.4
1.3E-01	8.4%	68%	Anode	EU-28: Copper Sheet Mix DKI/ECI
1.3E-01	8.0%	76%	BMS	GLO: market for electronic component, passive, unspecified ecoinvent 3.4
1.0E-01	6.4%	83%	Pack packaging	GLO: market for electronic component, passive, unspecified ecoinvent 3.4

Table H.16: The most important paths for ecotoxicity freshwater impacts of the NMC622 battery manufacturing

Absolute [CTUe]	Relative	Cumulative		
5.0E-01	31%	31%	Module packaging	GLO: market for electronic component, passive, unspecified ecoinvent 3.4
4.6E-01	29%	60%	Pack packaging	GLO: market for electronic component, passive, unspecified ecoinvent 3.4
1.3E-01	8.3%	68%	Anode	EU-28: Copper Sheet Mix DKI/ECI
1.3E-01	8.2%	76%	BMS	GLO: market for electronic component, passive, unspecified ecoinvent 3.4
1.0E-01	6.5%	83%	Pack packaging	GLO: market for electronic component, passive, unspecified ecoinvent 3.4

H.9 Photochemical ozone formation

Table H.17: The most important paths for photochemical ozone formation impacts of the NMC333 battery manufacturing

Absolute [kg NMVOC eq.]	Relative	Cumulative			
8.8E-05	18%	18%	Cathode	Nickel sulfate <LC>	Nickel refining (Ni institute) <u-so>
4.0E-05	8.4%	27%	Cathode	Transport of active material <LC>	GLO: Bulk commodity carrier, average, ocean going ts <u-so>
3.5E-05	7.4%	34%	Anode	GLO: market for graphite, battery grade ecoinvent 3.4	
2.8E-05	5.9%	40%	Anode	Transport of active material <LC>	GLO: Bulk commodity carrier, average, ocean going ts <u-so>
2.2E-05	4.5%	45%	Pack packaging	EU-28: Aluminium ingot mix ts	
1.9E-05	3.9%	48%	Module packaging	GLO: market for electronic component, passive, unspecified ecoinvent 3.4	
1.8E-05	3.7%	52%	Pack packaging	GLO: market for electronic component, passive, unspecified ecoinvent 3.4	
1.7E-05	3.6%	56%	Cathode	DE: Soda (Na2CO3) ts	
1.6E-05	3.3%	59%	Electrolyte	GLO: market for lithium hexafluorophosphate ecoinvent 3.4	
1.4E-05	3.0%	62%	Cathode	EU-28: Electricity grid mix 1kV-60kV ts	
1.3E-05	2.7%	65%	Electrolyte	Transport of active material <LC>	GLO: Bulk commodity carrier, average, ocean going ts <u-so>
9.5E-06	2.0%	67%	Module packaging	Transport of cell from China, Korea or Japan to Europe <LC>	GLO: Bulk commodity carrier, average, ocean going ts <u-so>
8.9E-06	1.9%	69%	Cathode	EU-28: Aluminium ingot mix ts	
8.4E-06	1.8%	70%	Manufacture of battery cells	Dry room maintenance	EU-28: Electricity grid mix 1kV-60kV ts
8.2E-06	1.7%	72%	Cell container	Transport of passive material <LC>	GLO: Bulk commodity carrier, average, ocean going ts <u-so>
7.7E-06	1.6%	74%	Cathode	EU-28: Thermal energy from natural gas ts	
7.5E-06	1.6%	75%	Cathode	Cobalt sulfate <LC>	EU-28: Thermal energy from light fuel oil (LFO) ts
6.9E-06	1.4%	77%	Cathode	EU-28: Sodium hydroxide (caustic soda) mix (100%) ts	
6.8E-06	1.4%	78%	Cathode	Nickel sulfate <LC>	Nickel primary extraction (Ni institute) <u-so>
6.2E-06	1.3%	79%	Manufacture of battery cells	Electrode drying & NMP recovery	EU-28: Thermal energy from natural gas ts
6.2E-06	1.3%	81%	Manufacture of battery cells	Dry room maintenance	EU-28: Thermal energy from natural gas ts

Table H.18: The most important paths for photochemical ozone formation impacts of the NMC622 battery manufacturing

Absolute [kg NMVOC eq.]	Relative	Cumulative			
1.3E-04	27%	27%	Cathode	Nickel sulfate <LC>	Nickel refining (Ni institute) <u-so>
3.5E-05	7.1%	34%	Anode	GLO: market for graphite, battery grade ecoinvent 3.4	
3.4E-05	7.0%	41%	Cathode	Transport of active material <LC>	GLO: Bulk commodity carrier, average, ocean going ts <u-so>
2.8E-05	5.7%	47%	Anode	Transport of active material <LC>	GLO: Bulk commodity carrier, average, ocean going ts <u-so>
2.1E-05	4.3%	51%	Pack packaging	EU-28: Aluminium ingot mix ts	
1.9E-05	3.9%	55%	Module packaging	GLO: market for electronic component, passive, unspecified ecoinvent 3.4	
1.7E-05	3.5%	58%	Pack packaging	GLO: market for electronic component, passive, unspecified ecoinvent 3.4	
1.5E-05	3.0%	62%	Electrolyte	GLO: market for lithium hexafluorophosphate ecoinvent 3.4	
1.4E-05	2.9%	64%	Cathode	DE: Soda (Na2CO3) ts	
1.2E-05	2.5%	67%	Electrolyte	Transport of active material <LC>	GLO: Bulk commodity carrier, average, ocean going ts <u-so>
1.2E-05	2.5%	69%	Cathode	EU-28: Electricity grid mix 1kV-60kV ts	
1.0E-05	2.1%	71%	Cathode	Nickel sulfate <LC>	Nickel primary extraction (Ni institute) <u-so>
9.1E-06	1.9%	73%	Module packaging	Transport of cell from China, Korea or Japan to Europe <LC>	GLO: Bulk commodity carrier, average, ocean going ts <u-so>
8.8E-06	1.8%	75%	Cathode	EU-28: Aluminium ingot mix ts	
8.3E-06	1.7%	77%	Manufacture of battery cells	Dry room maintenance	EU-28: Electricity grid mix 1kV-60kV ts
6.5E-06	1.3%	78%	Cathode	EU-28: Thermal energy from natural gas ts	
6.2E-06	1.3%	79%	Manufacture of battery cells	Dry room maintenance	EU-28: Thermal energy from natural gas ts
6.2E-06	1.3%	81%	Manufacture of battery cells	Electrode drying & NMP recovery	EU-28: Thermal energy from natural gas ts

H.10 Ozone depletion

Table H.19: The most important paths for ozone depletion impacts of the NMC333 battery manufacturing

Absolute [kg CFC-11 eq.]	Relative	Cumulative		
2.5E-09	44%	44%	Cathode	World: Polyvinylidene fluoride (PVDF)
1.3E-09	23%	67%	Anode	World: Polyvinylidene fluoride (PVDF)
6.2E-10	11%	77%	Electrolyte	GLO: market for lithium hexafluorophosphate ecoinvent 3.4
4.5E-10	7.8%	85%	Anode	GLO: market for graphite, battery grade ecoinvent 3.4

Table H.20: The most important paths for ozone depletion impacts of the NMC622 battery manufacturing

Absolute [kg CFC-11 eq.]	Relative	Cumulative		
2.1E-09	41%	41%	Cathode	World: Polyvinylidene fluoride (PVDF)
1.3E-09	24%	65%	Anode	World: Polyvinylidene fluoride (PVDF)
5.7E-10	11%	76%	Electrolyte	GLO: market for lithium hexafluorophosphate ecoinvent 3.4
4.4E-10	8.4%	84%	Anode	GLO: market for graphite, battery grade ecoinvent 3.4

H.11   Ionizing radiation

Table H.21: The most important paths for ionizing radiation impacts of the NMC333 battery manufacturing

Absolute [kBq U235 eq.]	Relative	Cumulative			
4.2E-03	29%	29%	Cathode	EU-28: Electricity grid mix 1kV-60kV ts	
2.5E-03	17%	45%	Manufacture of battery cells	Dry room maintenance	EU-28: Electricity grid mix 1kV-60kV ts
1.5E-03	10%	56%	Pack packaging	EU-28: Aluminium ingot mix ts	
9.1E-04	6.1%	62%	Cathode	EU-28: Sodium hydroxide (caustic soda) mix (100%) ts	
6.3E-04	4.3%	66%	Cathode	EU-28: Aluminium ingot mix ts	
5.9E-04	3.9%	70%	Cathode	Cobalt sulfate <LC>	EU-28: Sodium hydroxide (caustic soda) mix (100%) ts
4.6E-04	3.1%	73%	Electrolyte	GLO: market for lithium hexafluorophosphate ecoinvent 3.4	
3.9E-04	2.6%	76%	Module packaging	EU-28: Aluminium ingot mix ts	
2.8E-04	1.9%	78%	Cathode	Nickel sulfate <LC>	EU-28: Electricity grid mix 1kV-60kV ts
2.7E-04	1.8%	79%	Module packaging	GLO: market for electronic component, passive, unspecified ecoinvent 3.4	
2.7E-04	1.8%	81%	Cathode	Manganese sulfate <LC>	EU-28: Electricity grid mix 1kV-60kV ts

Table H.22: The most important paths for ionizing radiation impacts of the NMC622 battery manufacturing

Absolute [kBq U235 eq.]	Relative	Cumulative			
3.6E-03	26%	26%	Cathode	EU-28: Electricity grid mix 1kV-60kV ts	
2.5E-03	18%	44%	Manufacture of battery cells	Dry room maintenance	EU-28: Electricity grid mix 1kV-60kV ts
1.5E-03	11%	55%	Pack packaging	EU-28: Aluminium ingot mix ts	
7.7E-04	5.6%	61%	Cathode	EU-28: Sodium hydroxide (caustic soda) mix (100%) ts	
6.2E-04	4.5%	65%	Cathode	EU-28: Aluminium ingot mix ts	
4.3E-04	3.1%	68%	Cathode	Nickel sulfate <LC>	EU-28: Electricity grid mix 1kV-60kV ts
4.2E-04	3.1%	71%	Electrolyte	GLO: market for lithium hexafluorophosphate ecoinvent 3.4	
4.0E-04	2.9%	74%	Cathode	Nickel sulfate <LC>	EU-28: Electricity grid mix 1kV-60kV ts
3.7E-04	2.7%	77%	Module packaging	EU-28: Aluminium ingot mix ts	
2.9E-04	2.1%	79%	Cathode	Cobalt sulfate <LC>	EU-28: Sodium hydroxide (caustic soda) mix (100%) ts
2.8E-04	2.0%	81%	Module packaging	GLO: market for electronic component, passive, unspecified ecoinvent 3.4	

H.12   Particulate matter/Respiratory inorganics

Table H.23: The most important paths for particulate matter/respiratory inorganics impacts of the NMC333 battery manufacturing

Absolute [kg PM2.5 eq.]	Relative	Cumulative			
6.2E-05	38%	38%	Cathode	Nickel sulfate <LC>	Nickel refining (Ni institute) <u-so>
4.1E-05	26%	64%	Cathode	Cobalt sulfate <LC>	CD: Cobalt mining <u-so>
9.3E-06	5.7%	69%	Anode	GLO: market for graphite, battery grade ecoinvent 3.4	
4.7E-06	2.9%	72%	Electrolyte	GLO: market for lithium hexafluorophosphate ecoinvent 3.4	
4.1E-06	2.6%	75%	Module packaging	GLO: market for electronic component, passive, unspecified ecoinvent 3.4	
4.0E-06	2.4%	77%	Pack packaging	GLO: market for electronic component, passive, unspecified ecoinvent 3.4	
3.2E-06	2.0%	79%	Cathode	Nickel sulfate <LC>	Nickel primary extraction (Ni institute) <u-so>
2.7E-06	1.7%	81%	Pack packaging	EU-28: Aluminium ingot mix ts	

Table H.24: The most important paths for particulate matter/respiratory inorganics impacts impacts of the NMC622 battery manufacturing

Absolute [kg PM2.5 eq.]	Relative	Cumulative			
9.3E-05	55%	55%	Cathode	Nickel sulfate <LC>	Nickel refining (Ni institute) <u-so>
2.1E-05	12%	68%	Cathode	Cobalt sulfate <LC>	CD: Cobalt mining <u-so>
9.1E-06	5.4%	73%	Anode	GLO: market for graphite, battery grade ecoinvent 3.4	
4.8E-06	2.8%	76%	Cathode	Nickel sulfate <LC>	Nickel primary extraction (Ni institute) <u-so>
4.4E-06	2.6%	78%	Electrolyte	GLO: market for lithium hexafluorophosphate ecoinvent 3.4	
4.2E-06	2.5%	81%	Module packaging	GLO: market for electronic component, passive, unspecified ecoinvent 3.4	

H.13 Water scarcity

Table H.25: The most important paths for water scarcity impacts of the NMC333 battery manufacturing

Absolute [m³ eq.]	Relative	Cumulative			
5.8E-04	25%	25%	Cathode	EU-28: Electricity grid mix 1kV-60kV ts	
3.5E-04	15%	40%	Manufacture of battery cells	Dry room maintenance	EU-28: Electricity grid mix 1kV-60kV ts
2.2E-04	9.3%	50%	Anode	EU-28: Copper Sheet Mix DKI/ECI	
1.8E-04	7.7%	57%	Pack packaging	EU-28: Aluminium ingot mix ts	
1.3E-04	5.6%	63%	Cathode	EU-28: Sodium hydroxide (caustic soda) mix (100%) ts	
8.3E-05	3.6%	67%	Cathode	Cobalt sulfate <LC>	EU-28: Sodium hydroxide (caustic soda) mix (100%) ts
7.3E-05	3.2%	70%	Cathode	EU-28: Aluminium ingot mix ts	
5.8E-05	2.5%	72%	Electrolyte	GLO: market for lithium hexafluorophosphate ecoinvent 3.4	
4.7E-05	2.0%	74%	Cell container	EU-28: Copper Sheet Mix DKI/ECI	
4.5E-05	2.0%	76%	Module packaging	EU-28: Aluminium ingot mix ts	
3.9E-05	1.7%	78%	Cathode	Nickel sulfate <LC>	EU-28: Electricity grid mix 1kV-60kV ts
3.8E-05	1.7%	80%	Cathode	DE: Soda (Na2CO3) ts	

Table H.26: The most important paths for water scarcity impacts impacts of the NMC622 battery manufacturing

Absolute [m³ eq.]	Relative	Cumulative			
4.9E-04	23%	23%	Cathode	EU-28: Electricity grid mix 1kV-60kV ts	
3.4E-04	16%	39%	Manufacture of battery cells	Dry room maintenance	EU-28: Electricity grid mix 1kV-60kV ts
2.1E-04	9.9%	49%	Anode	EU-28: Copper Sheet Mix DKI/ECI	
1.7E-04	8.1%	57%	Pack packaging	EU-28: Aluminium ingot mix ts	
1.1E-04	5.1%	62%	Cathode	EU-28: Sodium hydroxide (caustic soda) mix (100%) ts	
7.2E-05	3.4%	66%	Cathode	EU-28: Aluminium ingot mix ts	
5.9E-05	2.8%	69%	Cathode	Nickel sulfate <LC>	EU-28: Electricity grid mix 1kV-60kV ts
5.5E-05	2.6%	71%	Cathode	Nickel sulfate <LC>	EU-28: Electricity grid mix 1kV-60kV ts
5.3E-05	2.5%	74%	Electrolyte	GLO: market for lithium hexafluorophosphate ecoinvent 3.4	
4.5E-05	2.1%	76%	Cell container	EU-28: Copper Sheet Mix DKI/ECI	
4.3E-05	2.0%	78%	Module packaging	EU-28: Aluminium ingot mix ts	
4.2E-05	2.0%	80%	Cathode	Cobalt sulfate <LC>	EU-28: Sodium hydroxide (caustic soda) mix (100%) ts

H.14 Abiotic resource depletion

Table H.27: The most important paths for abiotic resource depletion impacts of the NMC333 battery manufacturing

Absolute [kg Sb eq.]	Relative	Cumulative		
1.9E-05	30%	30%	Module packaging	GLO: market for electronic component, passive, unspecified ecoinvent 3.4
1.9E-05	28%	58%	Pack packaging	GLO: market for electronic component, passive, unspecified ecoinvent 3.4
7.6E-06	12%	70%	Electrolyte	GLO: market for lithium hexafluorophosphate ecoinvent 3.4
5.7E-06	8.7%	78%	Cathode	CL: Concentrated lithium brine (60,000 pm) <u-so>
5.1E-06	7.8%	86%	BMS	GLO: market for electronic component, passive, unspecified ecoinvent 3.4

Table H.28: The most important paths for abiotic resource depletion impacts of the NMC622 battery manufacturing

Absolute [kg Sb eq.]	Relative	Cumulative		
2.0E-05	31%	31%	Module packaging	GLO: market for electronic component, passive, unspecified ecoinvent 3.4
1.8E-05	28%	59%	Pack packaging	GLO: market for electronic component, passive, unspecified ecoinvent 3.4
7.0E-06	11%	70%	Electrolyte	GLO: market for lithium hexafluorophosphate ecoinvent 3.4
5.2E-06	8.1%	78%	BMS	GLO: market for electronic component, passive, unspecified ecoinvent 3.4
4.8E-06	7.4%	86%	Cathode	CL: Concentrated lithium brine (60,000 pm) <u-so>

H.15   Land use

Table H.29: The most important paths for land use impacts of the NMC333 battery manufacturing

Absolute [kg C deficit eq.]	Relative	Cumulative		
8.0E-03	16%	16%	Electrolyte	GLO: market for lithium hexafluorophosphate ecoinvent 3.4
7.4E-03	15%	31%	Module packaging	GLO: market for electronic component, passive, unspecified ecoinvent 3.4
7.1E-03	14%	45%	Pack packaging	GLO: market for electronic component, passive, unspecified ecoinvent 3.4
5.2E-03	10%	55%	Anode	GLO: market for graphite, battery grade ecoinvent 3.4
4.5E-03	9.1%	64%	Cathode	EU-28: Electricity grid mix 1kV-60kV ts
2.7E-03	5.4%	70%	Manufacture of battery cells	Dry room maintenance · EU-28: Electricity grid mix 1kV-60kV ts
1.9E-03	3.9%	74%	BMS	GLO: market for electronic component, passive, unspecified ecoinvent 3.4
1.6E-03	3.2%	77%	Cathode	RoW: market for ammonia, liquid ecoinvent 3.4
1.5E-03	3.1%	80%	Pack packaging	GLO: market for electronic component, passive, unspecified ecoinvent 3.4

Table H.30: The most important paths for land use impacts of the NMC622 battery manufacturing

| Absolute [kg C deficit eq.]	Relative	Cumulative		
7.6E-03	16%	16%	Module packaging	GLO: market for electronic component, passive, unspecified ecoinvent 3.4
7.4E-03	16%	32%	Electrolyte	GLO: market for lithium hexafluorophosphate ecoinvent 3.4
6.9E-03	15%	46%	Pack packaging	GLO: market for electronic component, passive, unspecified ecoinvent 3.4
5.1E-03	11%	57%	Anode	GLO: market for graphite, battery grade ecoinvent 3.4
3.8E-03	8.1%	65%	Cathode	EU-28: Electricity grid mix 1kV-60kV ts
2.7E-03	5.6%	70%	Manufacture of battery cells	Dry room maintenance	EU-28: Electricity grid mix 1kV-60kV ts
2.0E-03	4.2%	75%	BMS	GLO: market for electronic component, passive, unspecified ecoinvent 3.4
1.6E-03	3.3%	78%	Pack packaging	GLO: market for electronic component, passive, unspecified ecoinvent 3.4
1.3E-03	2.8%	81%	Cathode	RoW: market for ammonia, liquid ecoinvent 3.4

I

Cobalt and nickel sulfate
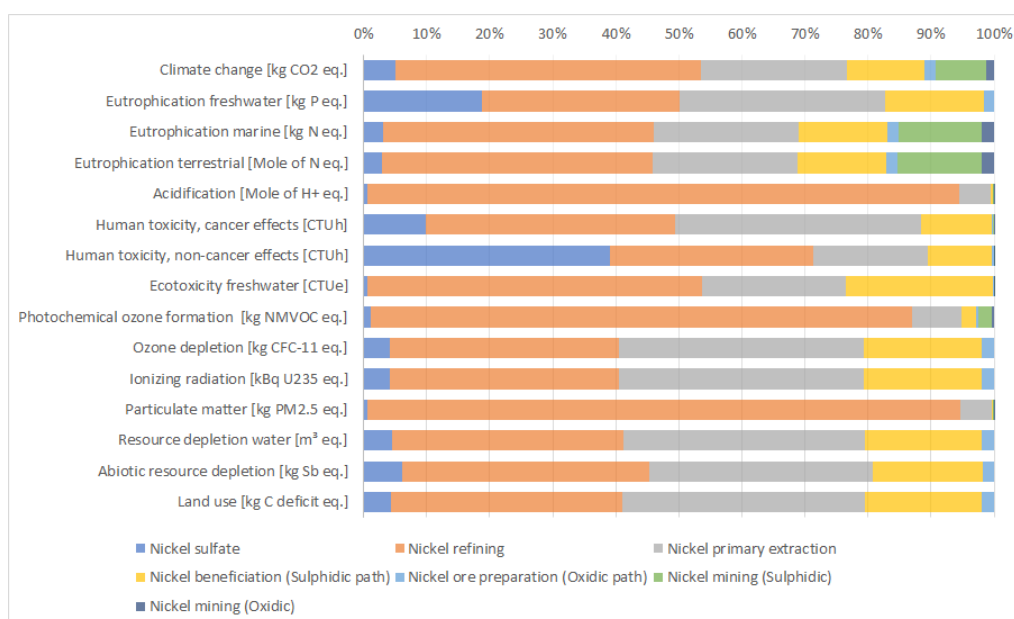
Figure I.1: Contribution of cradle-to-grave impacts from each step in the production of nickel sulfate
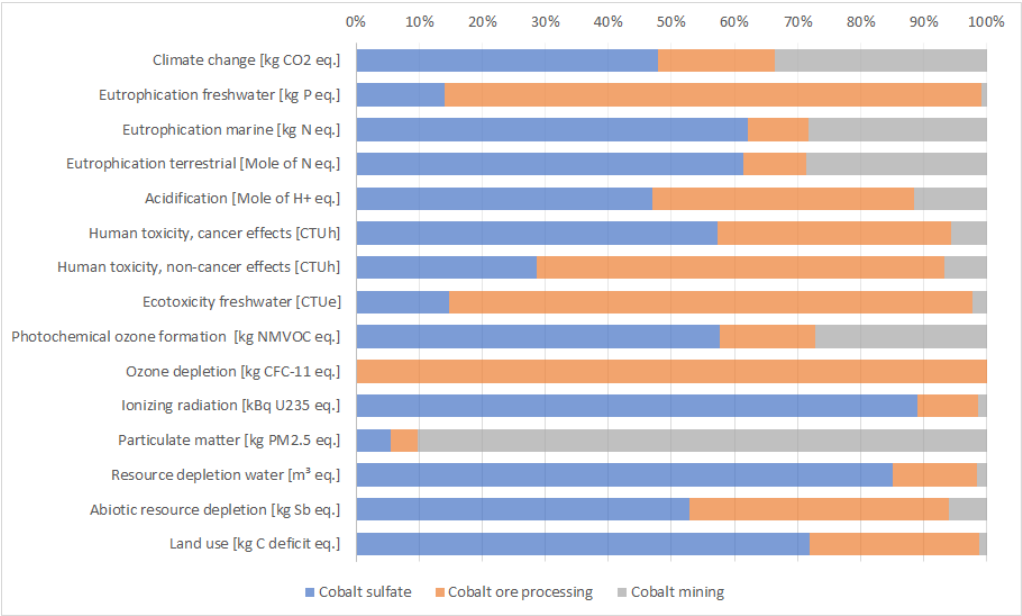
Figure I.2: Contribution of cradle-to-grave impacts from each step in the production of cobalt sulfate